Reconstructed Discontinuous Galerkin Methods for Computational Fluid Dynamics on Unstructured Grids

Hong Luo
Department of Mechanical and Aerospace Engineering
North Carolina State University

Presented at 2014 CFD Summer School
Beijing, China
July 7-11, 2014

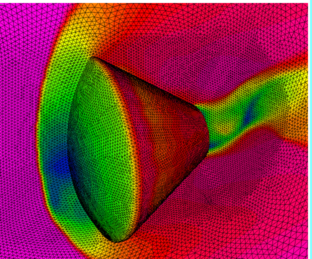
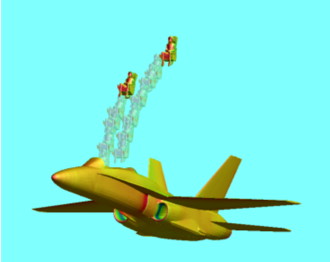
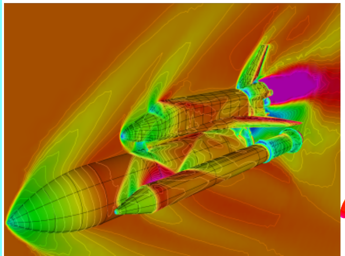
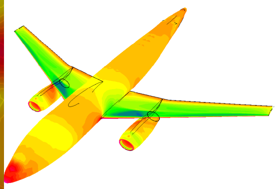
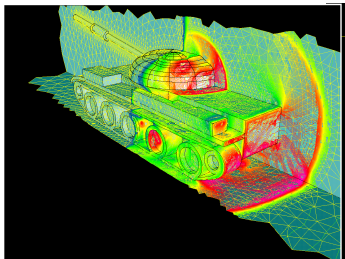
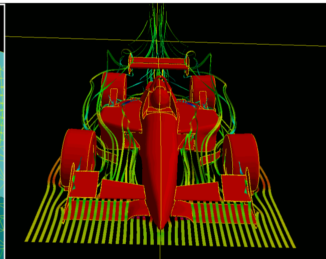

Start by saying thank you

- The main organizer
  - Prof. Li-Shi Luo

- Funding agencies to help enable this
  - NASA, AFOSR, Navy, Army, DOE, INL, DTRA, and NSF

- Collaborators and post-docs and students over time
  - Prof. R. Löhner, Prof. J. Edwards, Prof. N. Dinh, Prof. K. Xu, Prof. C. Cai, and Prof. Z. Jiang, Dr. J. Baum, Dr. J. White, Dr. M. Christan, Dr. R. Nourgaliev, Dr. V. Mousseau, Dr. R. Berry
  - Dr. Yidong Xia, Dr. Seth Spiegel, Dr. L. Luo, Dr. Douglas Stefanski, Dr. B. Halashi, Dr. B. Segawa, Megan Frisby, X. Liu, L. Luo, J. Lou, C. Zhang

You for taking the time

- Lecture 1: Overview of unstructured grid technologies for CFD
- Lecture 2: Review of discontinuous Galerkin methods
- Lecture 3: Reconstructed discontinuous Galerkin methods
- Lecture 4: Discontinuous Galerkin methods for elliptic problems

Lecture 1

Overview of unstructured grid technologies for CFD

Outline

- Background and Motivation
  - Why Unstructured Grids ?
- 2nd Order Finite Volume Methods on Unstructured Grids
  - Well Established, Very Mature
  - Widely Used in the Production CFD Codes
- Higher-order (>2nd) Reconstructed Discontinuous Galerkin Finite Element Methods on Arbitrary Grids
  - Hierarchical WENO Reconstruction
  - Ongoing Research
  - Choice → Next Generation of CFD Codes
- Concluding Remarks

Why Unstructured Grids ?

- Unstructured Grids Provide Great Flexibility to Handle Complex Geometries
  - Typical Configurations of Engineering Interest, Such as Cars, Ships, and Airplanes Are Complex.

- Unstructured Grids Offer a Natural Framework for Grid Adaptation to Local Features
  - Flow Fields Exhibit a Wide Range of Local Features, Such as Shock Waves, Contact Discontinuities, and Vortices.

CAD Model for a Indy-Type Race Car

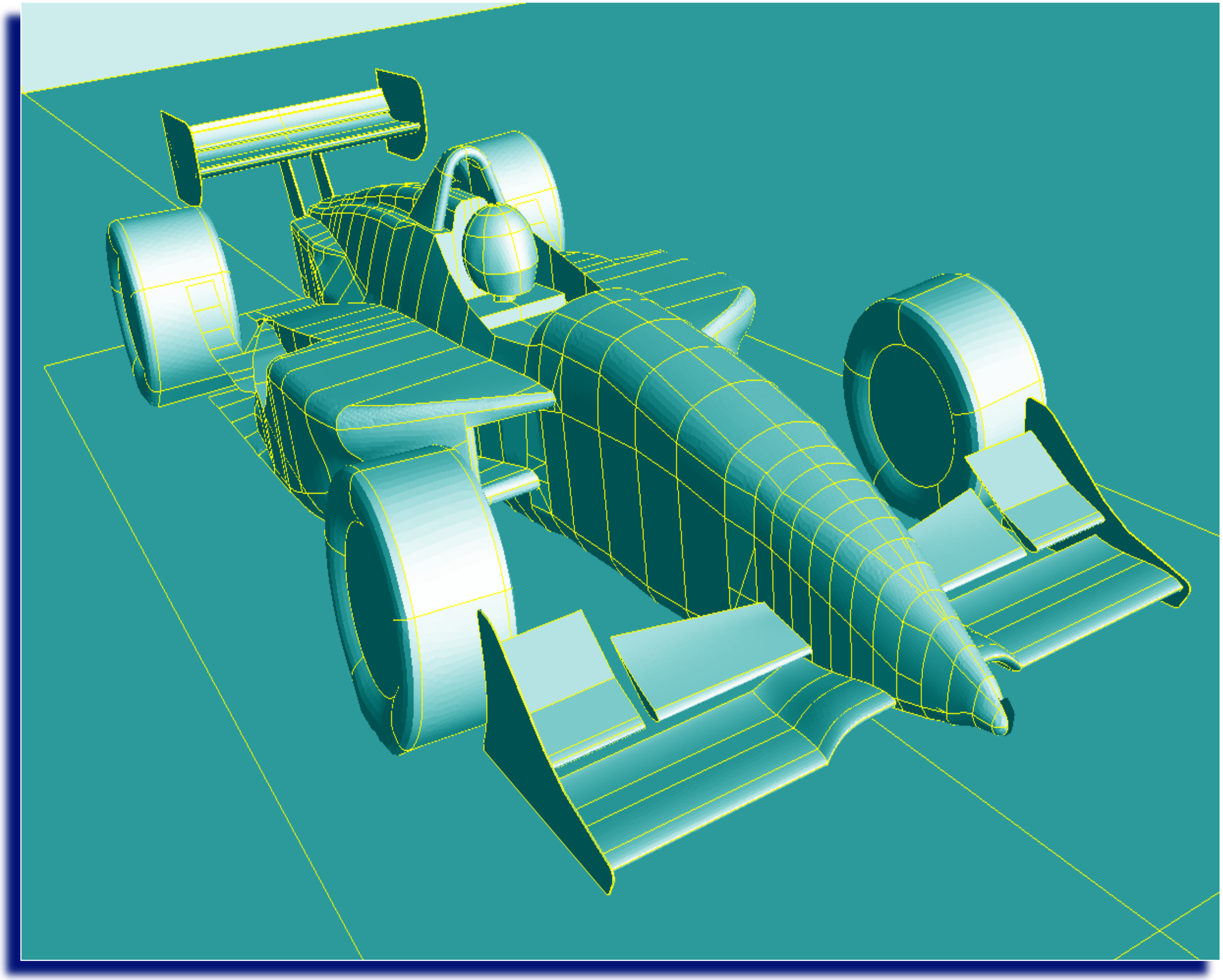

Surface Mesh for Indy-Type Race Car

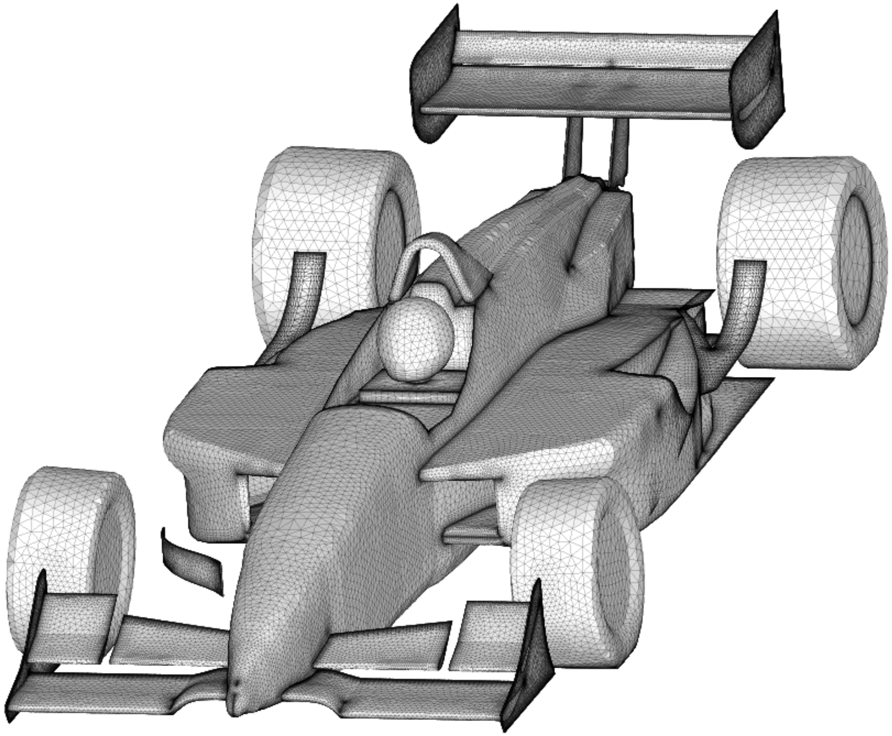

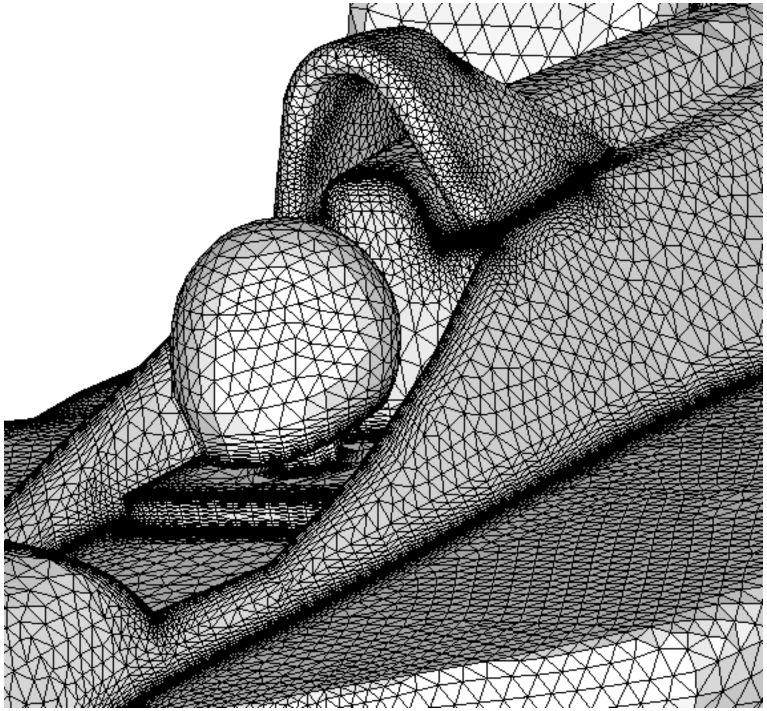

Slices of the Volume Mesh across the Car's Spoiler, and Driver's Compartment

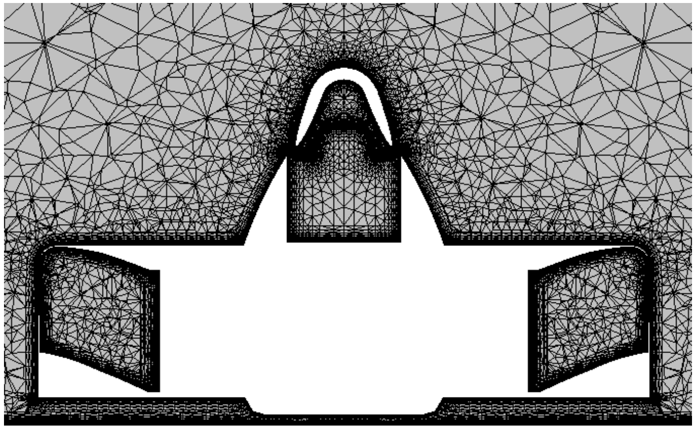

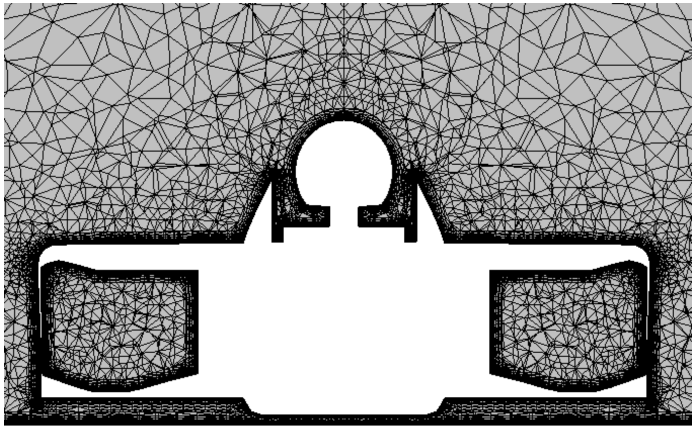

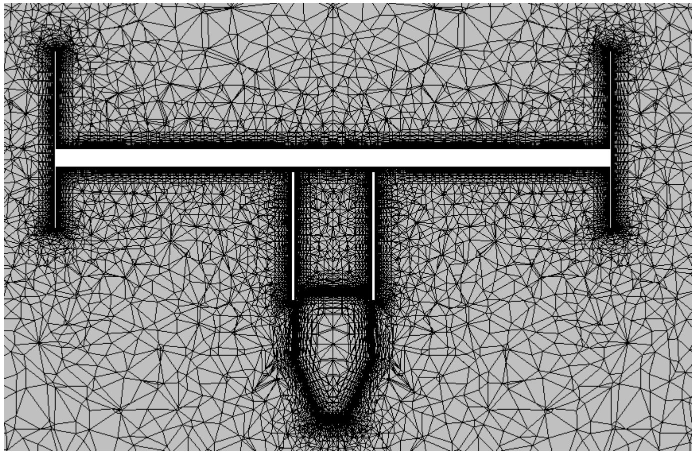

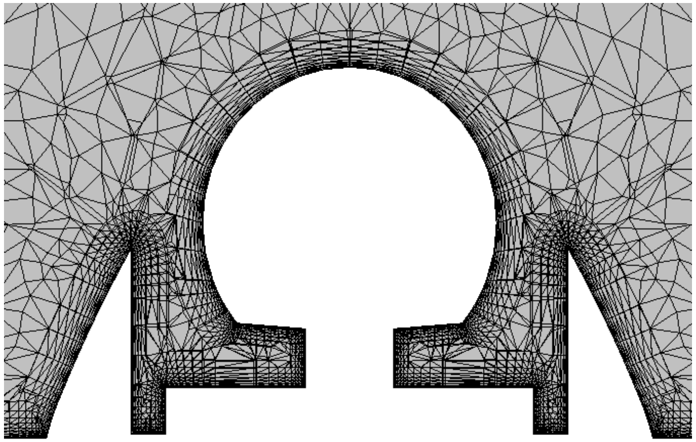

NURBE Model and Surface Mesh

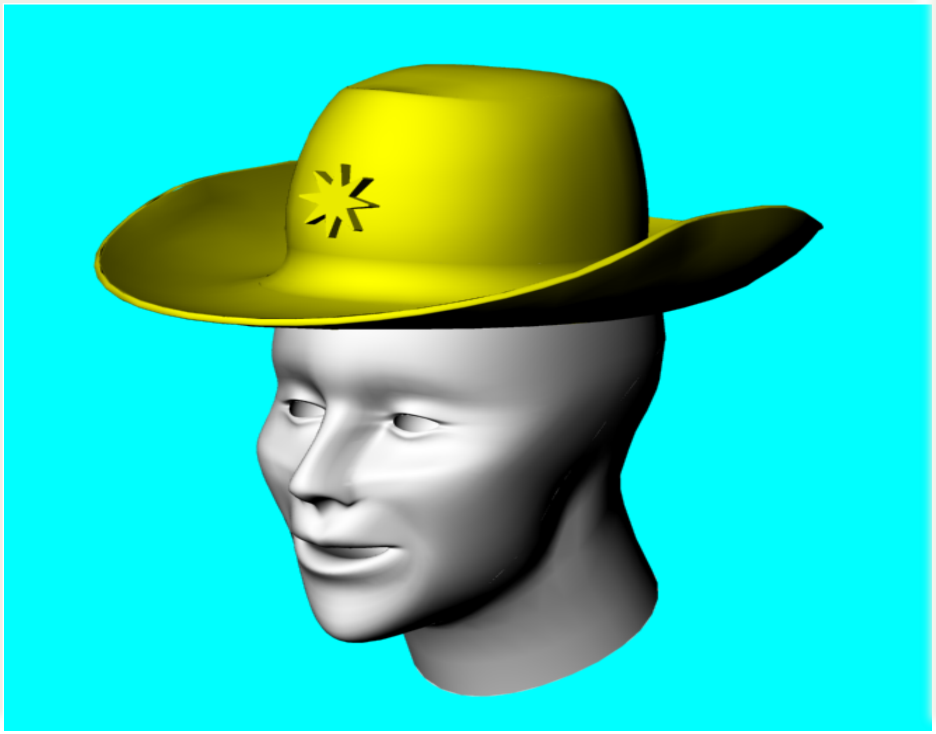

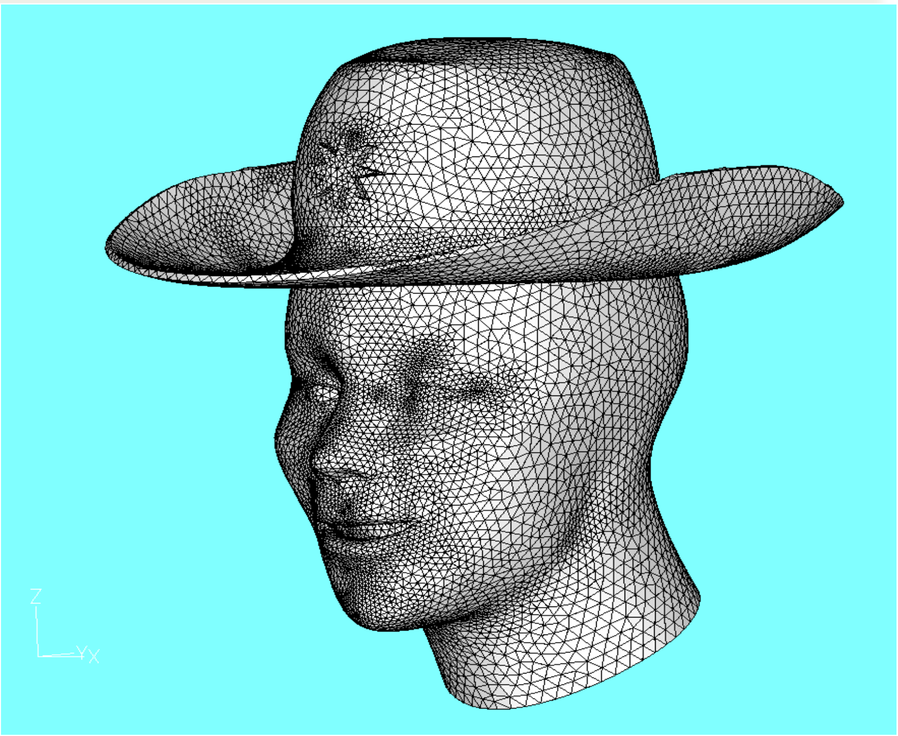

Hypersonic Flow past a Cylinder

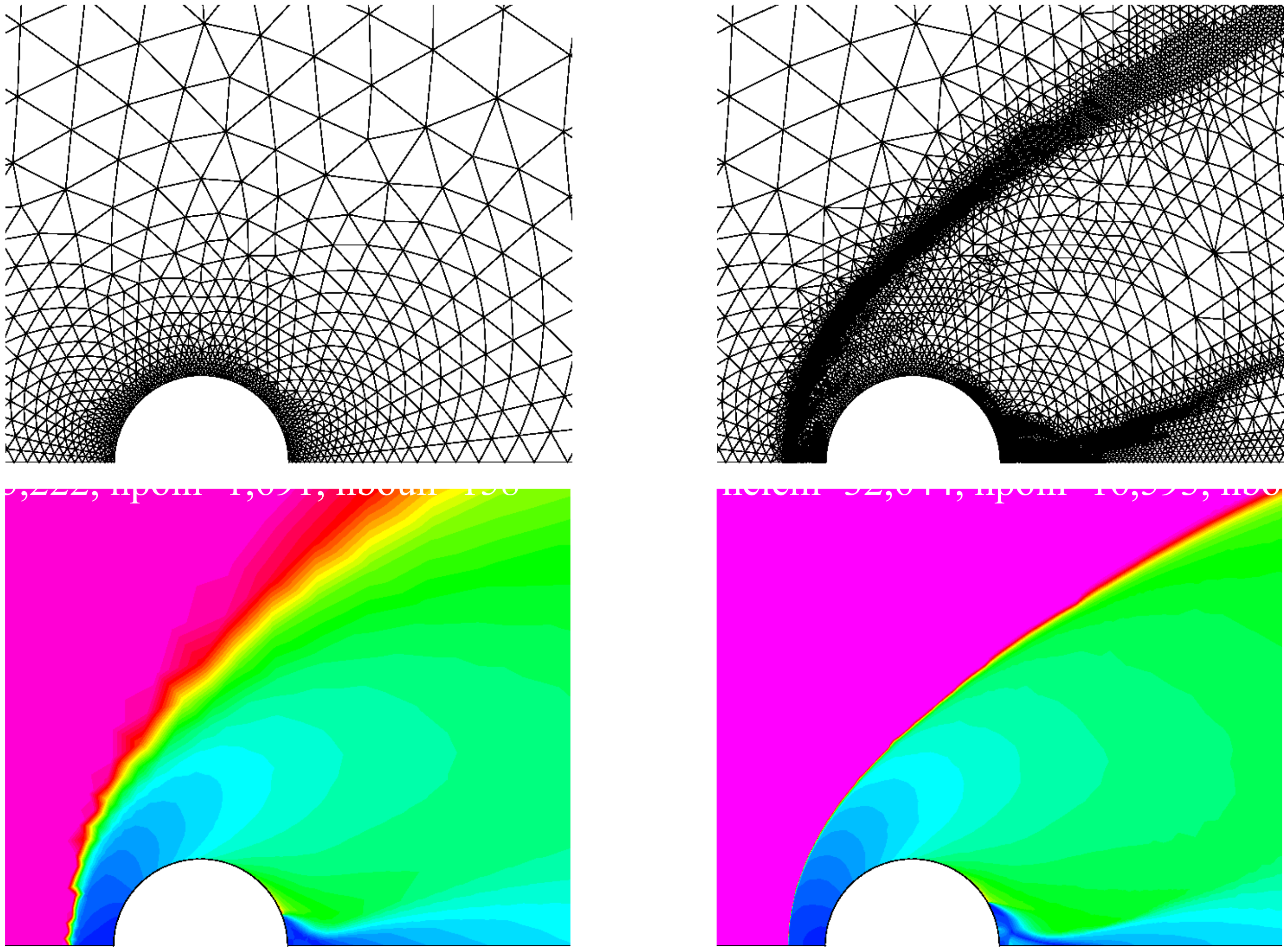

Shock and Tank Interaction

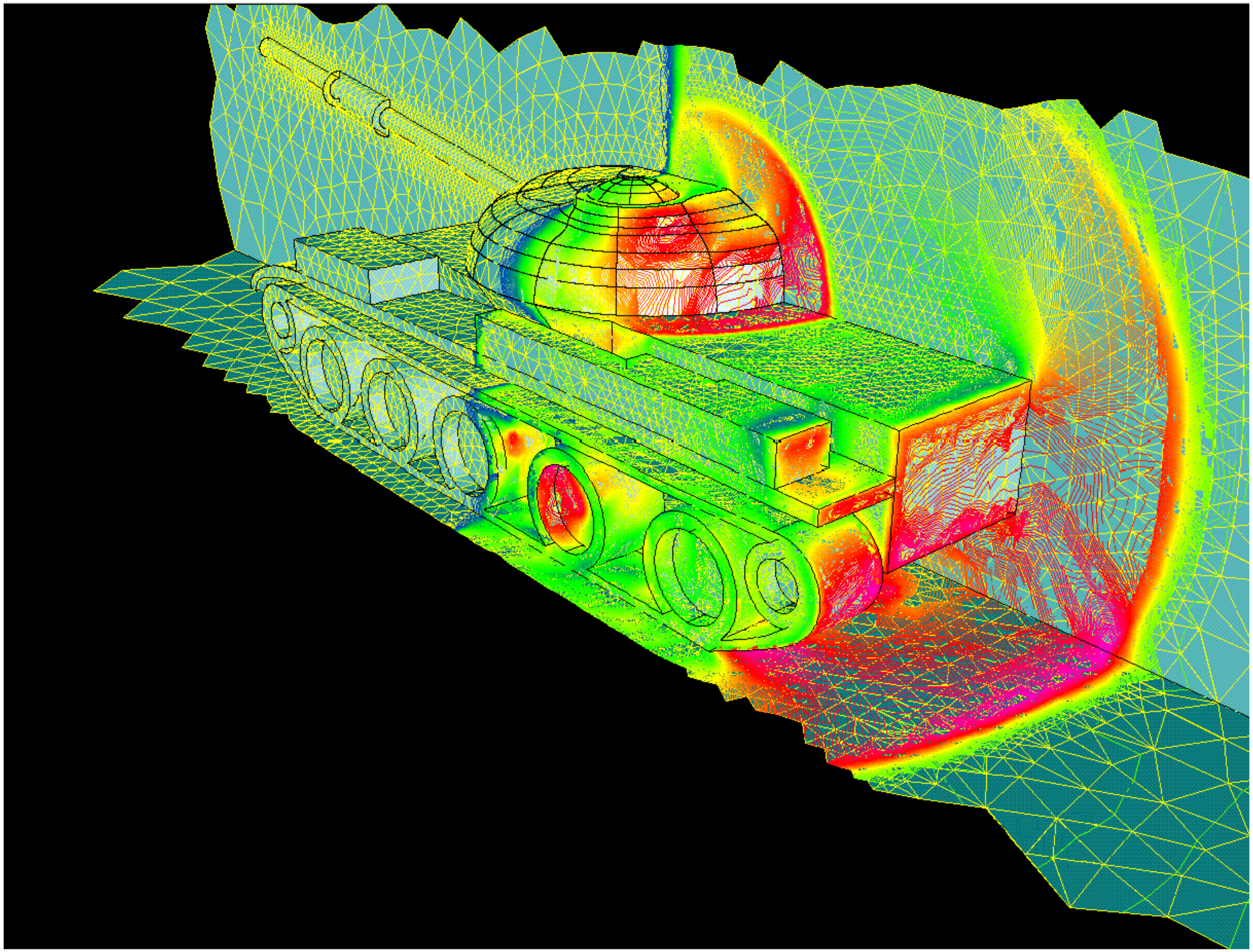

FVFLO-NCSU: Flow Solver

- Physics
  - Compressible flow for all speeds
  - Inviscid, Laminar, Turbulent, and DES
  - Real Air, Sesame, and JWL EOS
  - 6 DOF Integrator, Moving Bodies

- Numerics
  - Unstructured Triangular/Tetrahedral Elements Mesh
  - Vertex-based Finite Volume/Finite Element approximation
  - Implicit / Explicit Time Integration
  - Upwind & FCT Spatial Discretization
  - Arbitrary Lagrangian Eulerian Formulation
  - Remeshing & H-Refinement Adaptation
  - Overlapping and Embedded Grid Capabilities

External Aerodynamics Applications

Example 1. Fully Turbulent Flow past DLR-F6 Wing/body/Pylon/Nacelle Configuration

Single Point Test Case: $C_L=0.5$, $M_\infty=0.75$, $Re=3\text{x}10^6$

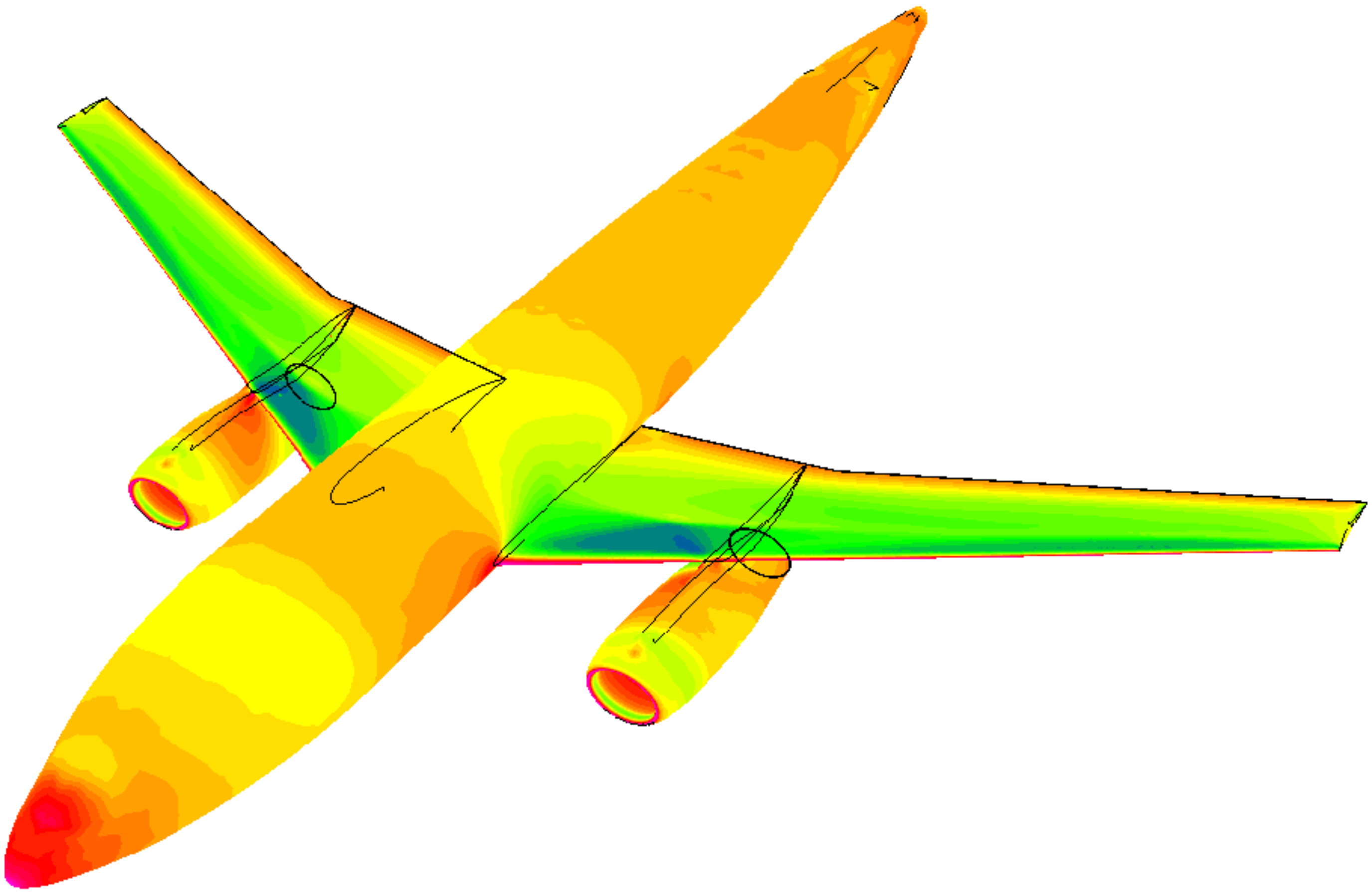

Luo, H., Baum, J. D., and Löhner, R. - High-Reynolds Number Viscous Flow Computations Using an Unstructured-Grid Method; **Journal of Aircraft**, Vol. 42, No. 2, pp. 483-492, 2005.

DLR-F6 Configuration

Single Point Case: Computed Cp vs. Experimental Data

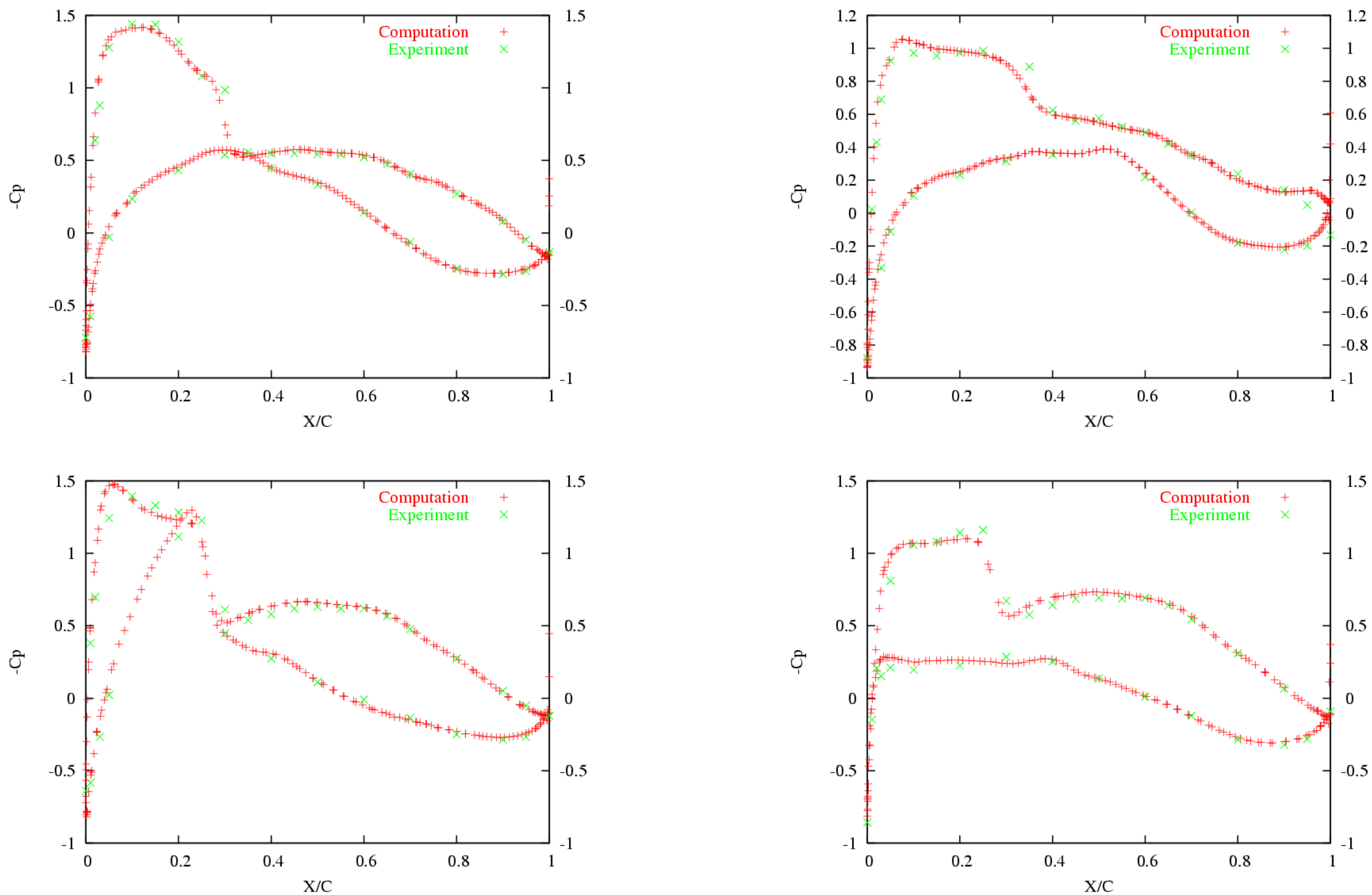

Example 2. Supersonic Flow Past a Space Shuttle

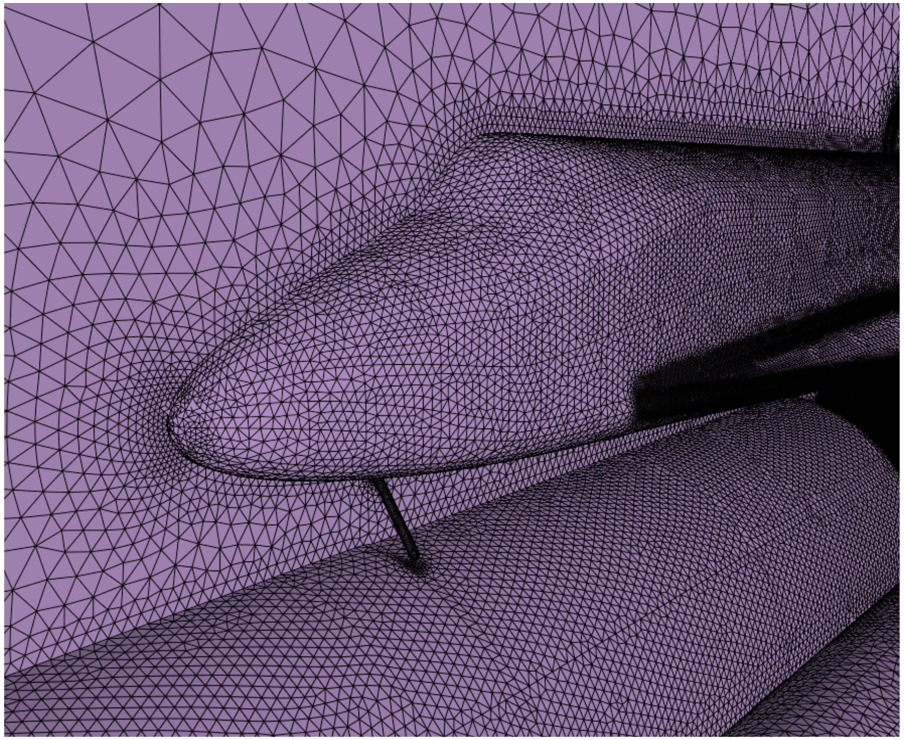

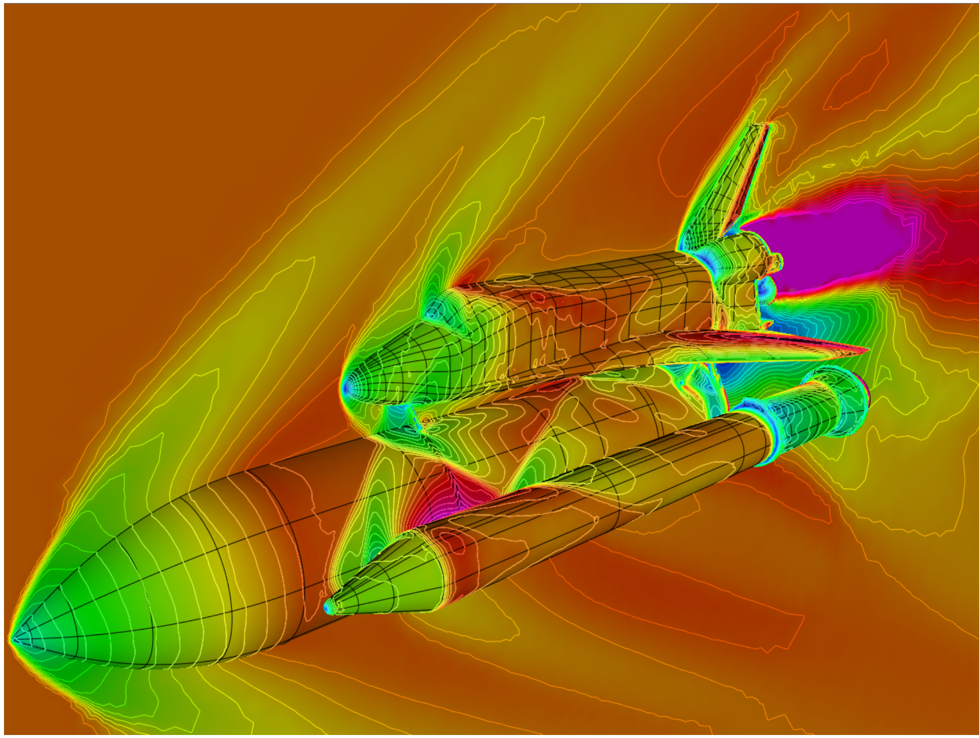

173,794 Boundary Points
2,679,754 Points
15,197,690 Elements

Mach Number Contours

Example 3. Viscous Flow past an Open-wheel Race Car

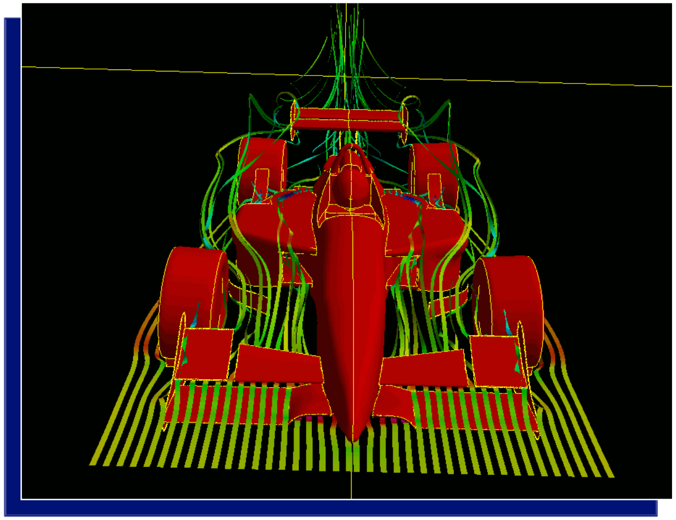

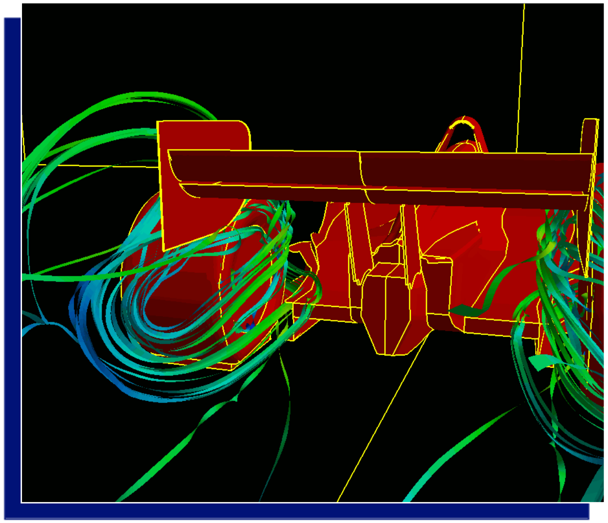

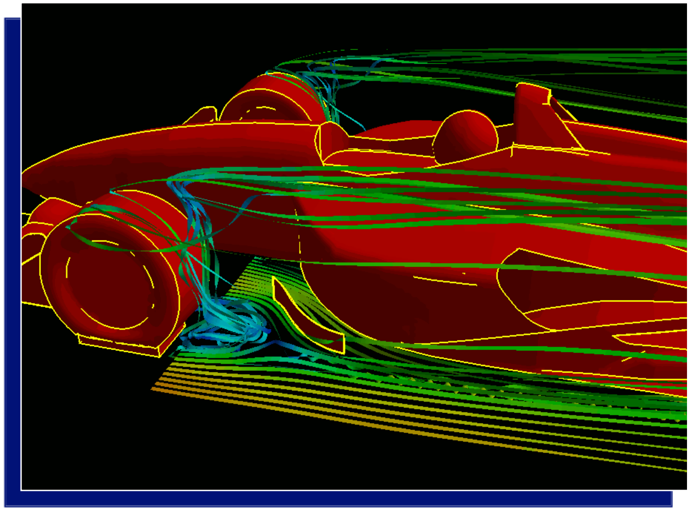

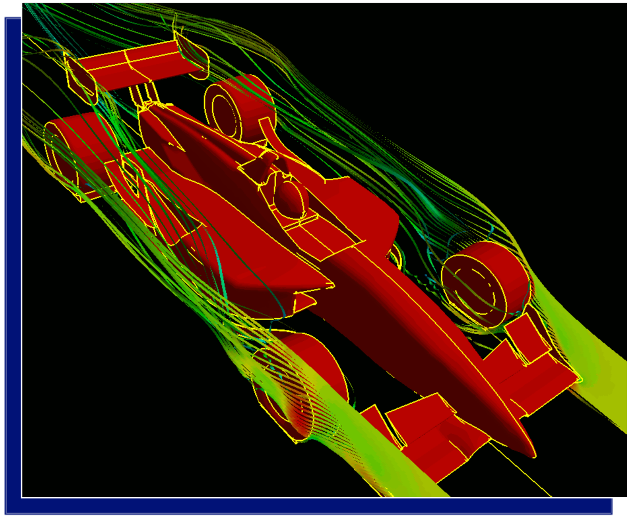

- Katz, J., Luo, H., Mestreau, E.L., Baum, J.D., and Löhner, R., Viscous Flow Simulation of an Open-Wheel Race Car; *SAE Publication* 983041, 1998.

Test case 4. Reactive Turbulent flow in REST Scramjet Inlet

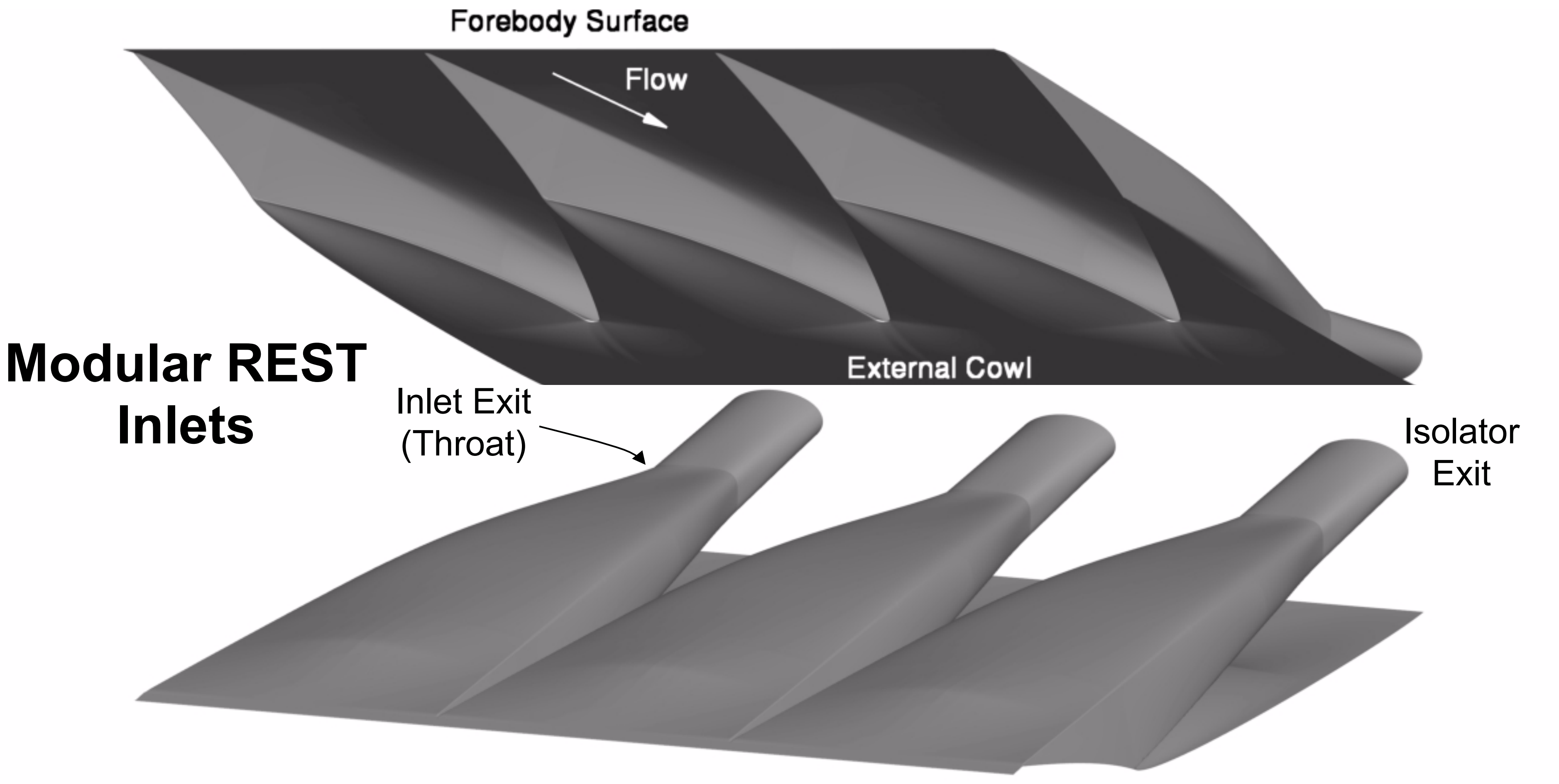

Spiegel, S., Stefanski, D., Edwards, J., and D., Luo, H., Regionally Structured/Unstructured Finite Volume Method for Chemically Reacting Flows, AIAA-2011-3048. 2011.

Test case 4. Reactive Turbulent flow in REST Scramjet Inlet

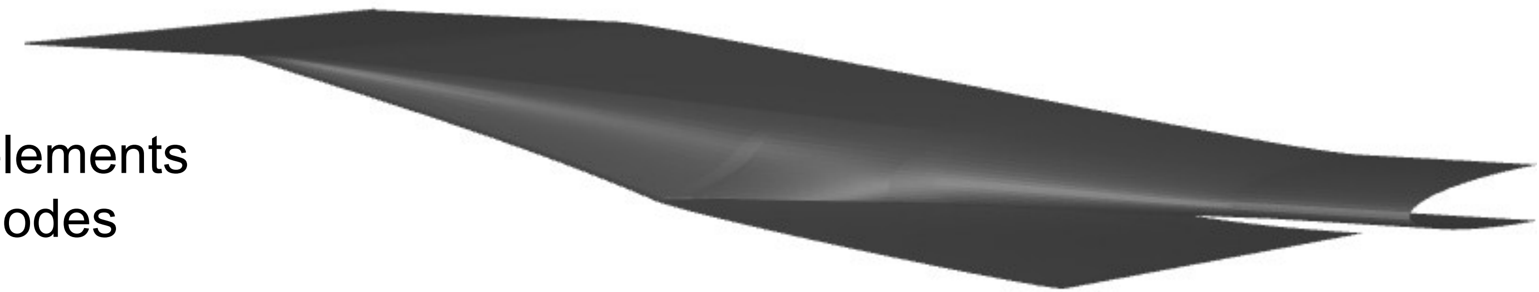

Grid

~ 4.1 million elements

~ 4.2 million nodes

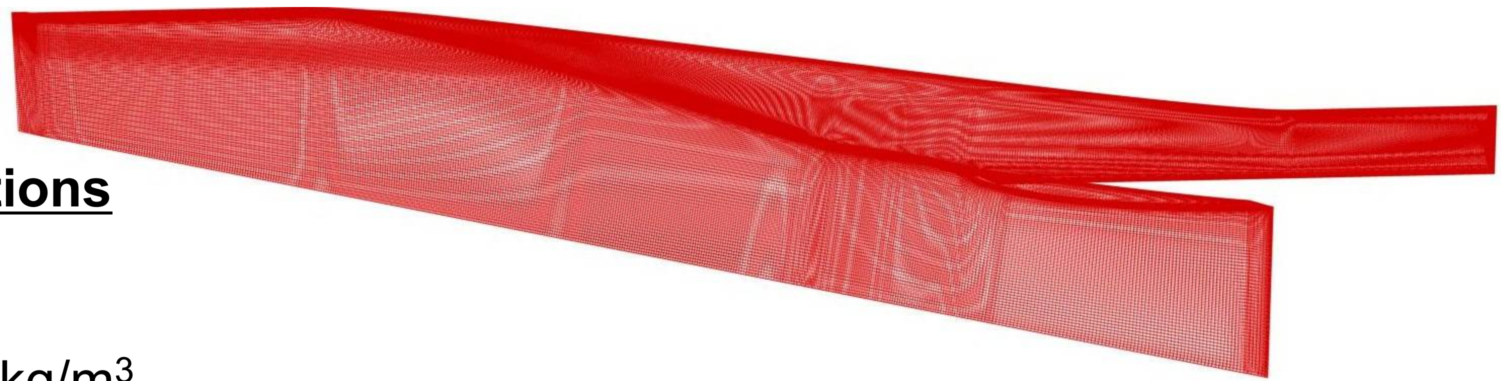

Inflow conditions

M = 6.64

T = 319.3 K

ρ = 0.003395 kg/m^3

P = 3.111 kPa

R_e = 4.17 million

Inlet geometry and mesh

Test case 4. Reactive Turbulent flow in REST Scramjet Inlet

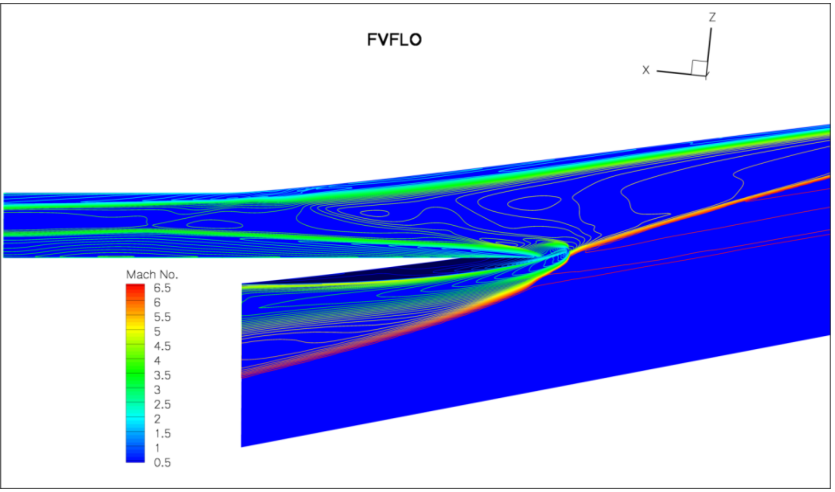

FVFLO

Top:
Mach no.

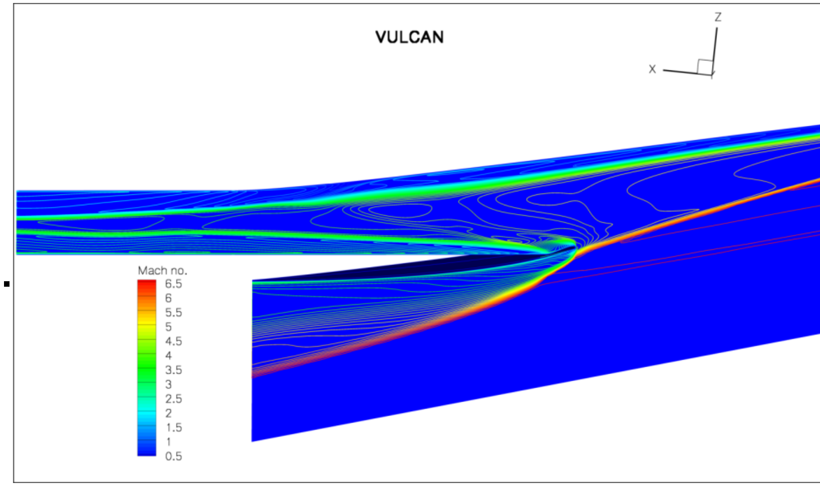

VULCAN

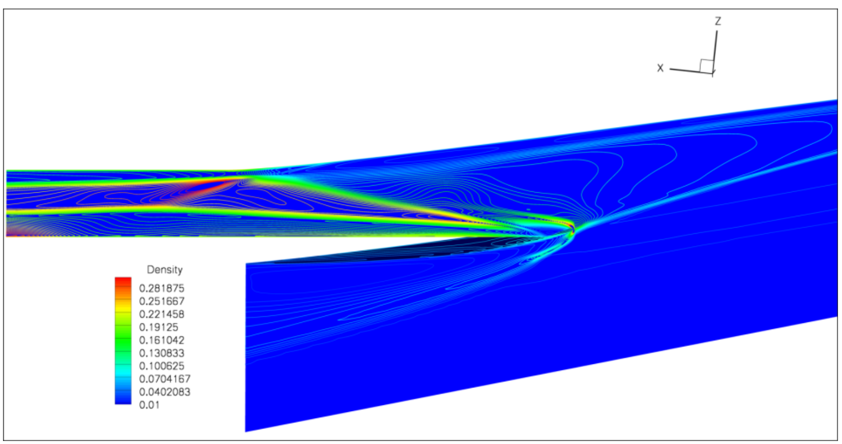

Bottom:
density

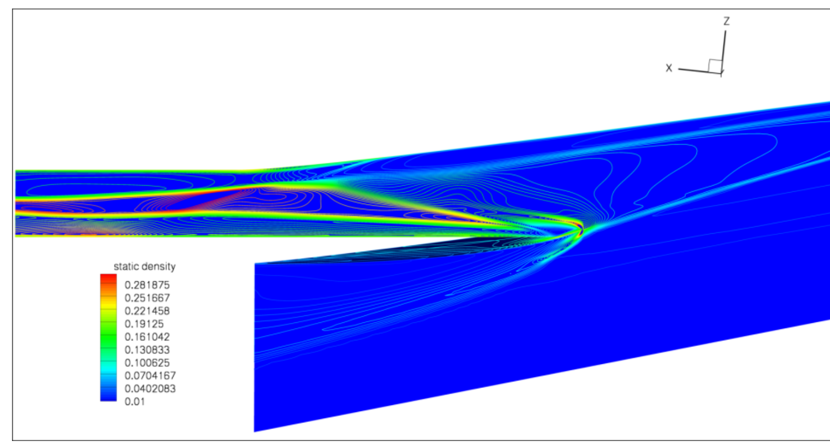

Test case 4. Reactive Turbulent flow in REST Scramjet Inlet

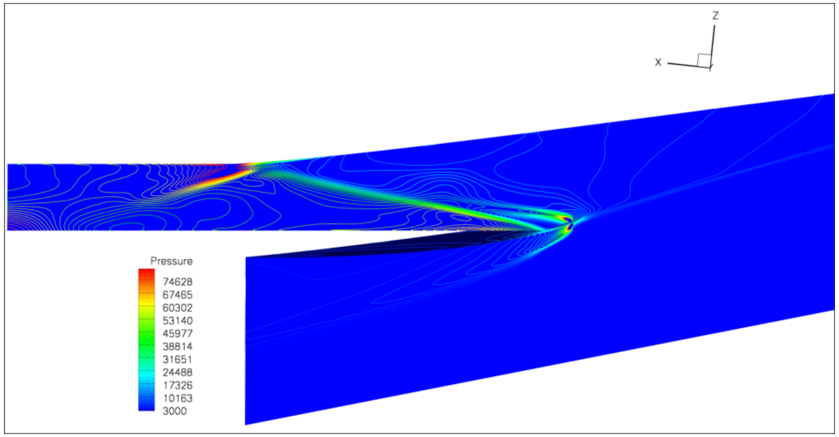

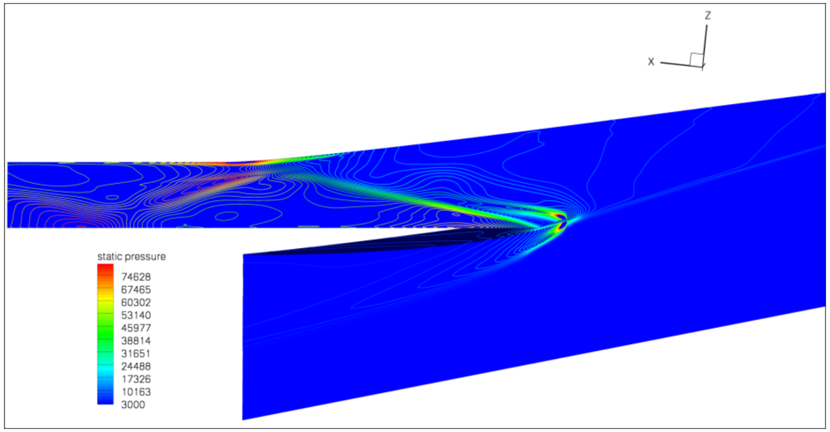

Top: Pressure

FVFLO

VULCAN

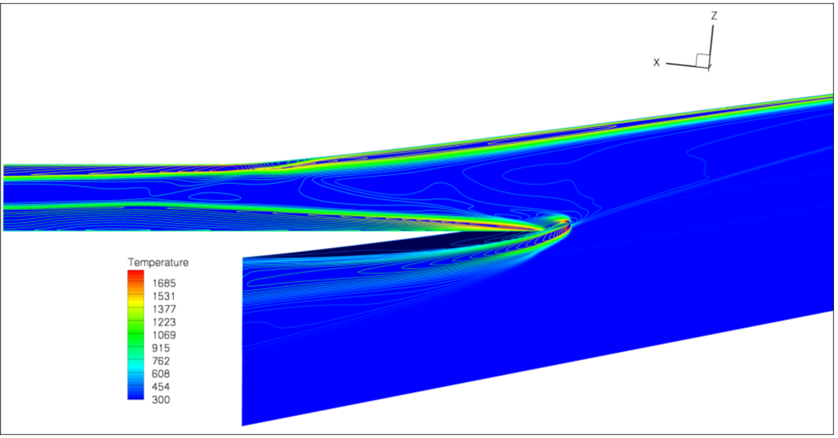

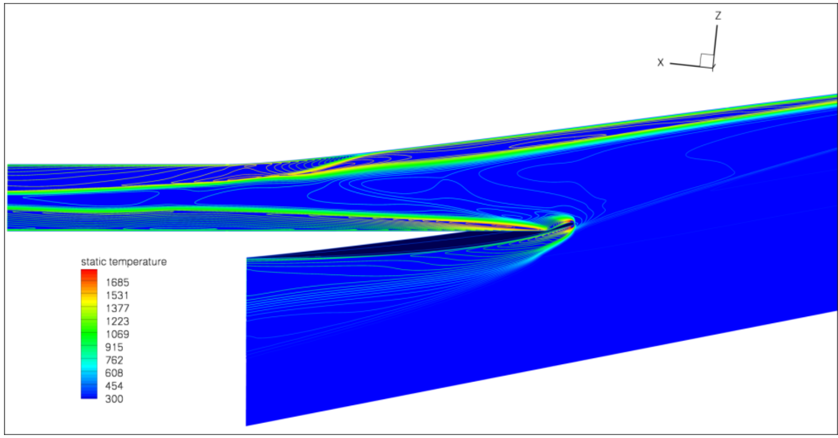

Bottom: Temp.

Blast and shock wave Applications

- Assess platform vulnerability and survivability
- Determine weapon lethality

Example 1. Blast in a Boeing 747

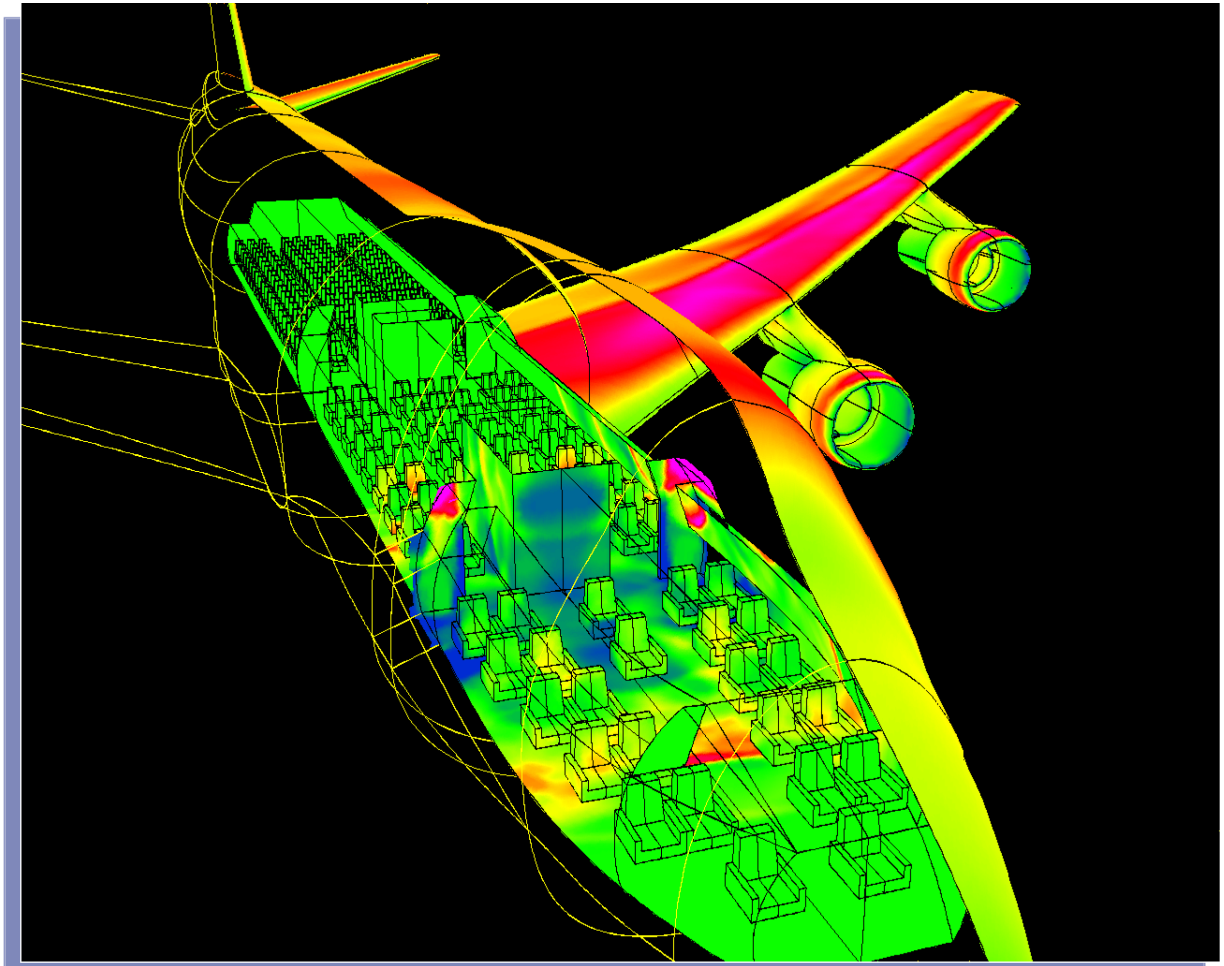

Baum, J. D., Luo, H., and Löhner, R., Numerical Simulation of a Blast inside a Boeing 747; AIAA-93-3091, 1993.

Example 2. Rear Blast Simulation for T62 Tank

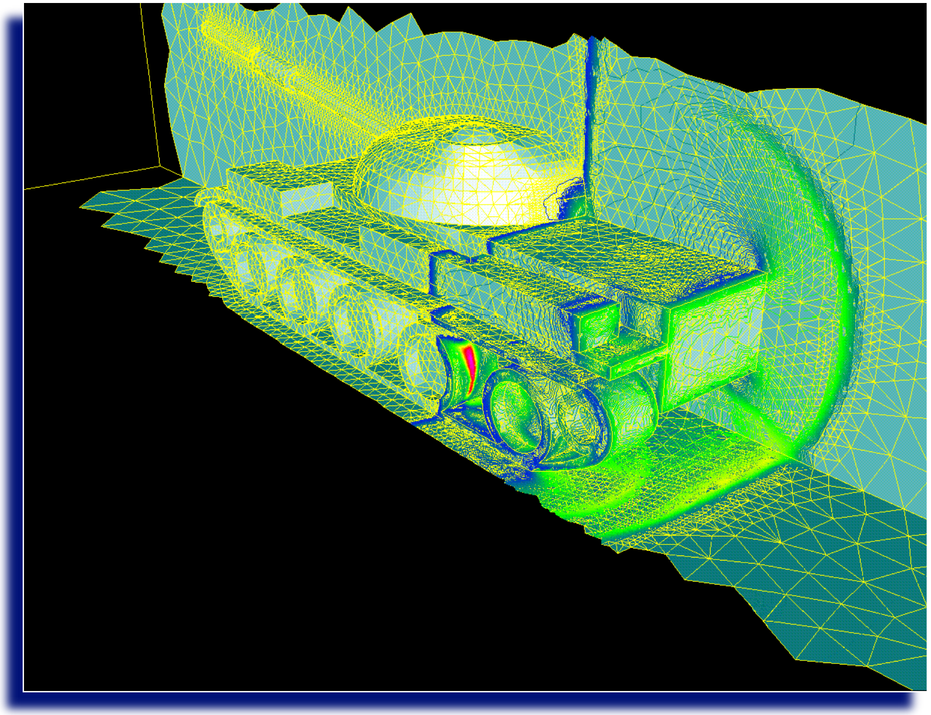

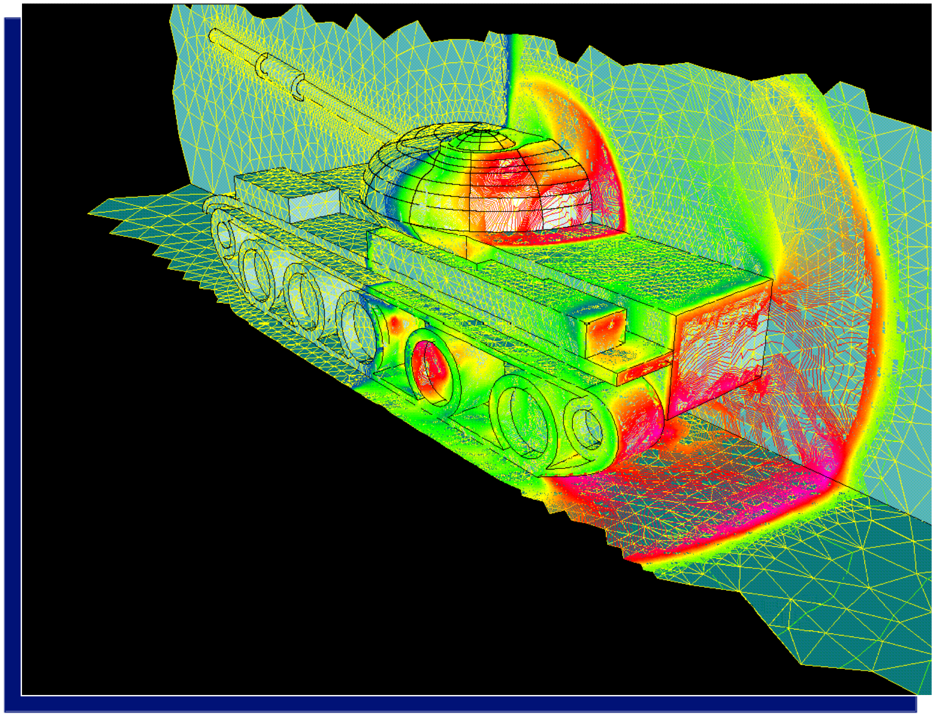

Example 3. World Trade Center Explosion (New York)

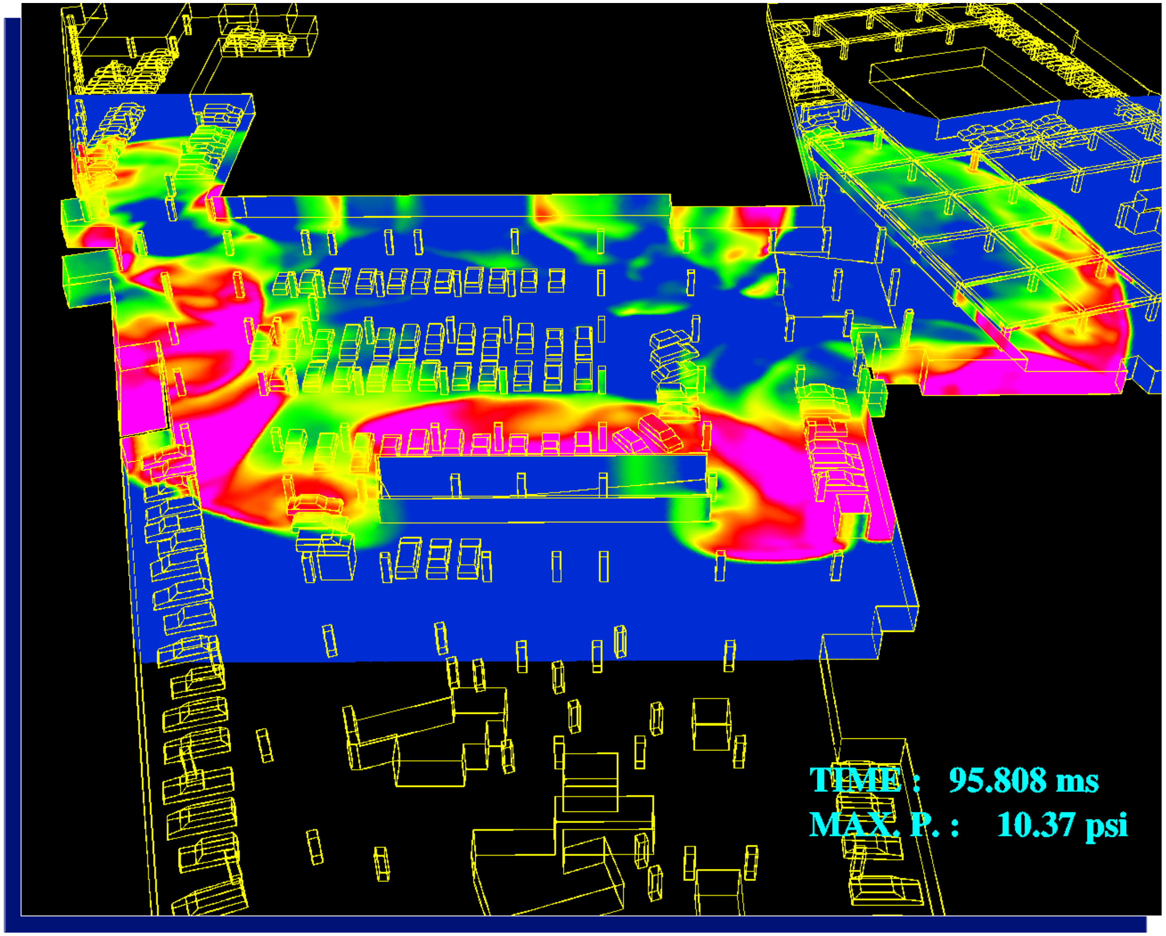

- Baum, J.D., Luo, H., and Löhner, R., Numerical Simulation of Blast in the World Trade Center; AIAA-95-0085, 1995

Example 4. Kenya Terrorist Attack

Example 4. Kenya Terrorist Attack (Blast Initialization)

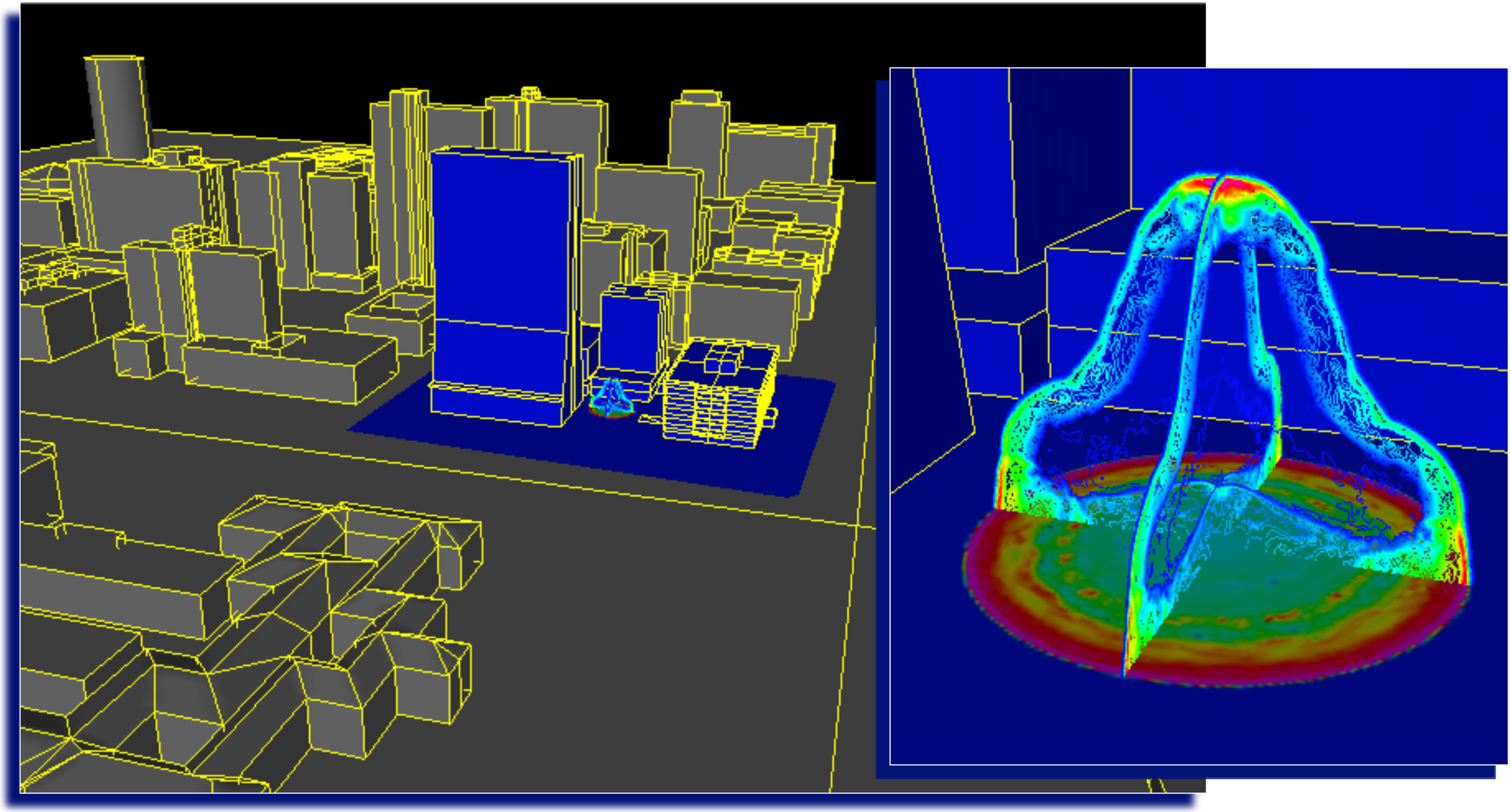

Example 4. Kenya Terrorist Attack
Pressure Field at Time=(2,2,172,512)ms

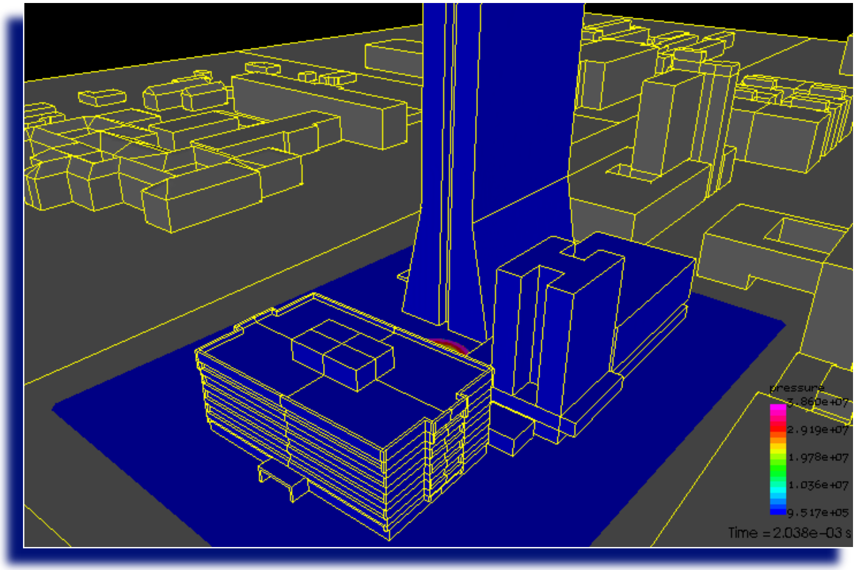

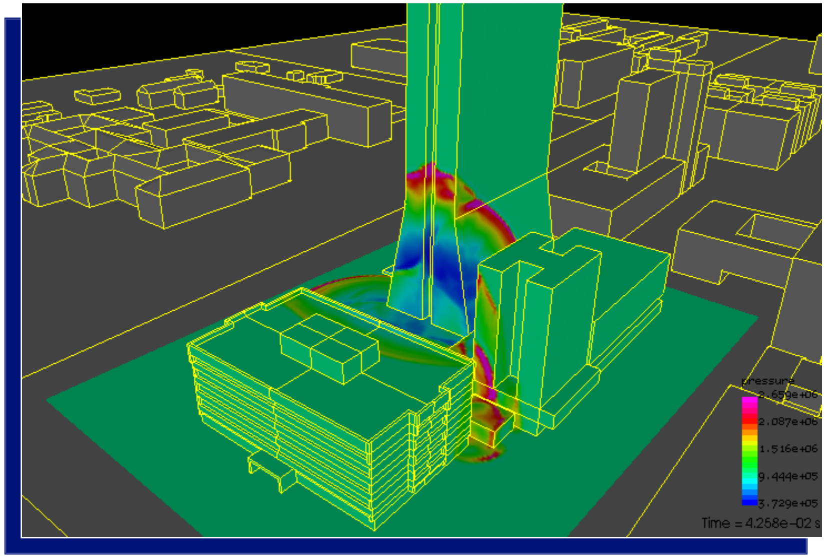

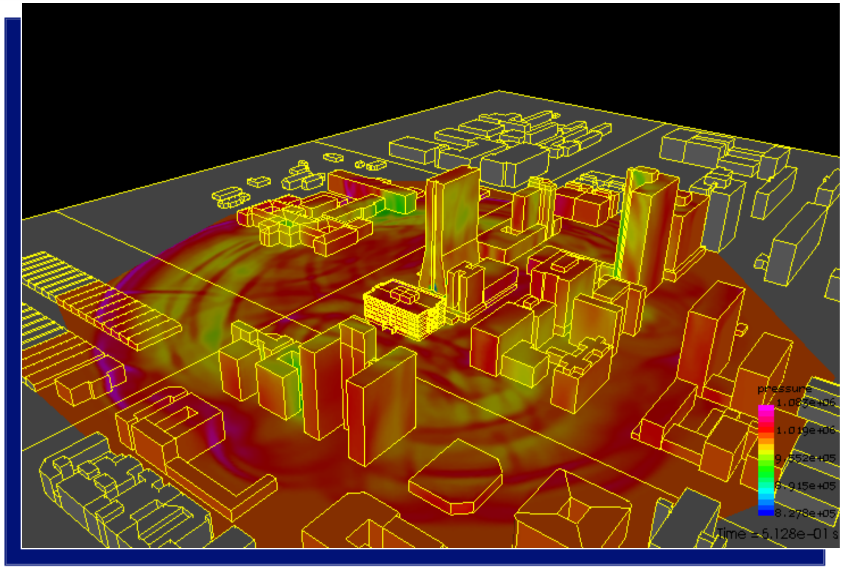

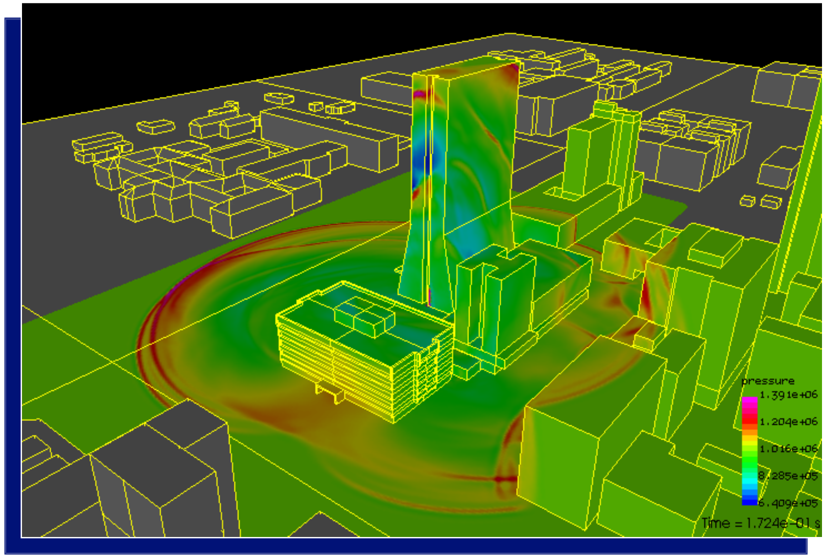

Example 4. Kenya Terrorist Attack (Adaptive mesh simulation)

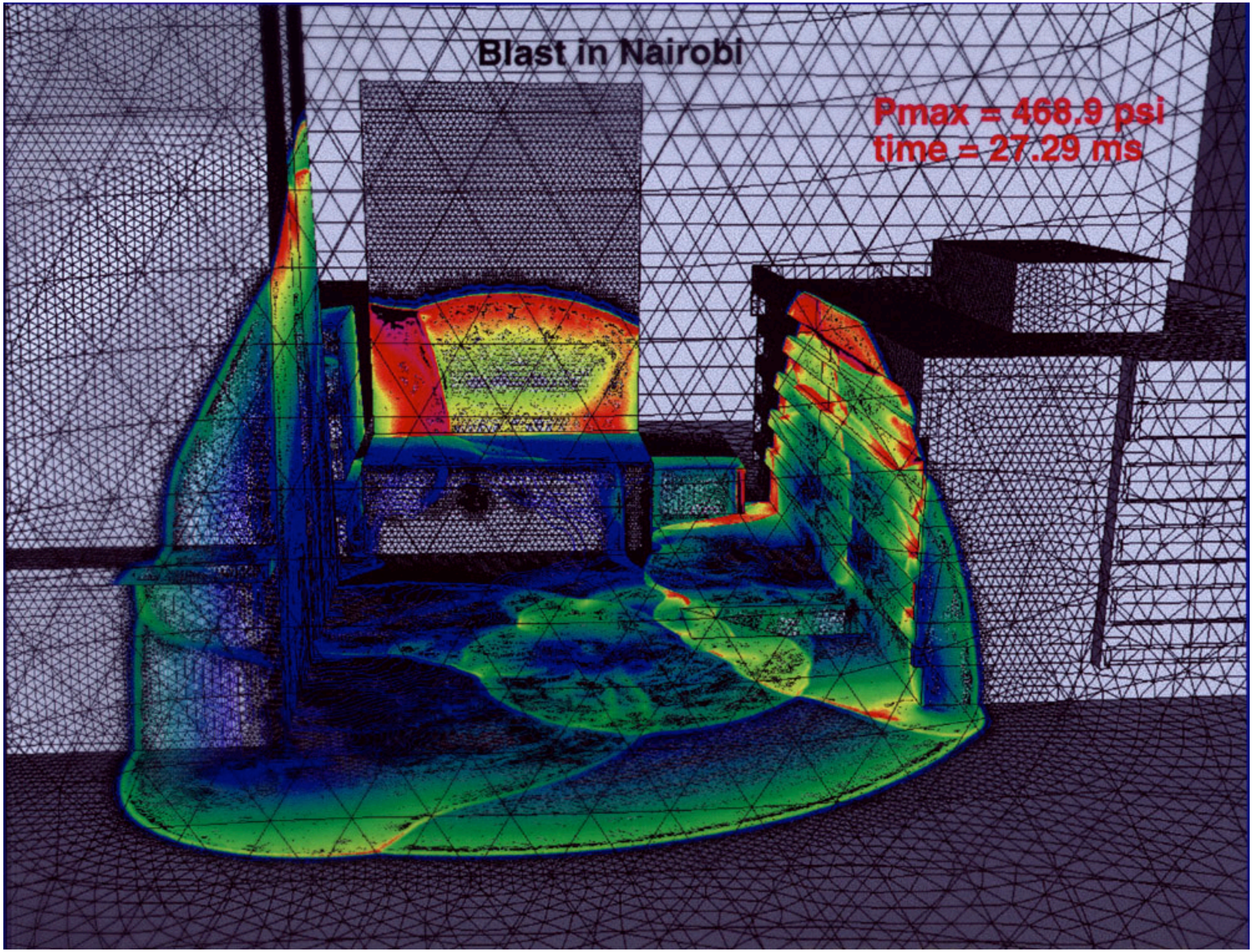

Moving Bodies Applications

F117 Store Separation

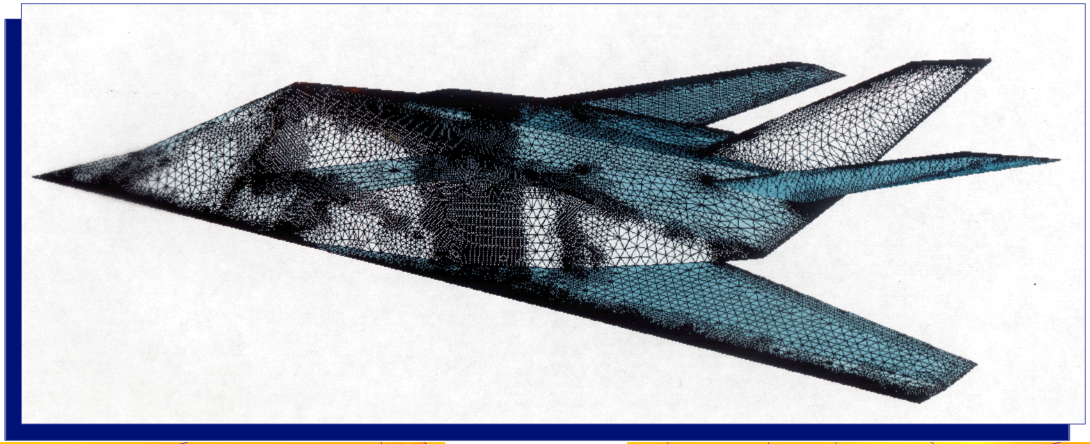

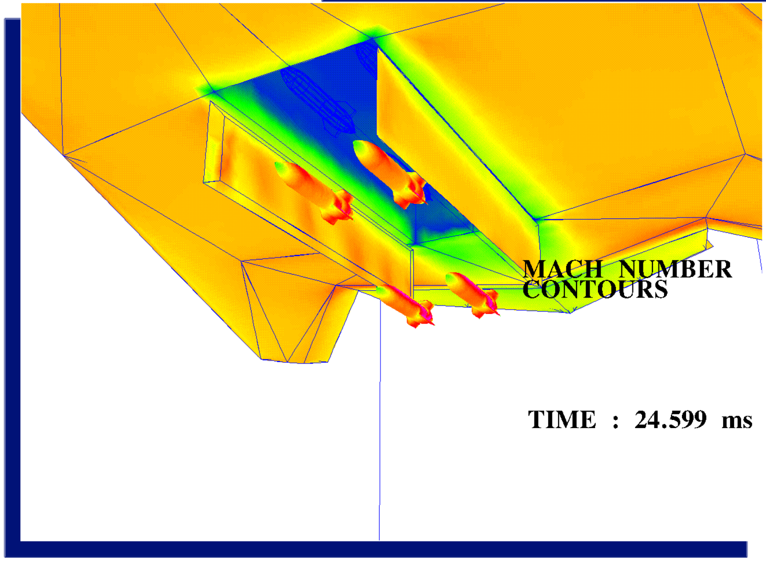

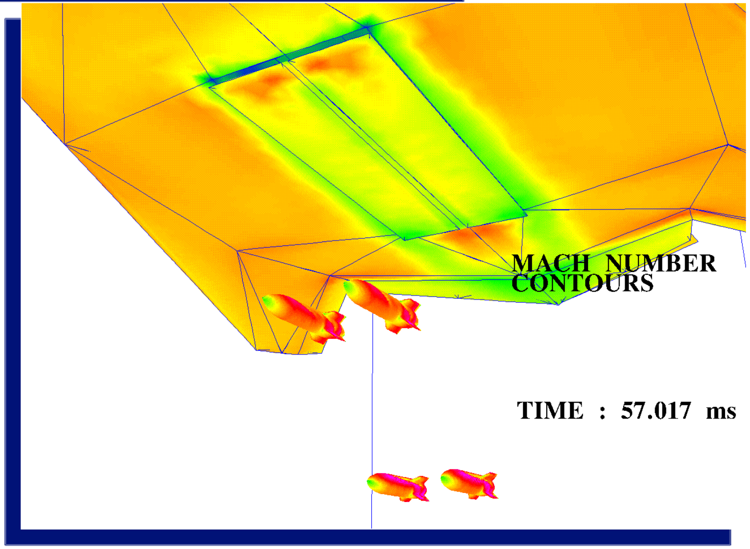

Baum, J.D., Luo, H., and Löhner, R., Validation of a New ALE Adaptive Unstructured Moving Body Methodology for Multi-Store Ejection; AIAA-95-1792, 1995.

F16 Fuel Tank Separation

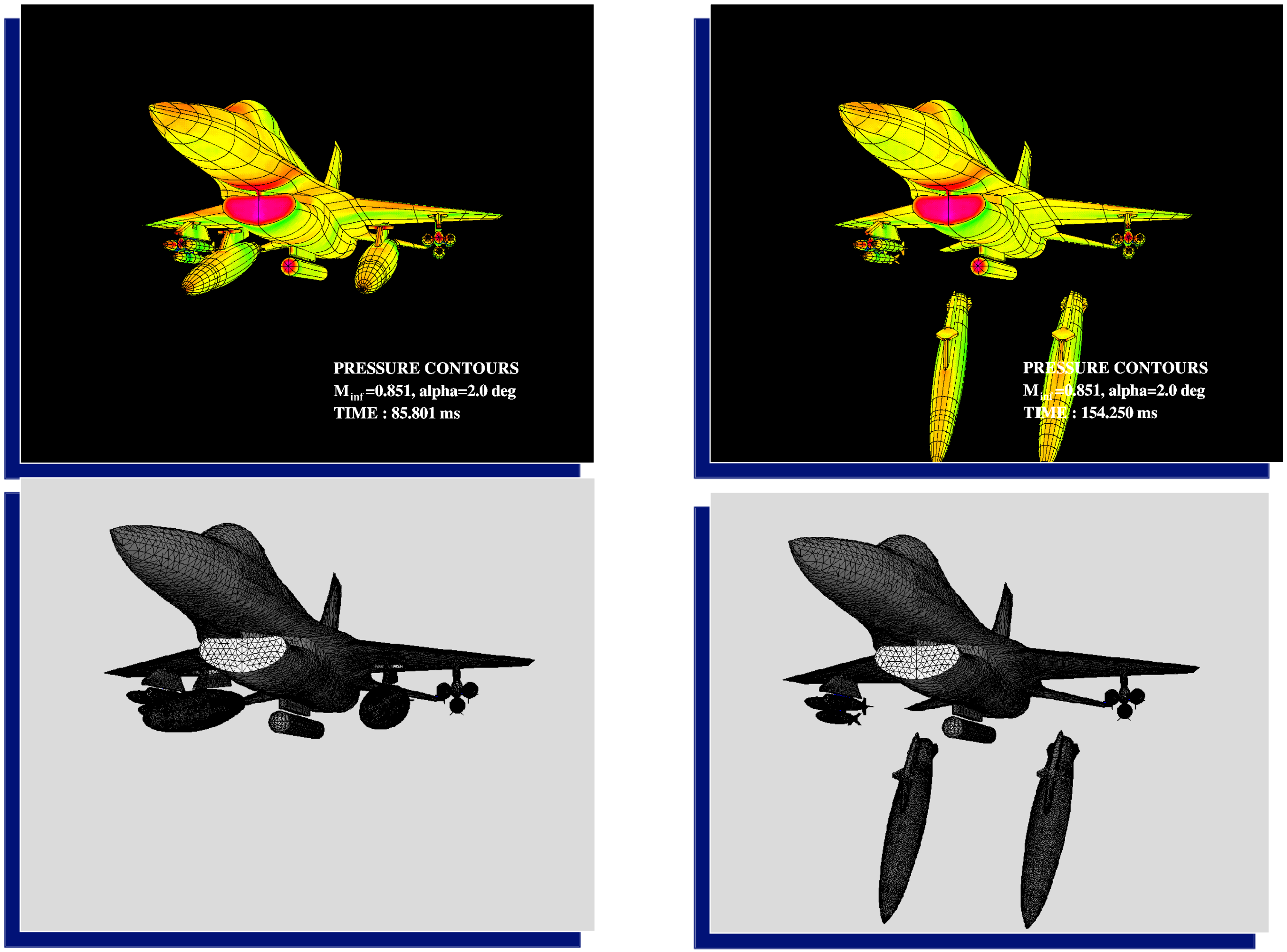

Baum, J.D., Luo, H., Löhner, R., Goldberg, E., and Feldhun, A., Application of Unstructured Adaptive Moving Body Methodology to the Simulation of Fuel Tank Separation From an F-16 C/D Fighter; AIAA-97-0166, 1997.

Canopy+2 Pilots Ejection

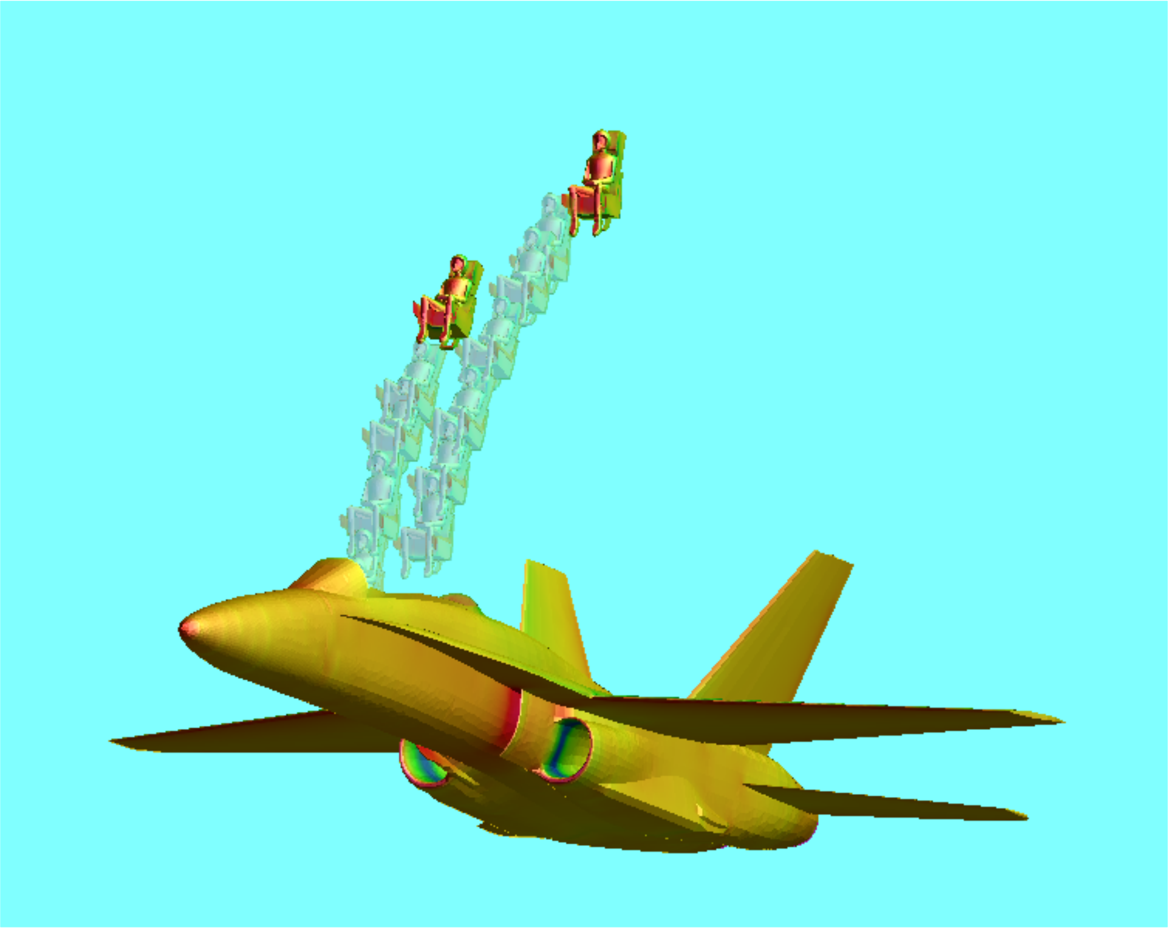

Baum, J.D., Löhner, R., Marquette, T. J., and Luo, H., Numerical Simulation of Aircraft Canopy Trajectory; AIAA-97-1885, 1997.

Fluid/Structure Interaction

Example 1. Truck and Blast Wave Interaction

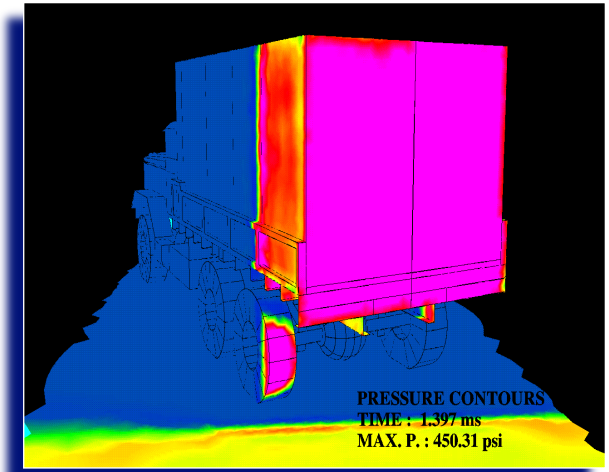

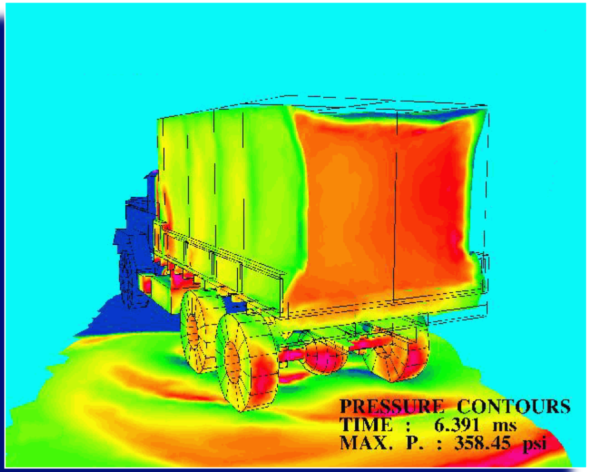

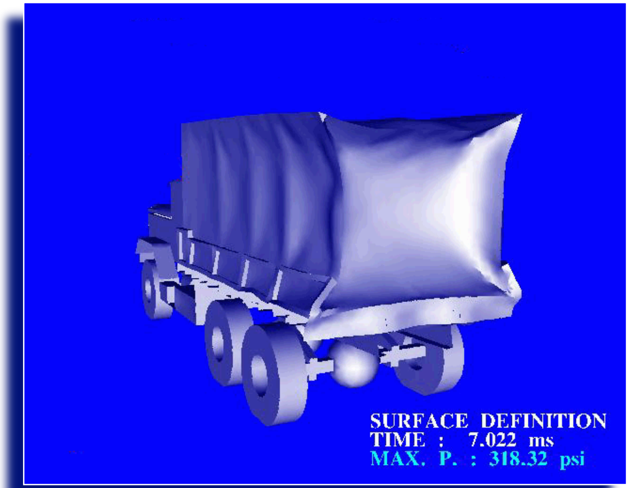

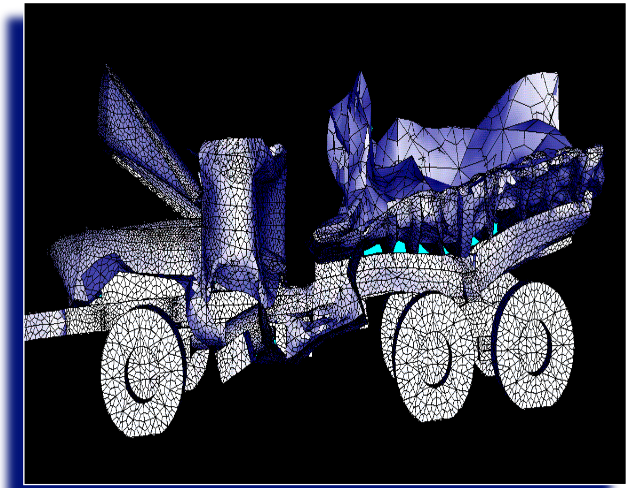

Baum, J.D., Luo, H., Löhner, R., Yang, C., Pelessone, D., and Charman, C., A Coupled Fluid-Structure Modeling of Shock Interaction with a Truck; AIAA-96-0796, 1996.

Example 2. Bomb Fragmentation CFD & CSD Meshes @ t=0.0 ms

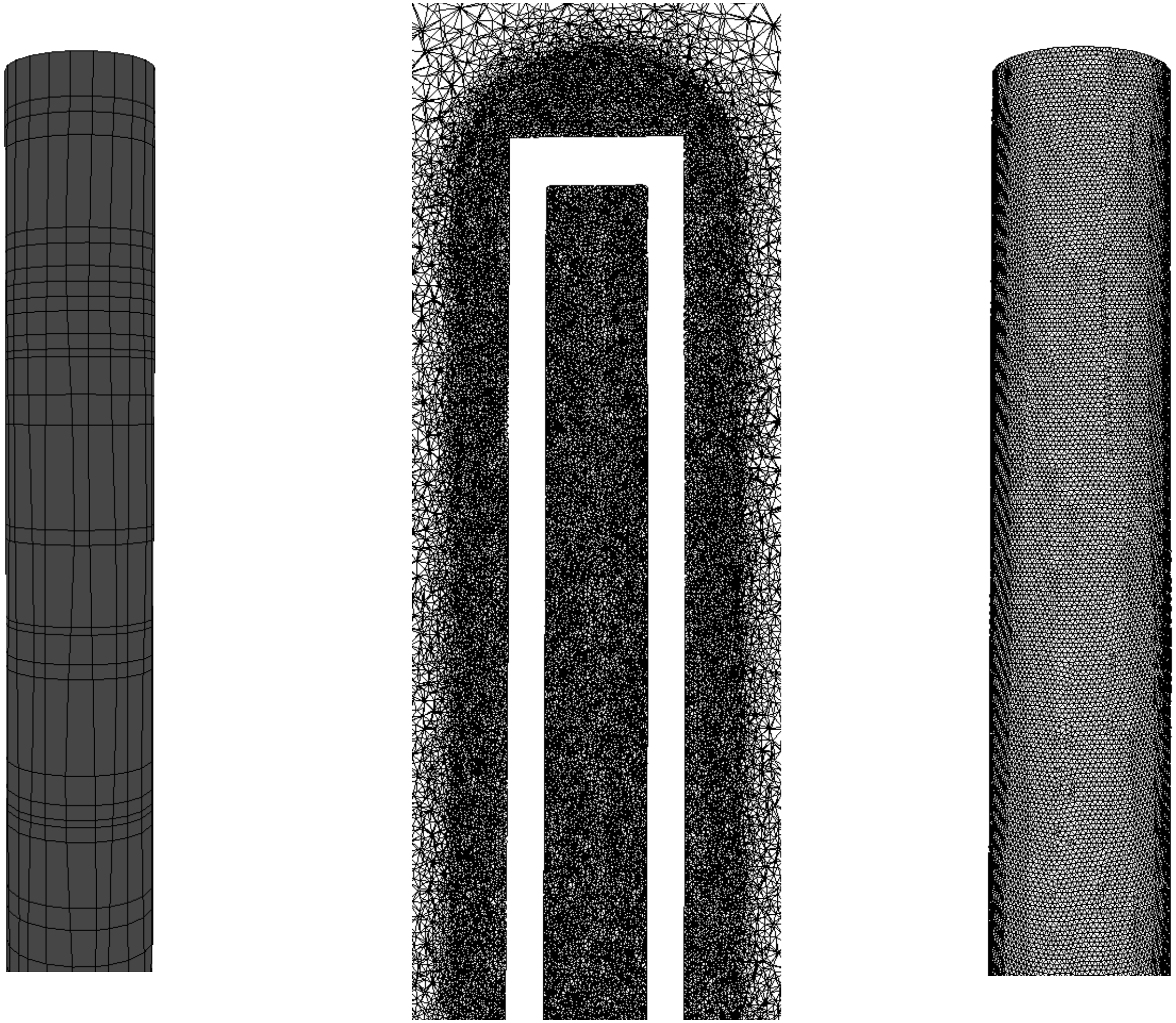

R. Löhner, R., Yang, C., Baum, J.D., Luo, H., Pelessone, D. and Charman, C. - The Numerical Simulation of Strongly Unsteady Flow with Hundreds of Moving Bodies; **International Journal for Numerical Methods in Fluids**, Vol. 31, pp. 113-120, 1999.

Example 2. Bomb Fragmentation CFD & CSD Meshes @ t=0.250 ms

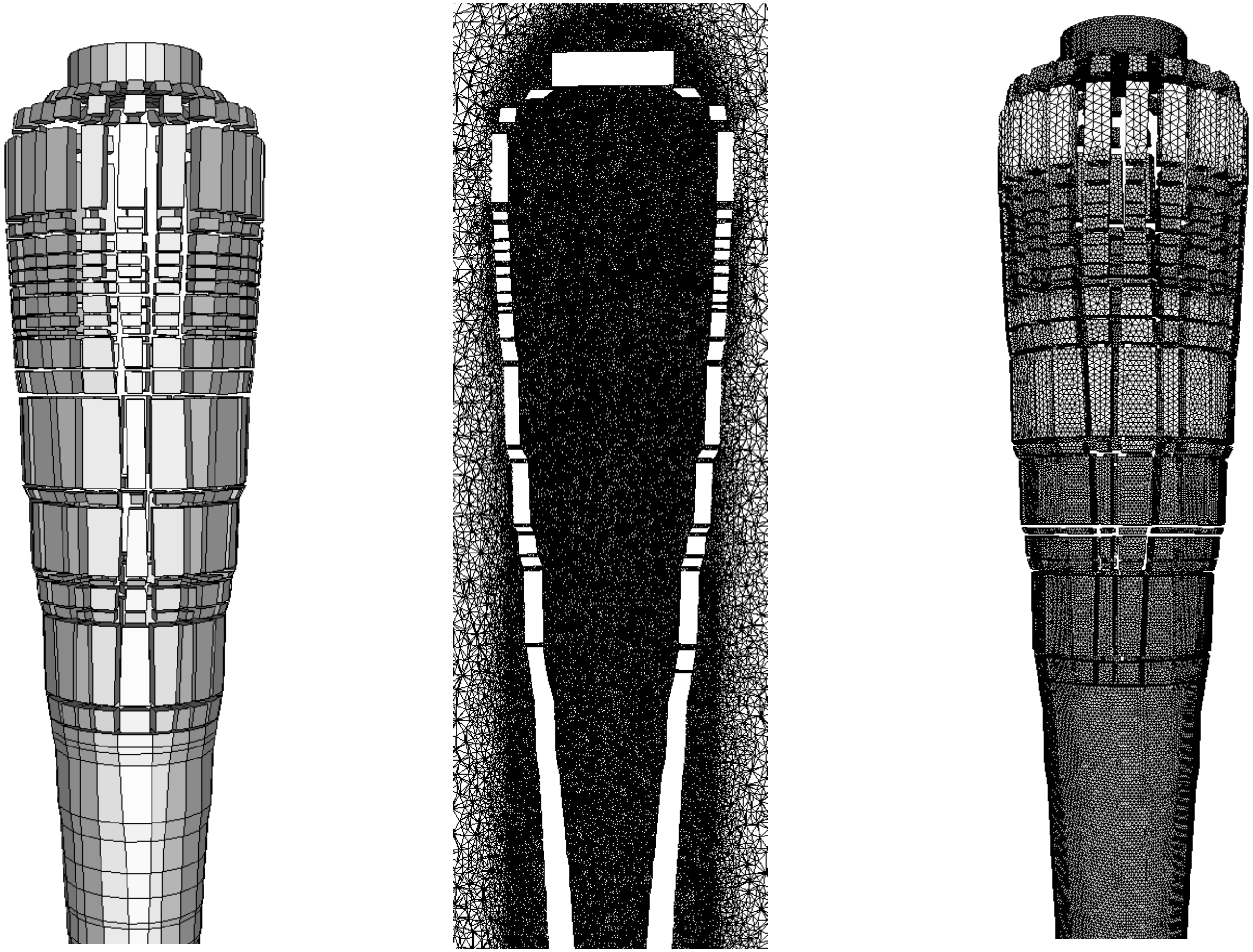

Example 2. Bomb Fragmentation
CFD & CSD Meshes @ t=0.550 ms

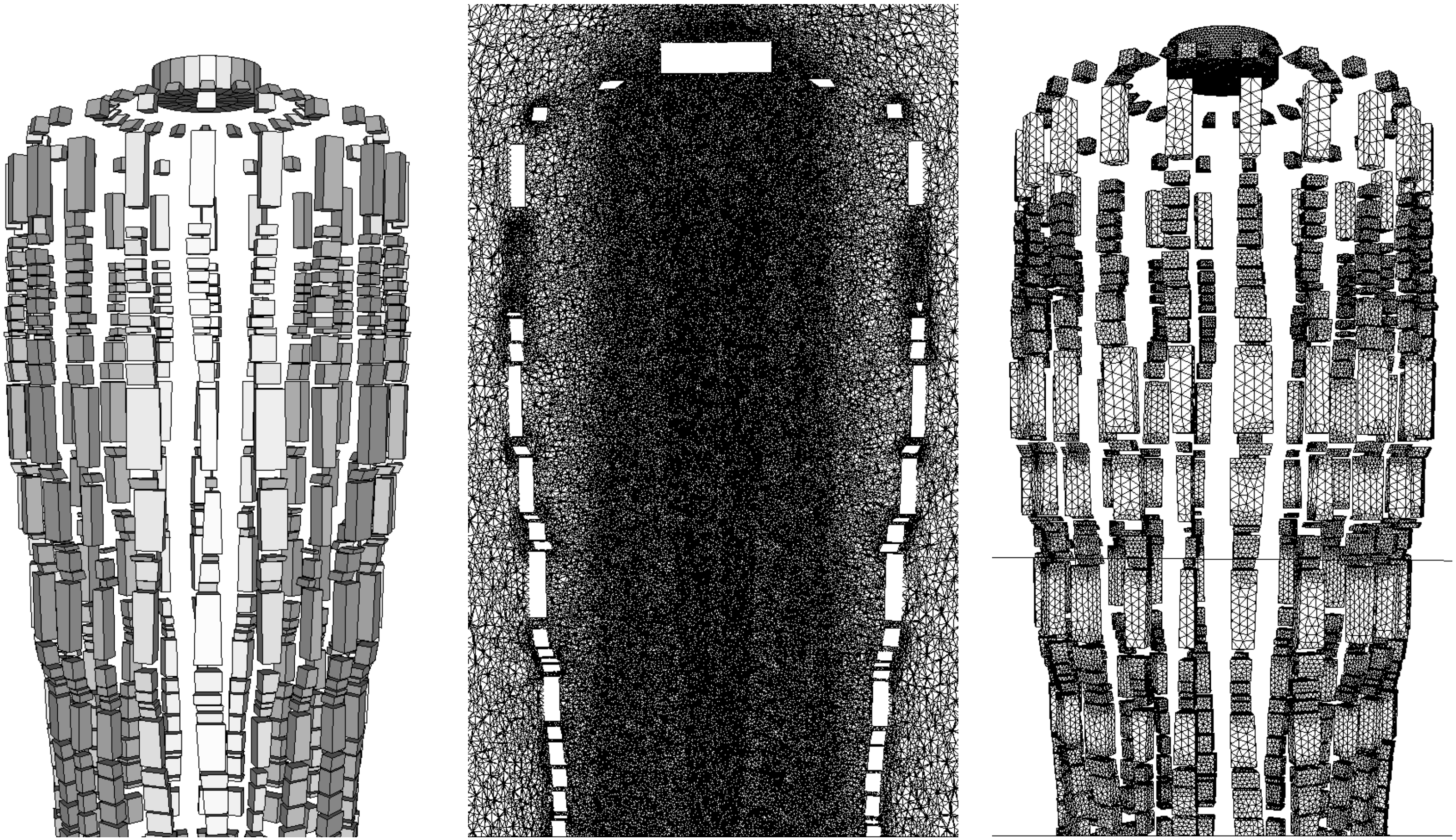

Example 2. Bomb Fragmentation
CFD & CSD Results @ t=0.101 ms

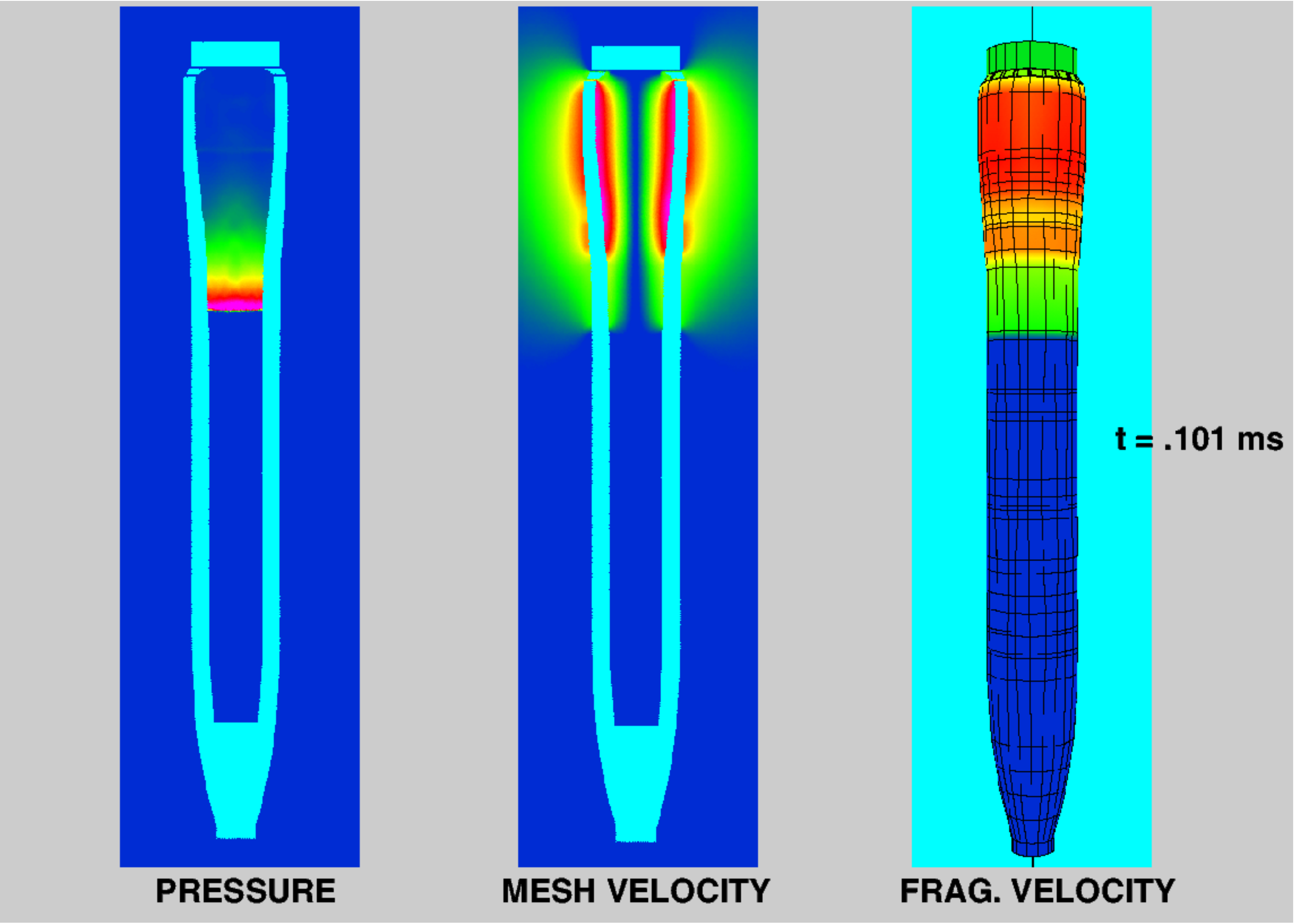

Example 2. Bomb Fragmentation
CFD & CSD Results @ t=0.250 ms

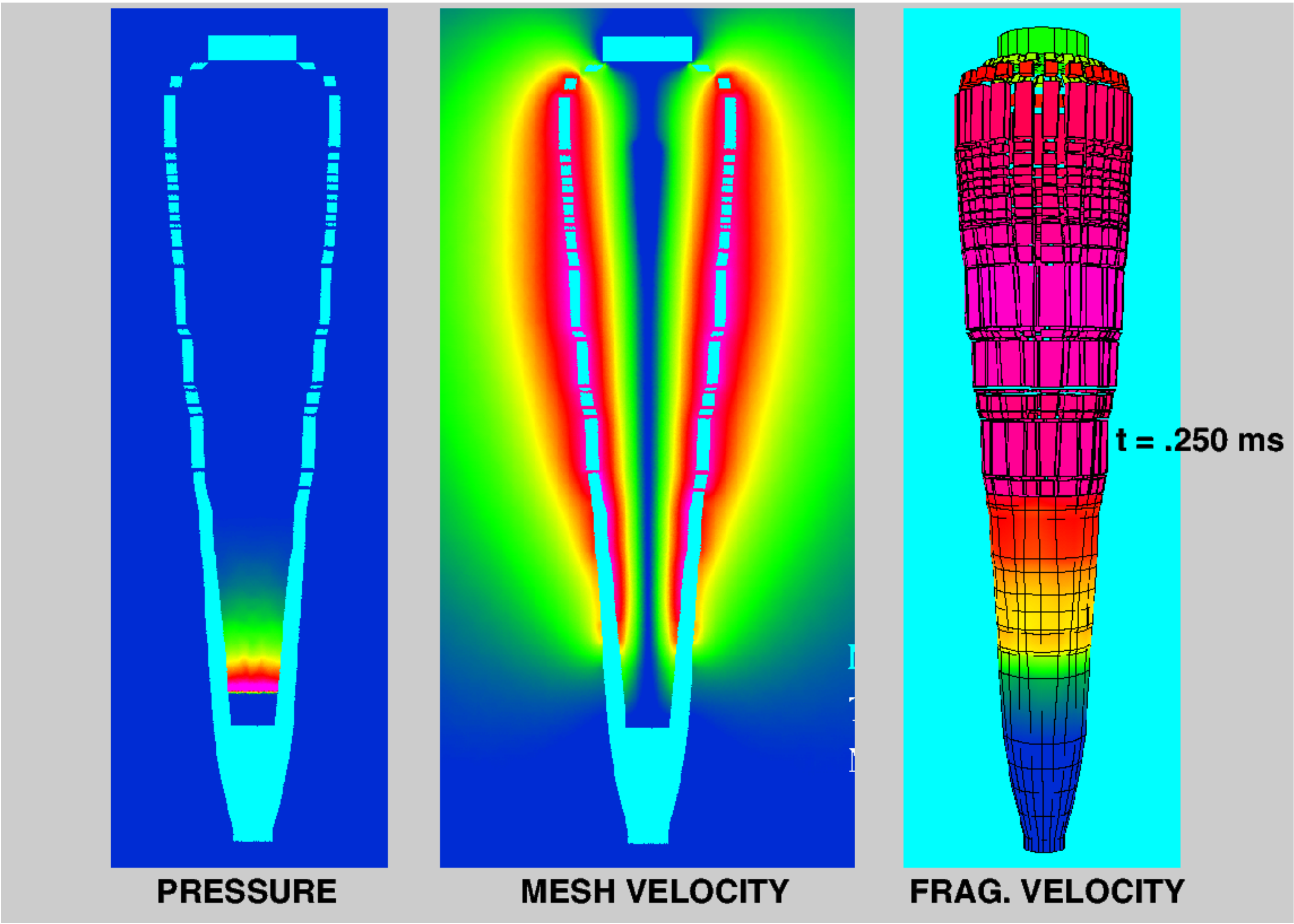

Example 2. Bomb Fragmentation CFD & CSD Results @ t=0.420 ms

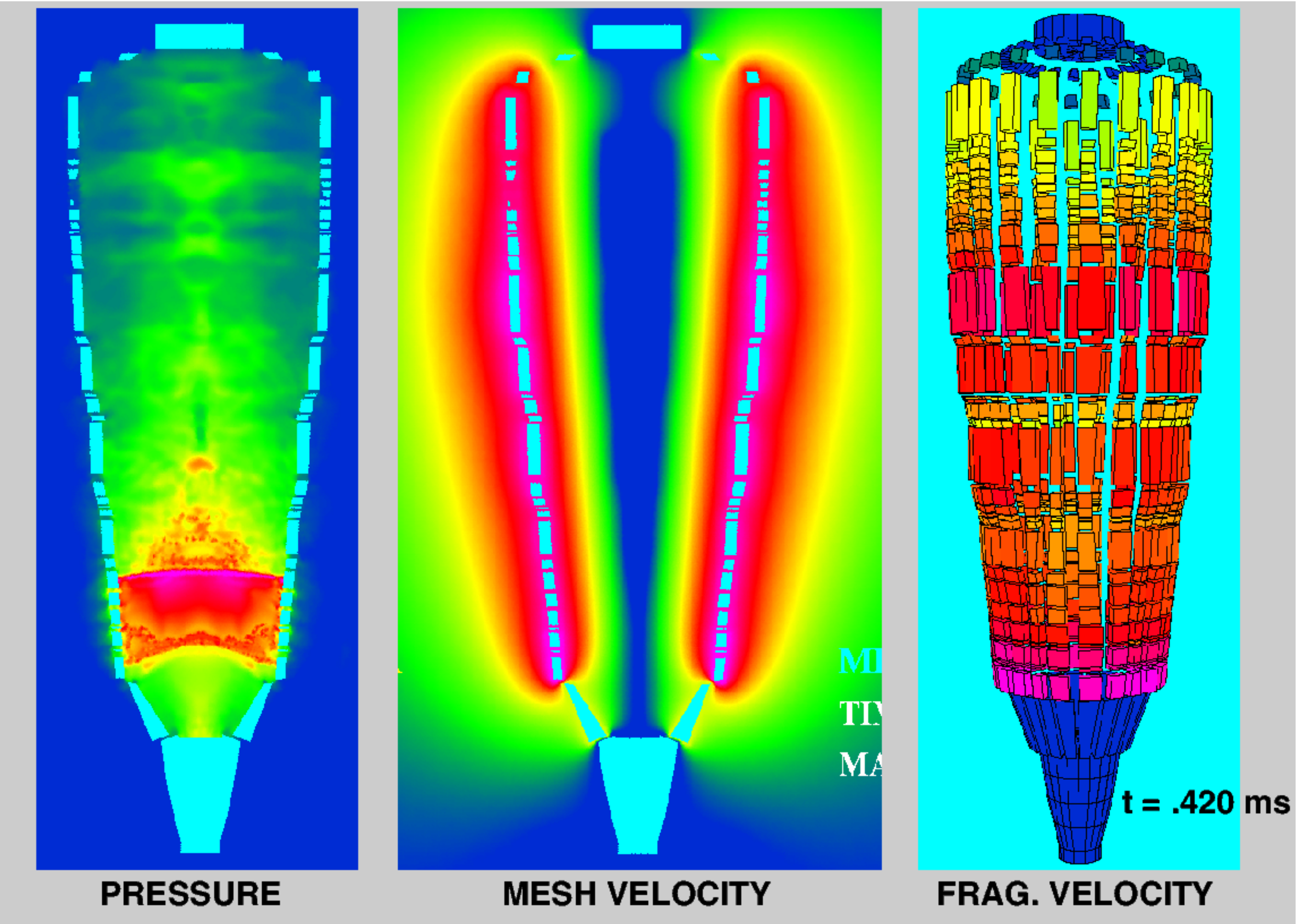

Challenges

- The second-order CFD methods simply can not deliver engineering-required accuracy in time for a variety of applications.
  - Large Eddy Simulation (LES)
  - Blade-Vortex Interaction (BVI)
- Turn-around time in minutes and at most in hours on a moderate computer cluster is necessary for engineering applications.
- The second-order CFD methods cannot provide Uncertainty Quantification (UQ) for a requested simulation.

Example 1: Large Eddy Simulation

- For flow problems with large regions of massive separation, there is a growing consensus that large eddy simulation techniques may offer the best hope for improving turbulence modelling.

- LES models are only reliable, when the numerical dissipation is low.

- Requirement ➔ Higher-order Methods

Example 2: Blade and Vortex Interaction

- Several revolutions of vortex are required to study BVI.
- The second order methods can barely keep any revolutions of vortex → making the computation meaningless.
- Requirement ➔ Higher-order Methods

Trend: Higher-order Methods

- One of intensive research efforts in the CFD is the development of higher-order (>2nd) methods for applications of scientific and engineering problems.

- Significant improvements in both accuracy and efficiency can be achieved by replacing second-order methods with higher-order (>2nd) methods for CFD applications.

  - ENO and WENO Methods
  - Compact Finite Difference Methods
  - Spectral Volume Methods
  - Discontinuous Galerkin Methods

Background

- Why DG ?
  - Several useful mathematical properties with respect to conservation, stability, and convergence.
  - Easy extension to higher-order (>2nd) schemes.
  - Well suited for complex geometries.
  - Easy adaptive strategies, allowing implementation of *hp*-refinement and hanging nodes.
  - Compact and highly parallelizable.
  - Accuracy for low Mach number flows.

Background

- Why not DG ?

  - High computing costs (more degrees of freedom)
    → CPU time
    → Storage requirements
  - Treatment of discontinuities (like all other high-order methods)
    → Sensitive to the implementation of limiters
    → Lead to loss of high-order accuracy
  - Requirement of higher-order boundary representation
    → Geometric modelling capability
    → Curved boundary elements
  - Efficient discretization of diffusion terms

Background

To reduce high computing costs of the DG methods, Reconstructed DG (RDG(P_nP_m)) schemes were introduced by Dumbser et al.

- P_n indicates that a piecewise polynomial of degree of n is used to represent a DG solution.
- P_m represents a reconstructed polynomial solution of degree of m ($m \geq n$) that is used to compute the fluxes and source terms.
- Provide a unified formulation for both finite volume and DG methods, and contain both classical finite volume and standard DG methods as two special cases of RDG(P_nP_m) schemes.

Background

Classification of the RDG(PnPm) Schemes

Order of Accuracy	Schemes			
O(1)	RDG(P_0P_0) (DG(P_0))			
O(2)	RDG(P_0P_1)	RDG(P_1P_1) (DG(P_1))		
O(3)	RDG(P_0P_2)	RDG(P_1P_2)	RDG(P_2P_2)	
O(4)	RDG(P_0P_3)	RDG(P_1P_3)	RDG(P_2P_3)	RDG(P_3P_3)
	:			
O(M+1)	RDG(P_0P_m) … FV	RDG(P_nP_m) New Class	…	RDG(P_mP_m) DG

Background

- A RDG method based on a hierarchical WENO reconstruction: HWENO(P_1P_2), has been developed for compressible flows with strong discontinuities on hybrid grids.
    - enhance the accuracy, and therefore reduce the high computational costs of the underlying DG methods
    - avoid the spurious oscillations in the vicinity of strong discontinuities, and therefore maintain the non-linear stability, and naturally linear stability.
- Effectively address the two weakest links of the DG methods !!!

Governing Equations

Compressible Navier-Stokes Equations

$$\frac{\partial \mathbf{U}(x,t)}{\partial t} + \frac{\partial \mathbf{F}_k(\mathbf{U}(x,t))}{\partial x_k} = \frac{\partial \mathbf{G}_k(\mathbf{U}(x,t))}{\partial x_k}$$

F: inviscid flux vector
G: viscous flux vector
U: conservative variable state vector

DG(P_n) Method

$$\frac{d}{dt}\int_{\Omega_e}\mathbf{U}_h B_i d\Omega + \int_{\Gamma_e}\mathbf{F}_k(\mathbf{U}_h)\mathbf{n}_k B_i d\Gamma - \int_{\Omega_e}\mathbf{F}_k(\mathbf{U}_h)\frac{\partial B_i}{\partial x_k}d\Omega = \int_{\Gamma_e}\mathbf{G}_k(\mathbf{U}_h)\mathbf{n}_k B_i d\Gamma - \int_{\Omega_e}\mathbf{G}_k(\mathbf{U}_h)\frac{\partial B_i}{\partial x_k}d\Omega, \quad 1 \le i \le \mathrm{N}$$

B_i(x): basis functions of the polynomials of degree Pn, $1 \le i \le$N.

N: dimension of the polynomial space Pn.

↑

Discontinuous Galerkin method of degree Pn (DG(Pn)) : O(h^{n+1})

$\mathbf{F}_k(\mathbf{U}_h)\mathbf{n}_k = \mathbf{H}_\mathrm{k}(\mathbf{U}^L{}_h, \mathbf{U}^R{}_h, \mathbf{n}_k)$ ← Numerical Riemann flux function

$$\mathbf{G}_k(\mathbf{U}_h, \frac{\partial \mathbf{U}_h}{\partial x_i})\mathbf{n}_k = \mathbf{H}_\mathrm{v}(\mathbf{U}_h^L, \mathbf{U}_h^R, \frac{\partial \mathbf{U}_h^L}{\partial x_i}, \frac{\partial \mathbf{U}_h^R}{\partial x_i}, \mathbf{n})$$

The computation of the viscous fluxes has to properly resolve the discontinuities at the interfaces.

Reconstructed Discontinuous Galerkine Method: RDG(PnPm)

$$\frac{d}{dt}\int_{\Omega_e} \mathbf{U}_{\mathrm{P_n}} B_i d\Omega + \int_{\Gamma_e} \mathbf{F}_k(\mathbf{U}^{\mathrm{R}}_{\mathrm{P_m}})\mathbf{n}_k B_i d\Gamma - \int_{\Omega_e} \mathbf{F}_k(\mathbf{U}^{\mathrm{R}}_{\mathrm{P_m}})\frac{\partial B_i}{\partial x_k} d\Omega = \int_{\Gamma_e} \mathbf{G}_k(\mathbf{U}^{\mathrm{R}}_{\mathrm{P_m}})\mathbf{n}_k B_i d\Gamma - \int_{\Omega_e} \mathbf{G}_k(\mathbf{U}^{\mathrm{R}}_{\mathrm{P_m}})\frac{\partial B_i}{\partial x_k} d\Omega, \quad 1 \le i \le N$$

$\mathbf{U}^{\mathrm{R}}_{\mathrm{P_m}}$: reconstructed polynomial solution of degree Pm

$B_i(\mathrm{x})$: basis functions of polynomials of degree Pn , $1 \le i \le \mathrm{N}$

N: dimension of the polynomial space $\mathrm{P_n}$

↑

Reconstructed Discontinuous Galerkin method RDG(PnPm) : $O(h^{m+1})$

HWENO reconstruction: HWENO(P_1P_2)

- A quadratic polynomial solution is obtained using a hierarchical WENO reconstruction by the following two steps:

  - Step 1: Reconstruct second derivatives by WENO : WENO(P_1P_2)
    - The second derivatives on each cell are first computed using underlying DG solution from its face-neighbouring cells using a 2-exact least-squares reconstruction.
    - The final second derivatives are obtained by WENO reconstruction using the least-squares reconstructed 2^{nd} order derivatives at the cell itself and its face-neighboring cells.

  - Step 2: Reconstruct first derivatives : HWENO(P_1P_2)
    - Reconstruct and modify the first derivatives of the resulting quadratic polynomial solution using WENO reconstruction.

References

- Luo, H., Xia Y., Spiegel, S., Nourgaliev, R., Jiang, Z., A Reconstructed Discontinuous Galerkin Method Based on a Hierarchical WENO Reconstruction for Compressible Flows on Tetrahedral Grids, **Journal of Computational Physics**, Vol. 236, pp. 477-492, 2013.
- Luo, H., Xia Y., Li. S., Nourgaliev, R., and Cai, C., A Hermite WENO Reconstruction-Based Discontinuous Galerkin Method for the Euler Equations on Tetrahedral Grids, **Journal of Computational Physics**, Vol. 231, pp. 5489-5503, 2012.
- Luo, H., Luo, L., and Nourgaliev, R., A Reconstructed Discontinuous Galerkin Method for the Euler Equations on Arbitrary Grids, **Communication in Computational Physics**, Vol. 12, No. 5, pp. 1495-1519, 2012.
- Luo, H., Luo, L., Ali, A., Nourgaliev, R., and Cai, C., A Parallel, Reconstructed Discontinuous Galerkin Method for the Compressible Flows on Arbitrary Grids, **Communication in Computational Physics**, Vol. 9, No. 2, pp. 363-389, 2011.
- Luo, H., Luo, L., Nourgaliev, R., Mousseau, V. A., and Dinh, N., A Reconstructed Discontinuous Galerkin Method for the Compressible Navier-Stokes Equations on Arbitrary Grids, **Journal of Computational Physics**, Vol. 229, pp. 6961-6978, 2010.

Cost Analysis (Tetrahedral Grids)

	RDG(P_0P_1)	RDG(P_1P_1)	RDG(P_1P_2)	RDG(P_2P_2)
Number of quadrature points for boundary integrals	1	3	4	7
Number of quadrature points for domain integrals	0	4	5	11
Reconstruction	Yes	No	Yes	No
Order of Accuracy	$O(h^2)$	$O(h^2)$	$O(h^3)$	$O(h^3)$
Storage for Implicit Diagonal Matrix	25 words Per element	400	400	2500

Cost Analysis (Hexahedral Grid)

Spatial method	RDG(P1P1))	RDG(P1P2)	RDG(P2P2)
Nr. of quadrature points for boundary integrals	4	4	9
Nr. of quadrature points for domain integrals	8	8	27
Reconstruction	NO	YES	NO
Order of spatial accuracy	$O(h^2)$	$O(h^3)$	$O(h^3)$
Storage for the implicit diagonal matrix per element	400 words	400 words	2500 words

The memory requirement for RDG(P1P2) is much smaller than DG(P2).

Design Goal

FVFLO	RDGFLO
Unstructured triangular/ tetrahedral grid	Unstructured arbitrary grid
Finite volume/finite element formulation	Reconstructed Discontinuous Galerkin formulation
h-adaptation	*hp*-adaptation
None	Error Estimation Uncertainty Quantification

RDGFLO

- Physics
  - Compressible flow for all speeds
  - Inviscid, Laminar, Turbulent (RDG(P_0P_1))
  - Chemically reactive flows (RDG(P_0P_1))
- Numerics
  - Unstructured Hybrid Mesh(tetrahedral, pyramidal, prismatic, and hexahedral)
  - Reconstructed Discontinuous Galerkin Formulation
  - Taylor basis
  - Explicit/Implicit (RK) Time Integration
  - LU-SGS/SGS/GMRES for linear systems
  - *p*-multigrid
  - HLLC, LDFSS, AUSM for Inviscid Fluxes
  - BR2, RDG for Viscous Fluxes
  - BGK for Inviscid+Viscou Fluxes
- Parallelization
  - MPI
- GPU
  - OpenACC

Numerical Examples

- Strengths of the RDG methods
  - Accuracy
  - Robustness
  - Essentially oscillation-free property

Strengths of the RDG methods

Accuracy Demonstration

Example 1: Convection of a Gaussian and a square wave

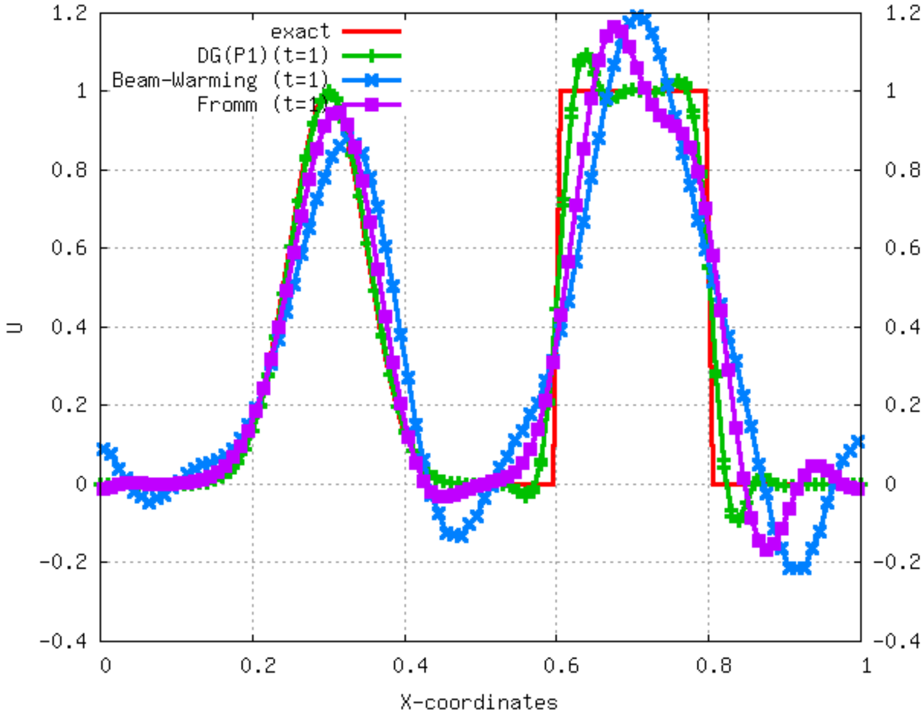

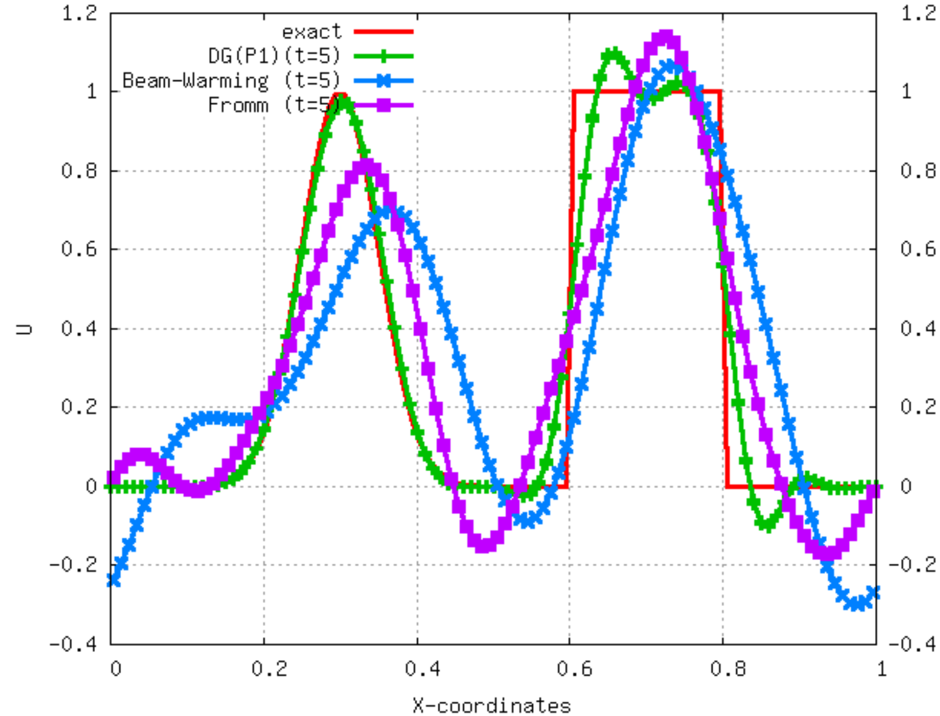

The superior dissipation and dispersion property of DG !

Convection of a Gaussian and a square wave

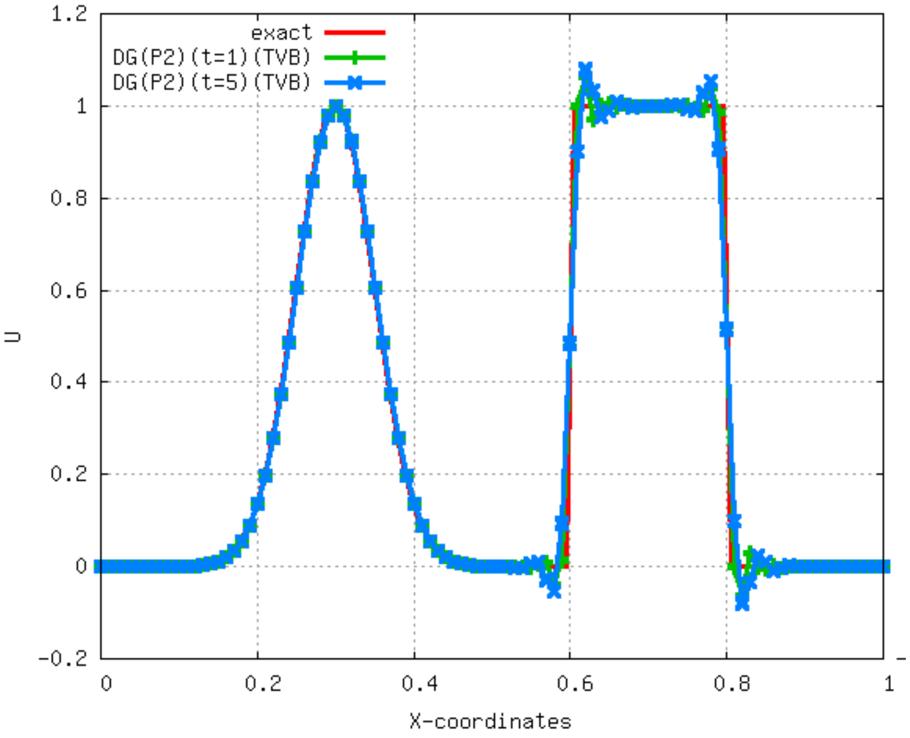

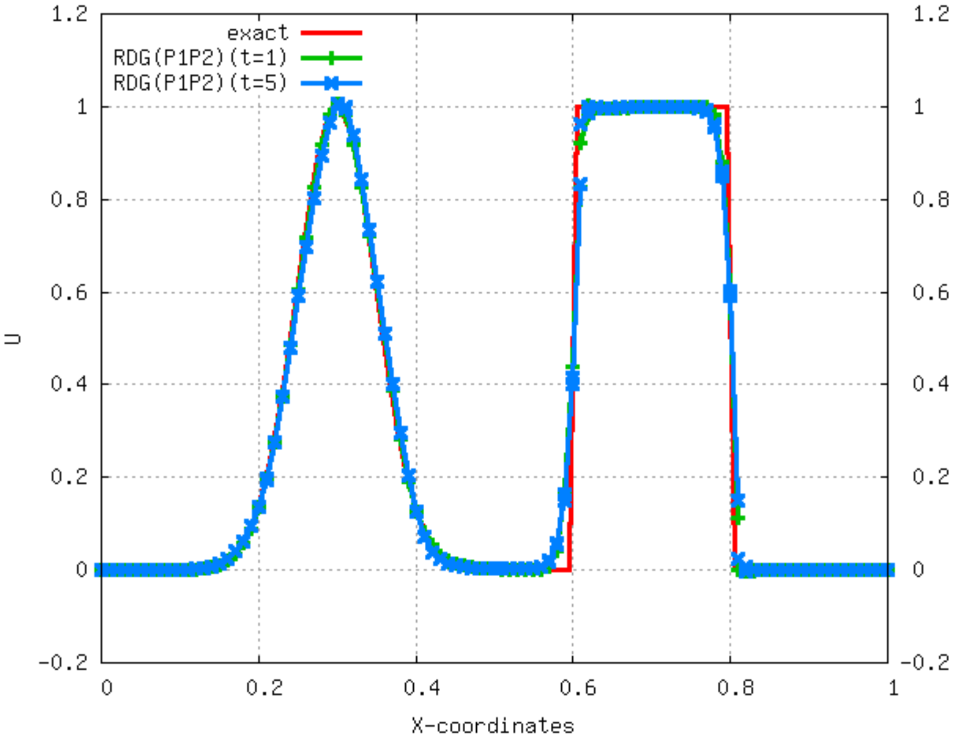

Note the high accuracy and oscillation-free of the RDG !

Example 2: Solution to a Heat Conduction Equation

Access the order of accuracy of RDG methods for diffusion

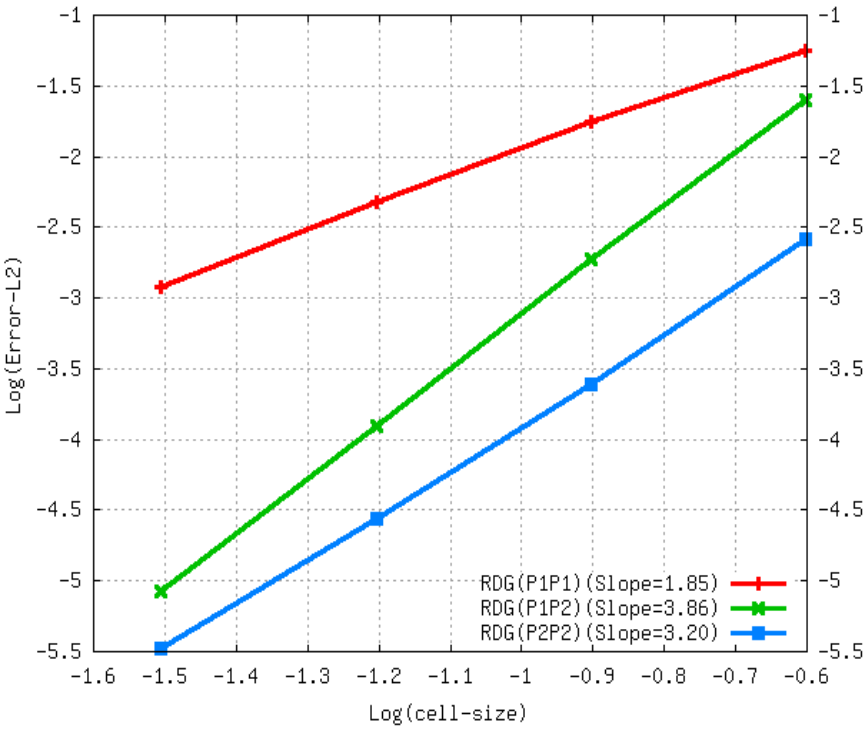

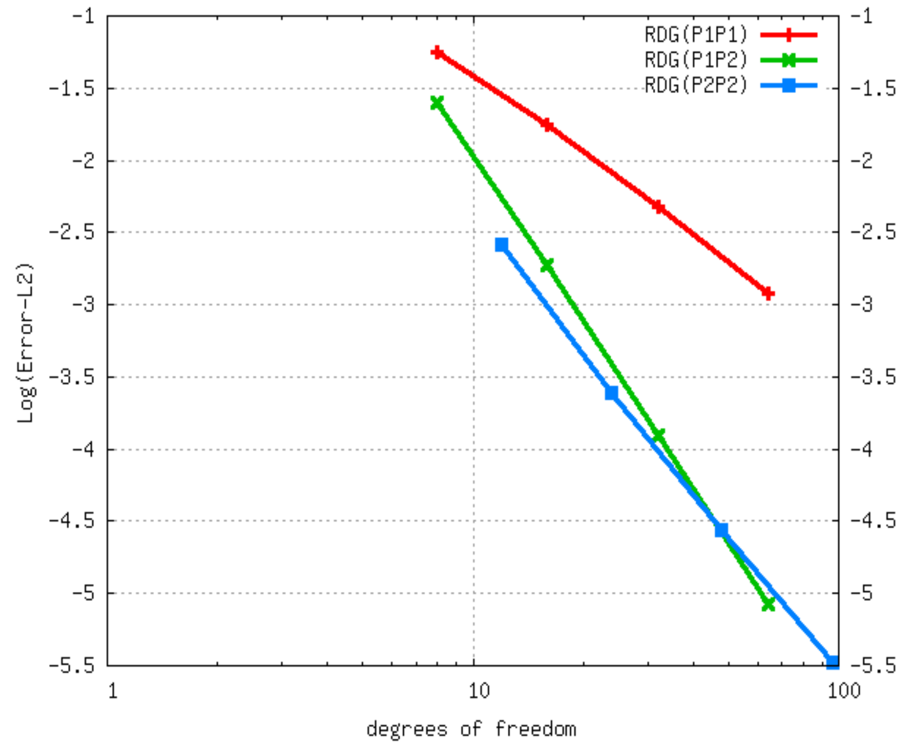

The superior convergence of RDG methods for diffusion!

Example 3. A Subsonic Flow through a Channel with a Smooth Bump (M_∞=0.5, α=0°)

- Access the order of accuracy of the RDG(P_1P_1), WENO(P_1P_2) and HWENO(P_1P_2) methods for internal flows.
- Entropy production is served as the error measurement.

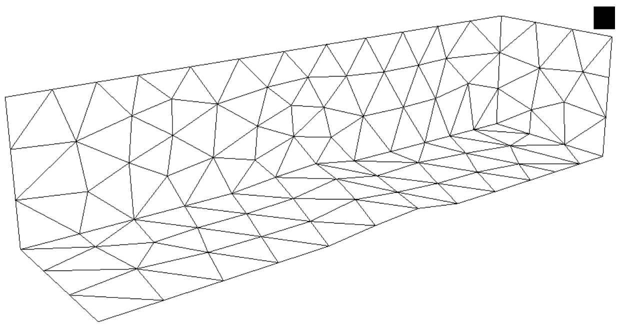

889 cells
254 pts
171 boundary pts

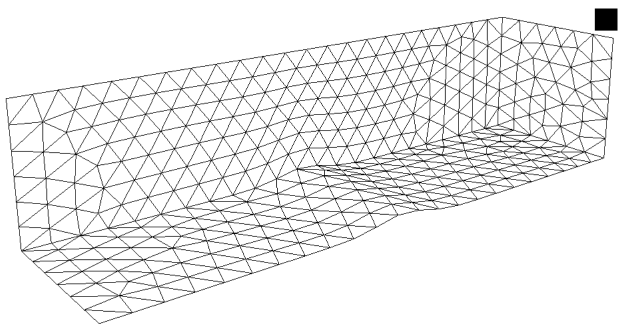

6986 cells
1555 pts
691 boundary pts

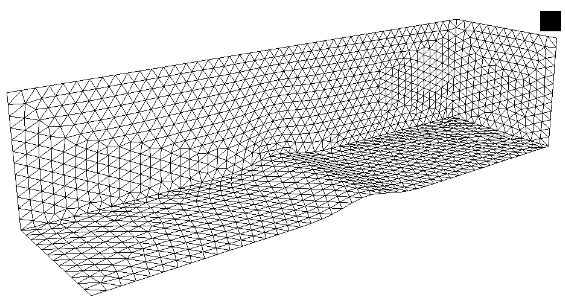

449522 cells
81567 pts
10999 boundary pts

Computed Velocity Contours by HWENO(P_1P_2)

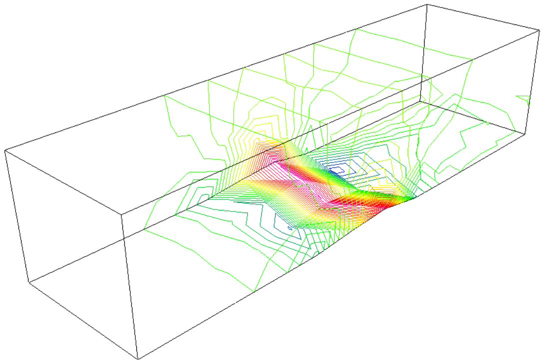

Coarse Grid

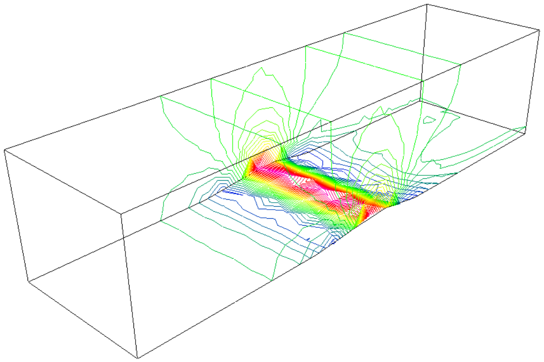

Medium Grid

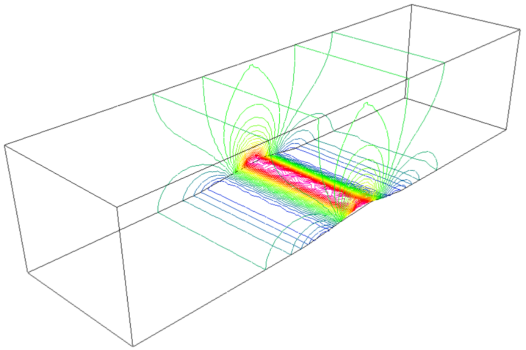

Fine Grids

Convergence Study for different RDG methods

L2-error and order of convergence for the RDG(P_1P_1), WENO(P_1P_2), and HWENO(P_1P_2) methods

	RDG(P_1P_1)		WENO(P_1P_2)		HWENO(P_1P_2)	
Length Scale	L^2-error	Order	L2-error	Order	L^2-error	Order
6.552E-2	2.438E-3		2.183E-3		2.220E-3	
3.295E-2	7.356E-4	1.744	2.794E-4	2.992	2.851E-4	2.987
1.650E-2	1.807e-4	2.032	4.539E-05	2.626	4.565E-5	2.647

Both WENO(P_1P_2) and HWENO(P_1P_2) deliver the designed 3rd order of convergence !!

Example 4. A Subsonic Flow past a Sphere (M_∞=0.5)

- Access the order of accuracy of the RDG(P_1P_1), WENO(P_1P_2) and HWENO(P_1P_2) methods for external flows.
- Entropy production is served as the error measurement.

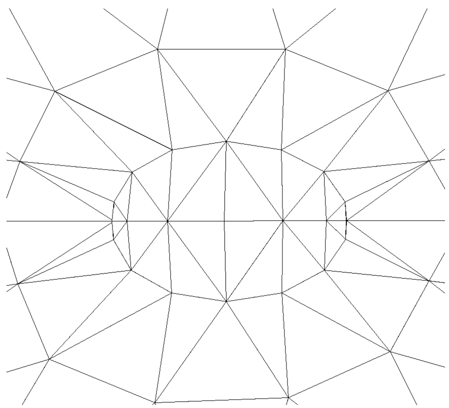

535 cells
167 points
124 boundary pts

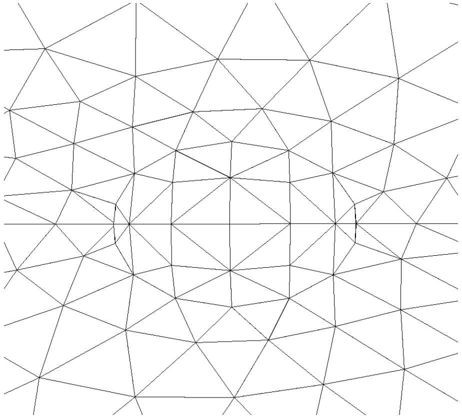

62426 cells
598 points
322 boundary pts

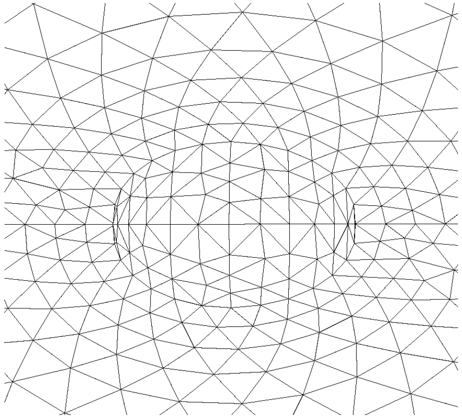

16467 cells
3425 points
1188 boundary pts

Computed Velocity Contours by HWENO(P_1P_2)

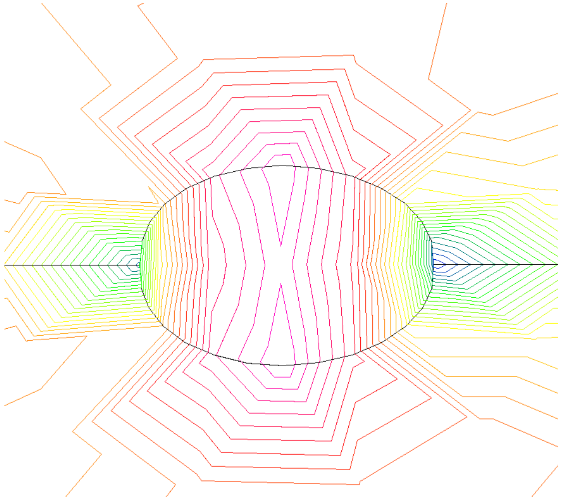

Coarse Grid

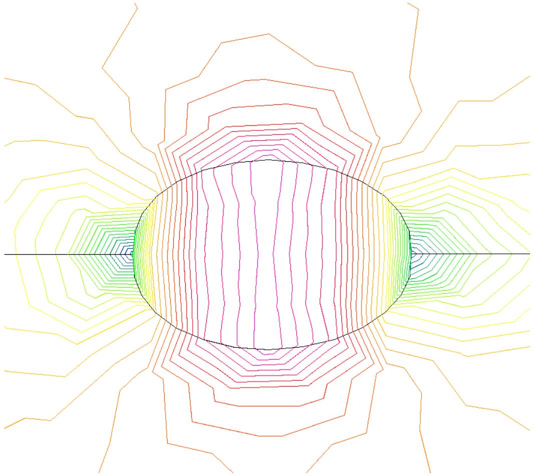

Medium Grid

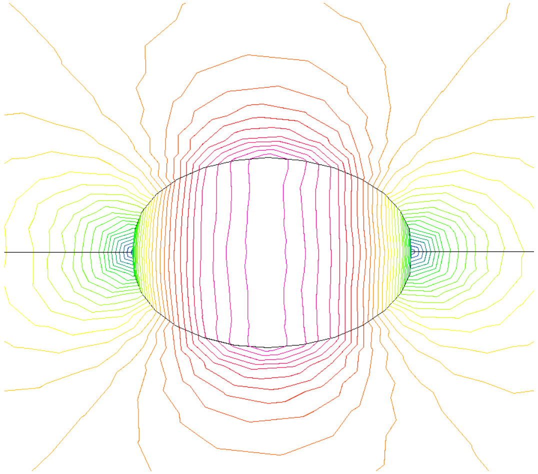

Fine Grids

Convergence Study for different RDG methods

L2-error and order of convergence for the RDG(P_1P_1), WENO(P_1P_2), and HWENO(P_1P_2) methods

	RDG(P_1P_1)		WENO(P_1P_2)		HWENO(P_1P_2)	
Length scale	L^2-error	Order	L^2-error	Order	L^2-error	Order
7.760E-2	1.783E-2		1.052E-2		1.117E-2	
4.688E-2	5.010E-3	2.519	1.317E-3	4.124	1.503E-3	3.980
2.476E-2	1.232E-3	2.198	1.978E-4	2.964	2.201E-4	3.009

Both WENO(P_1P_2) and HWENO(P_1P_2) deliver the designed 3rd order of convergence !!

Efficiency Comparison for Different RDG Methods

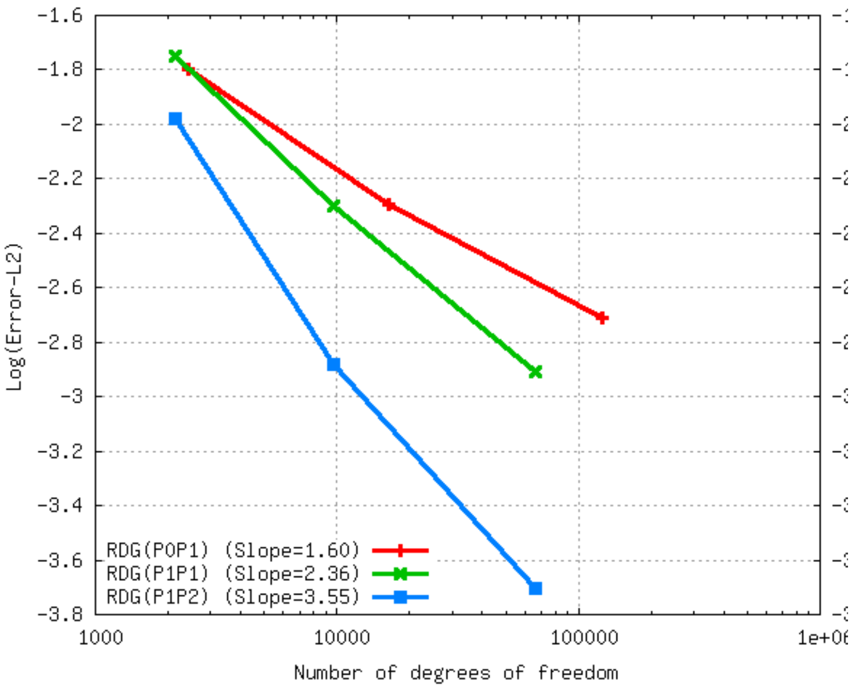

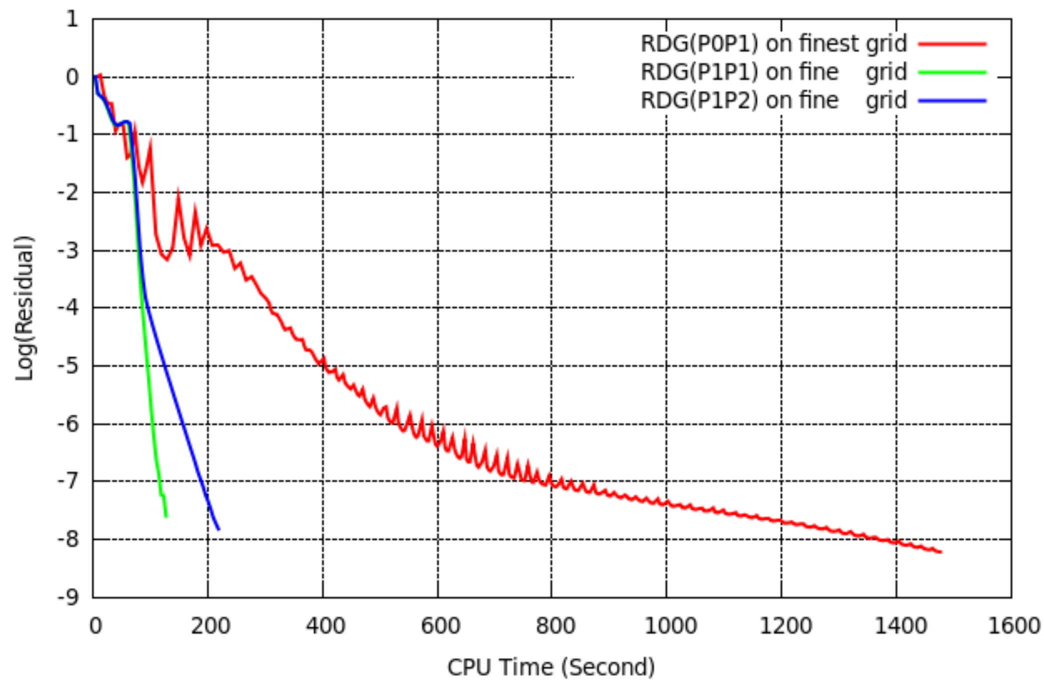

Convergence order
versus
number of degree of freedom

Convergence history
versus
CPU time (Second)

Efficiency Comparison for Different RDG Methods

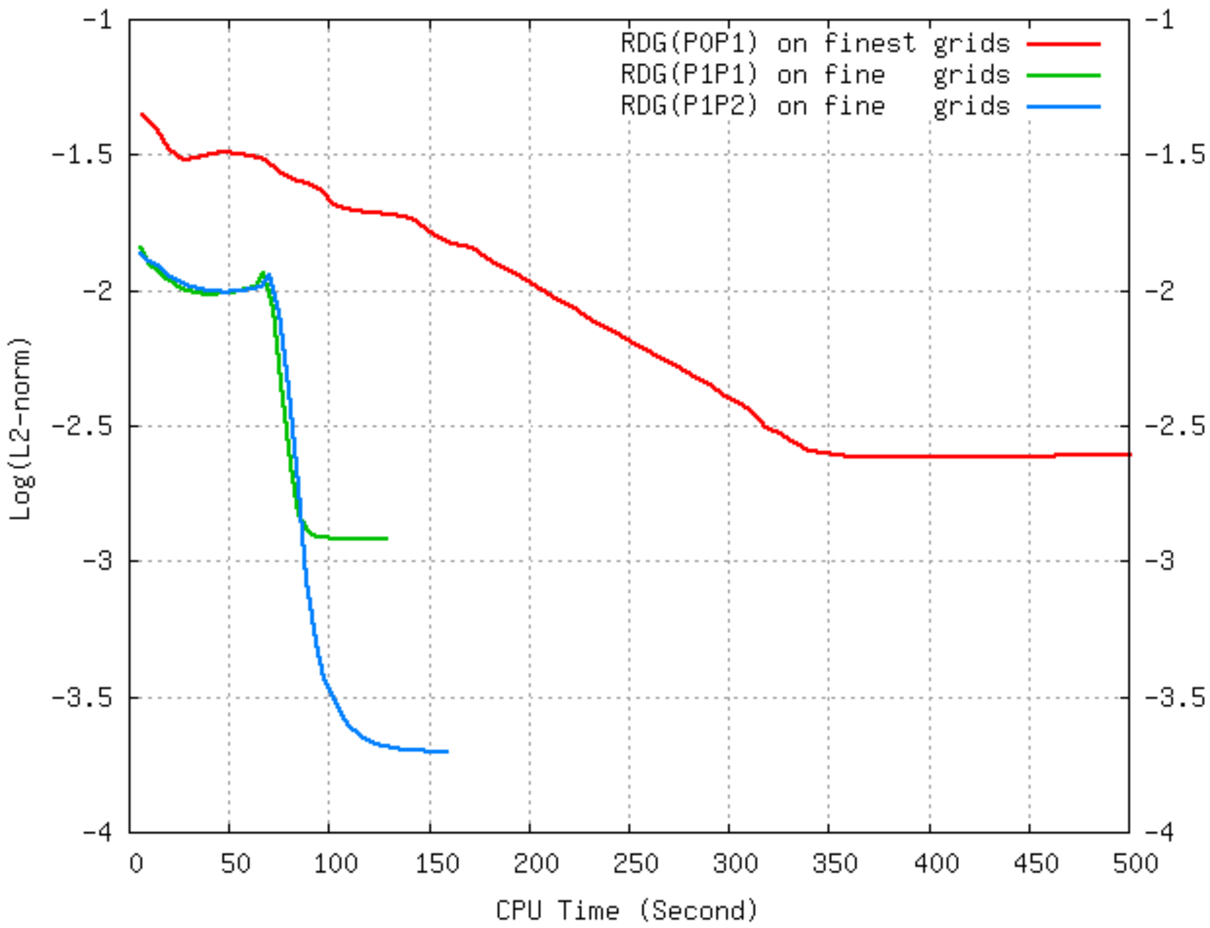

L2 norm versus CPU time

Example 5. Blasius Boundary Layer (M=0.2, Re=100,000)

61x17x1
40 cells on the plate

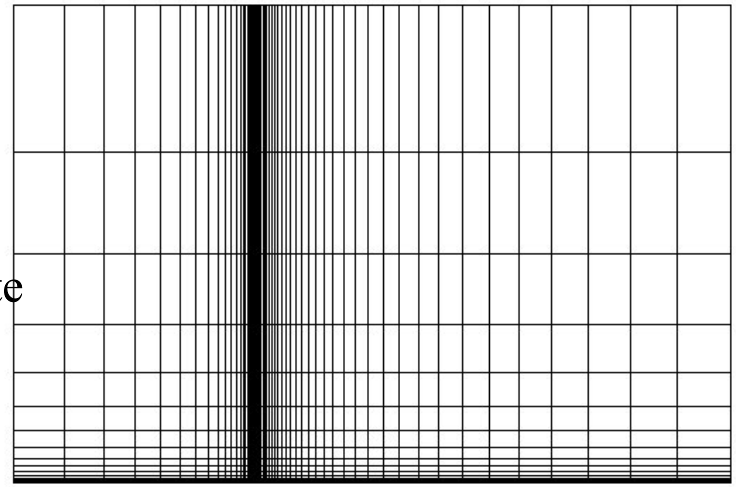

Eta =1.2
dy= 0.1291E-2

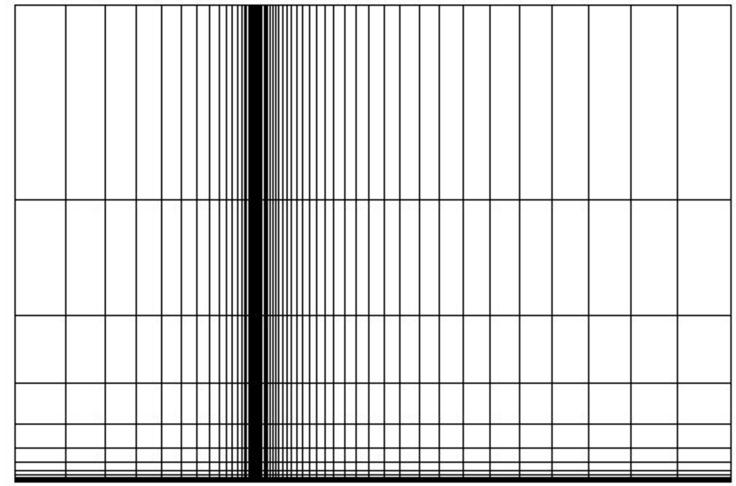

Eta=1.3
dy= 0.155869E-3

Npoin=1800
Nboun=210
62 grid points on the flat plate.
Dy=0.3464E-03 at LE,

Dy=0.82649E-03 at TE

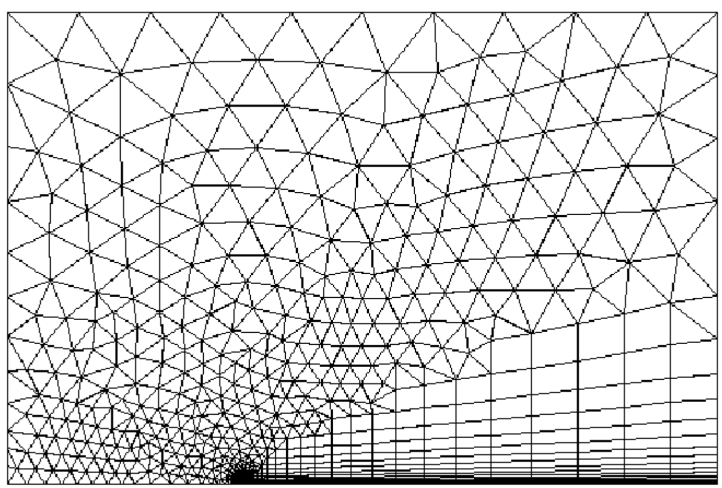

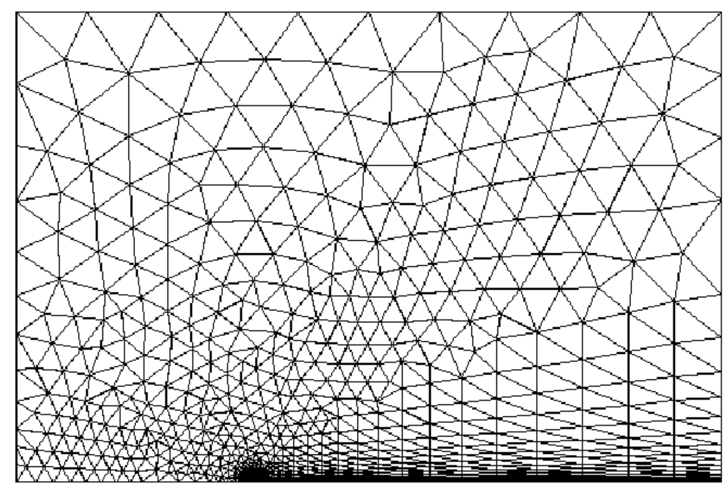

Computed skin friction coefficients (RDG(P1))

Eta=1.2

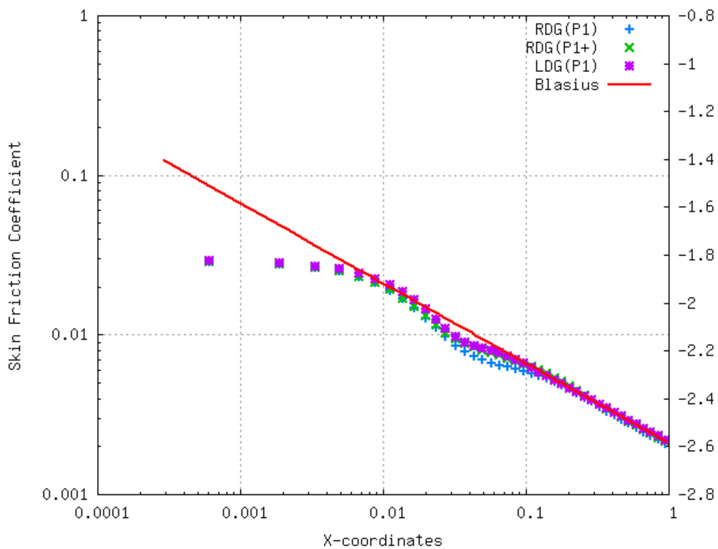

Eta=1.3

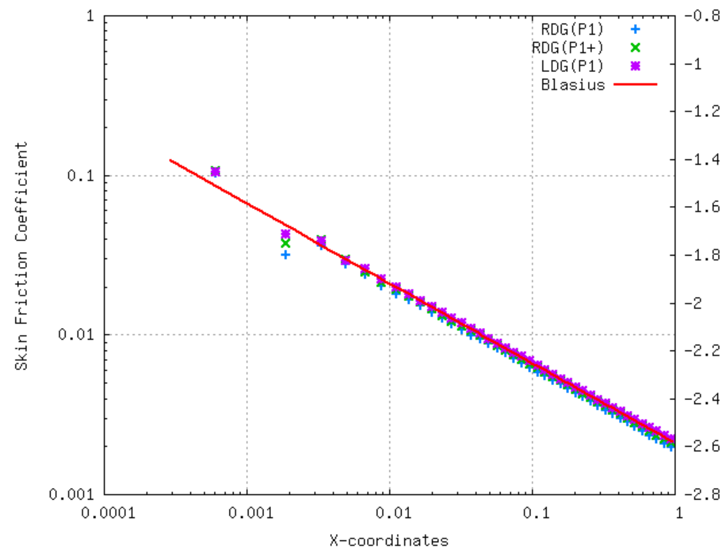

Hybrid

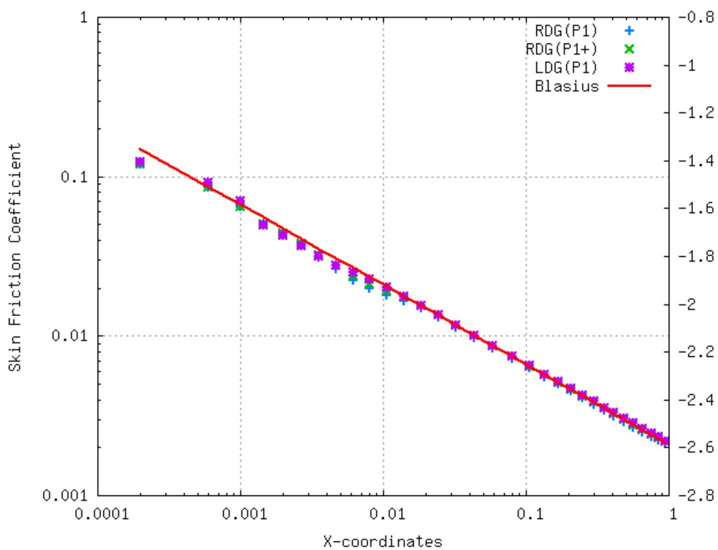

Triangular

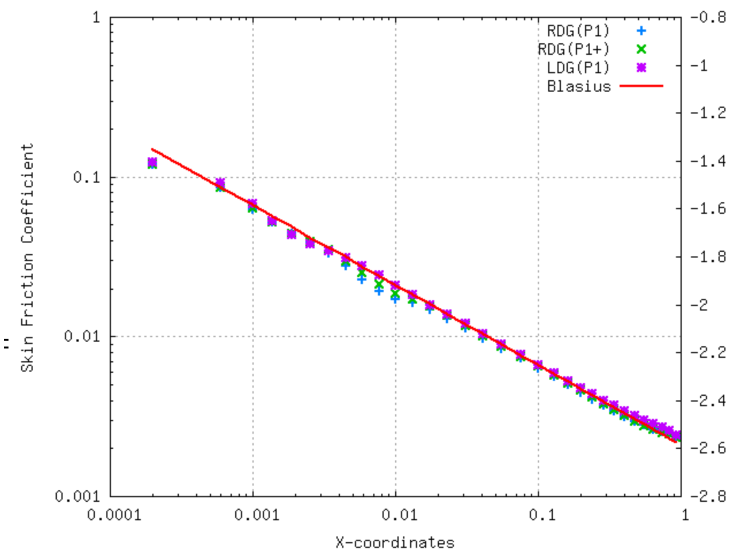

Computed skin friction coefficients (RDG(P2))

Eta=1.2

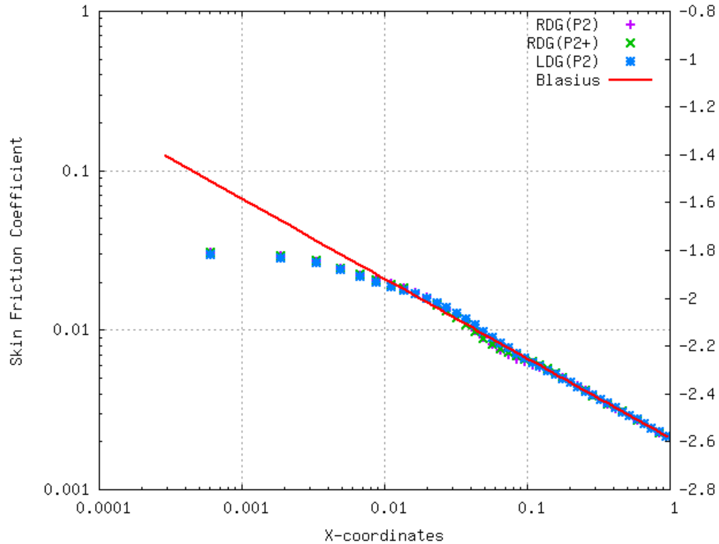

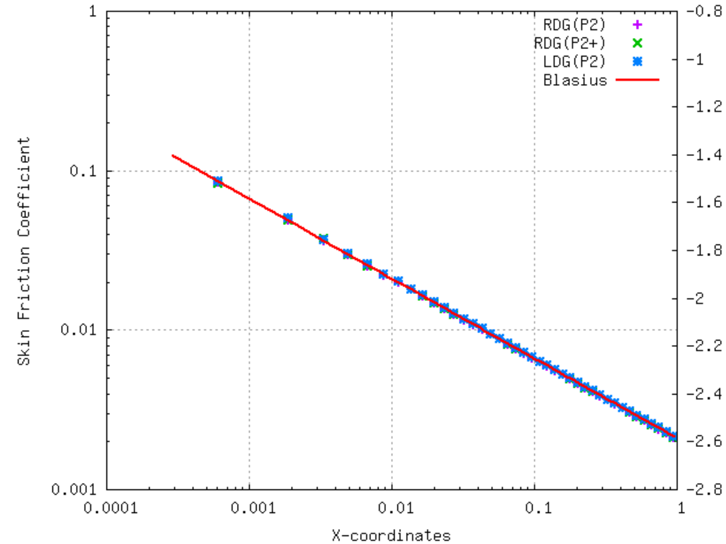

Eta=1.3

Hybrid

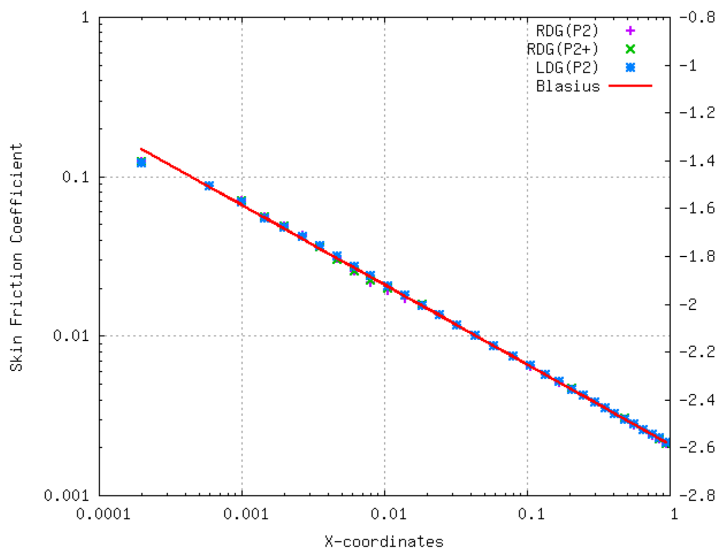

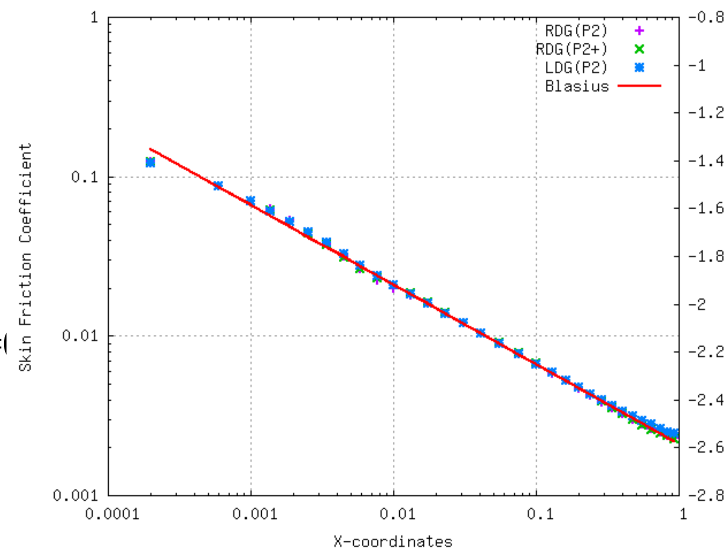

Triangular

Computed X-velocity profiles at x=0.2(RDG(P1))

Eta=1.2

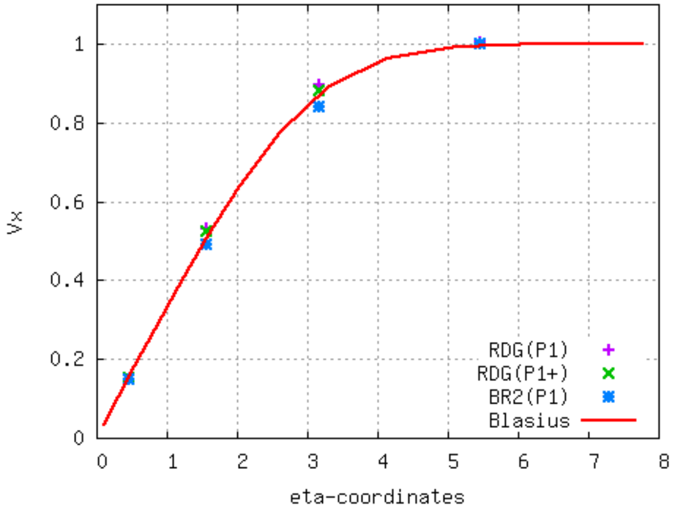

Eta=1.3

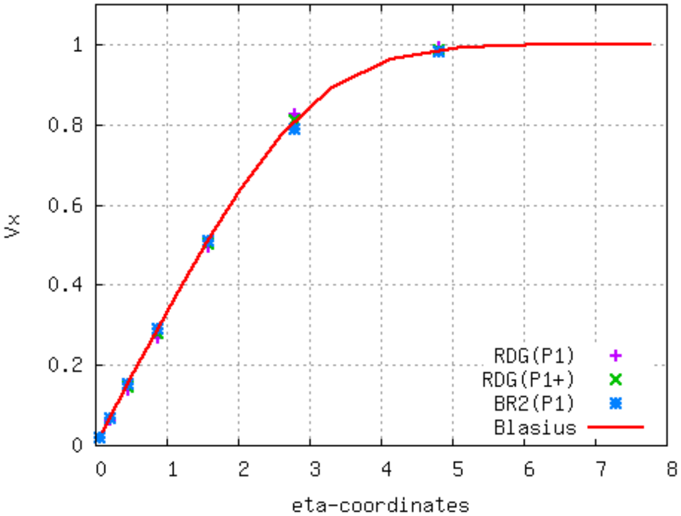

Hybrid

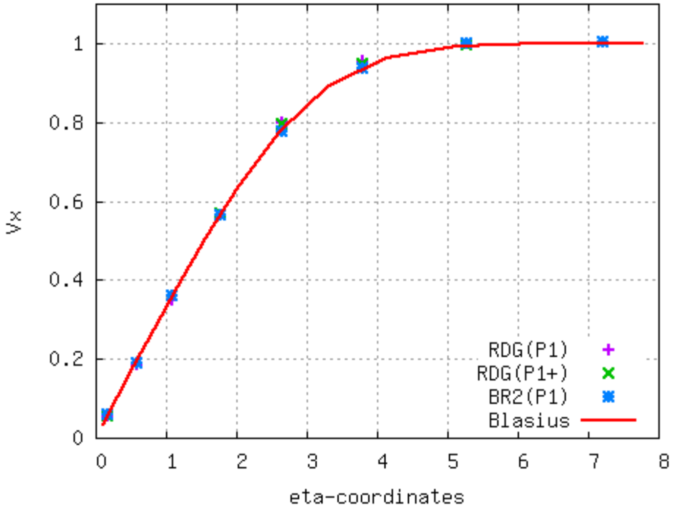

Triangular

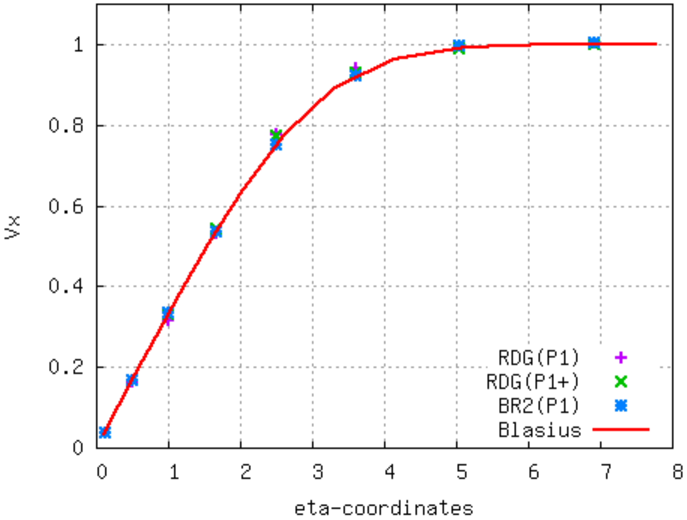

Computed X-velocity profiles at x=0.2(RDG(P2))

Eta=1.2

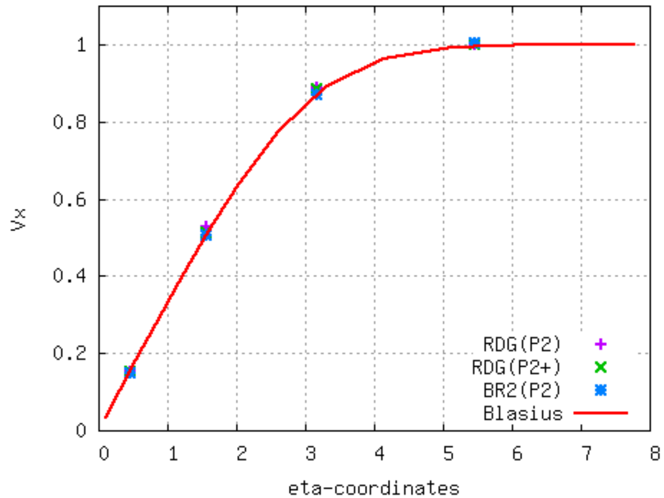

Eta=1.3

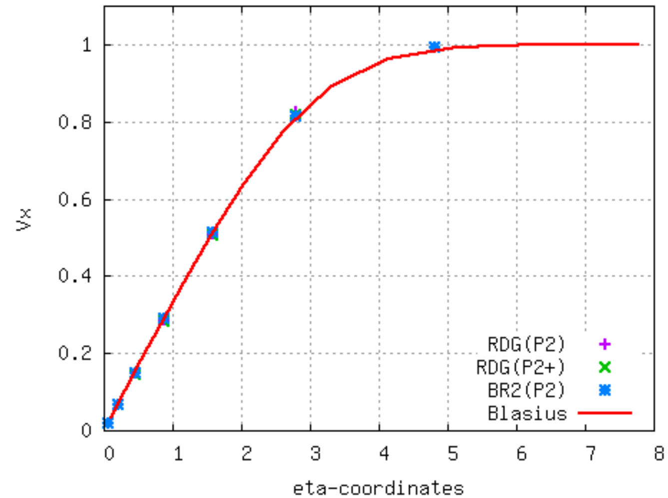

Hybrid

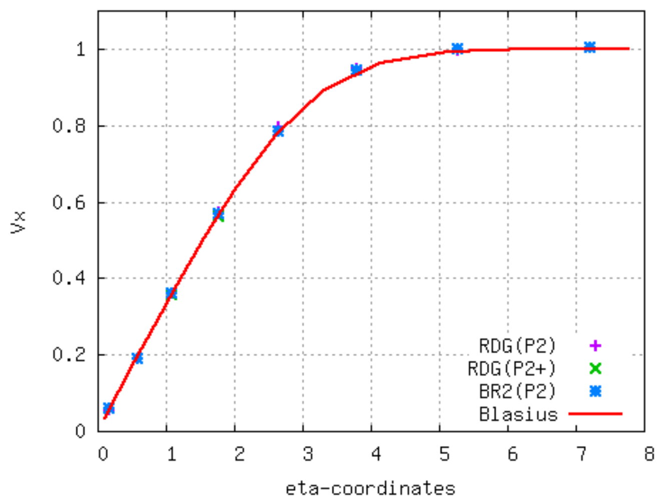

Triangular

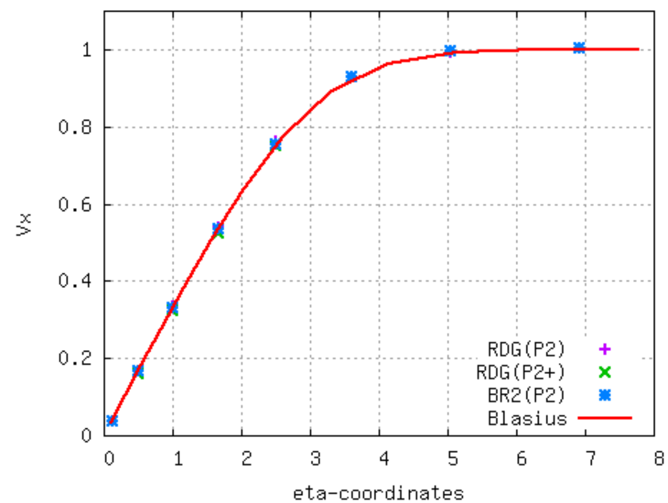

Computed Y-velocity profiles at x=0.2(RDG(P1))

Eta=1.2

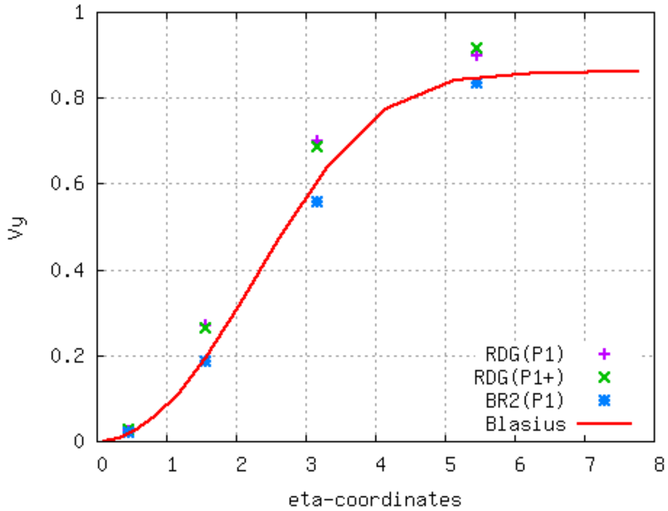

Eta=1.3

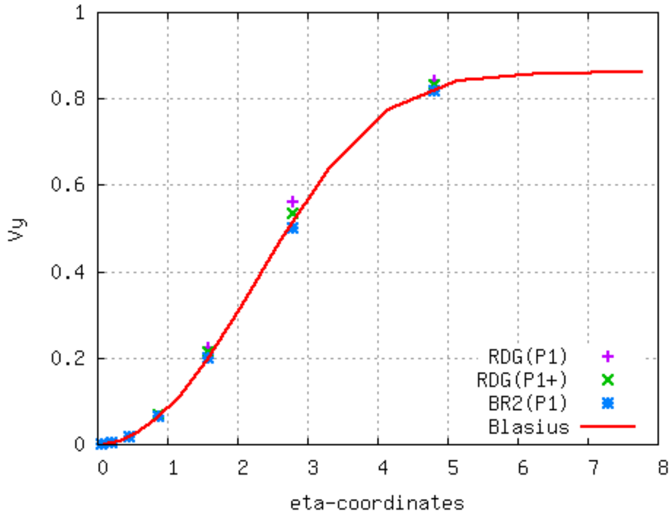

Hybrid

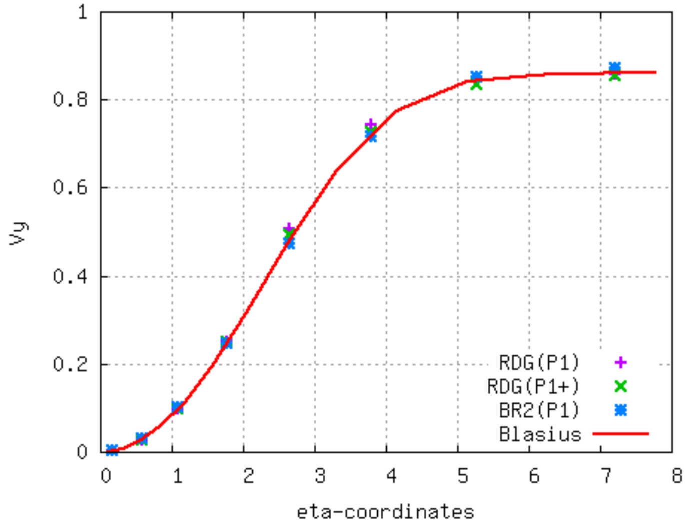

Triangular

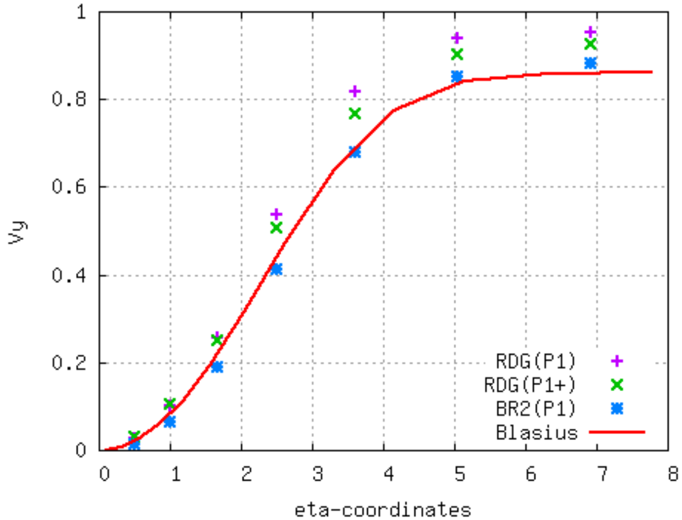

Computed Y-velocity profiles at x=0.2(RDG(P2))

Eta=1.2

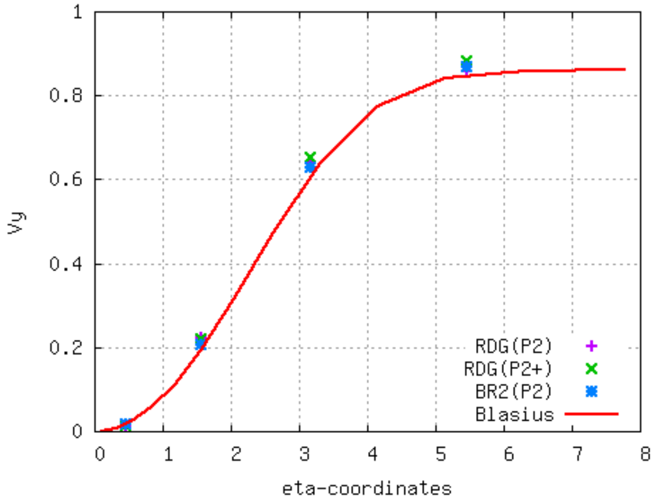

Eta=1.3

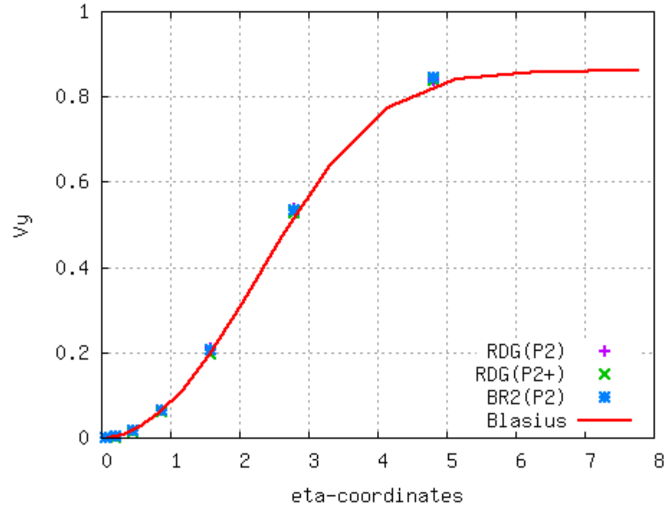

Hybrid

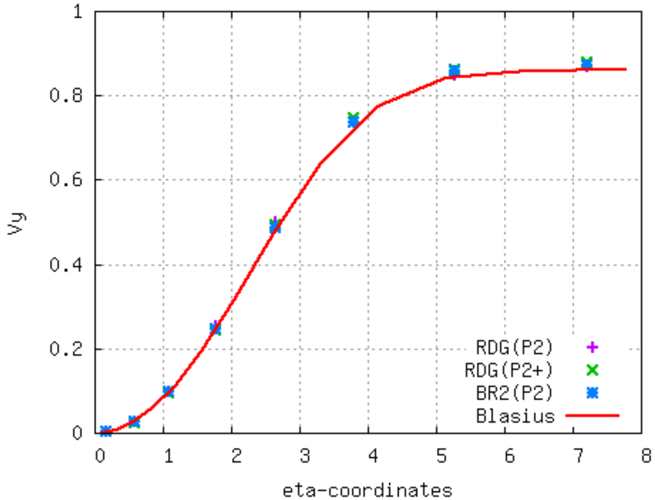

Triangular

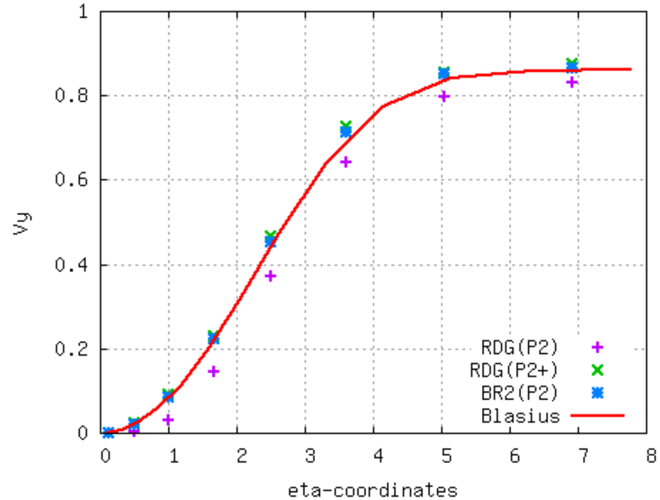

Strengths of the RDG method

Robustness Demonstration

Example 1. Water flow in a convergent-divergent nozzle

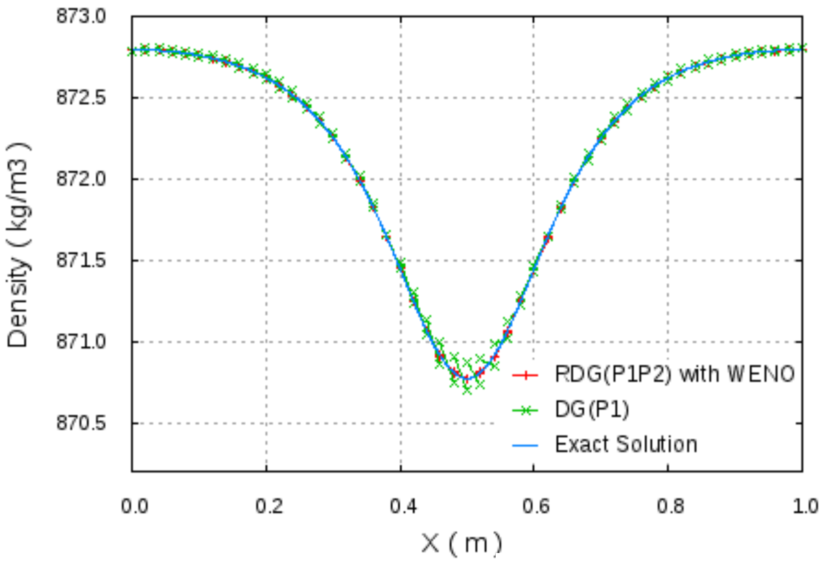

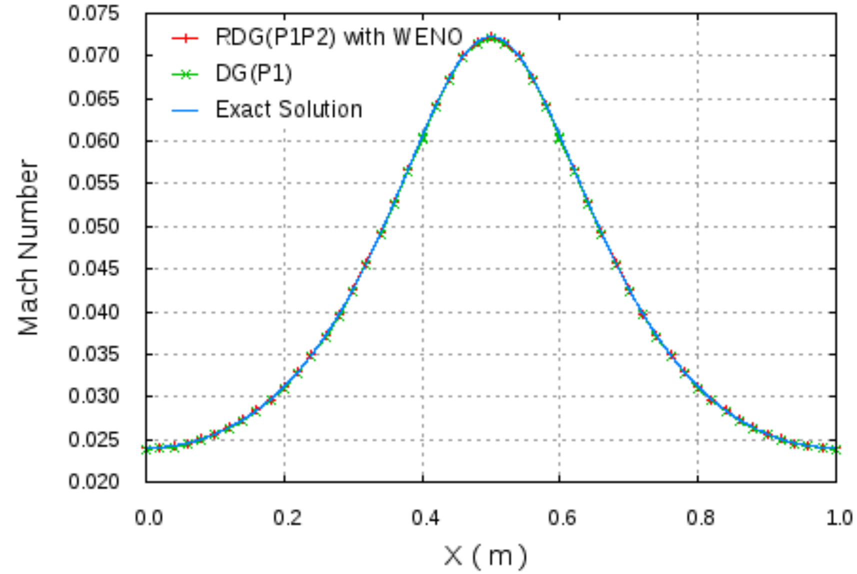

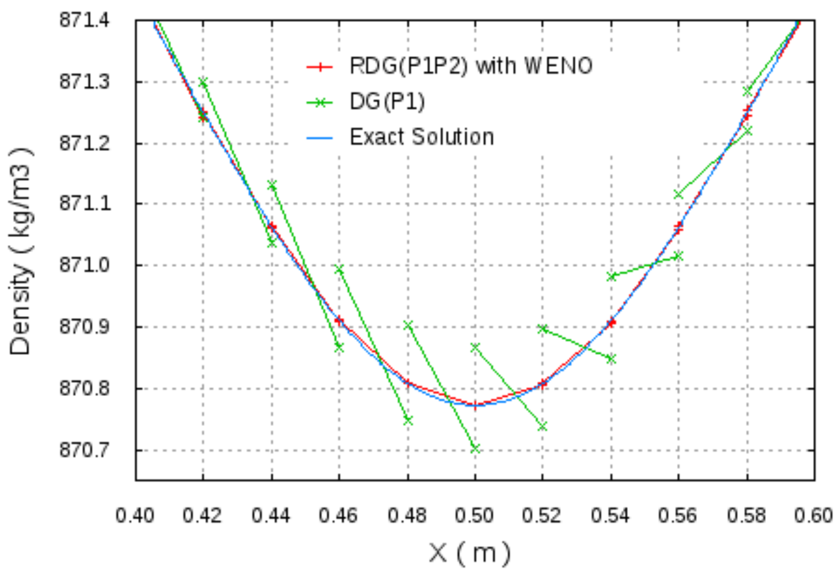

Vapor flow in a convergent-divergent nozzle

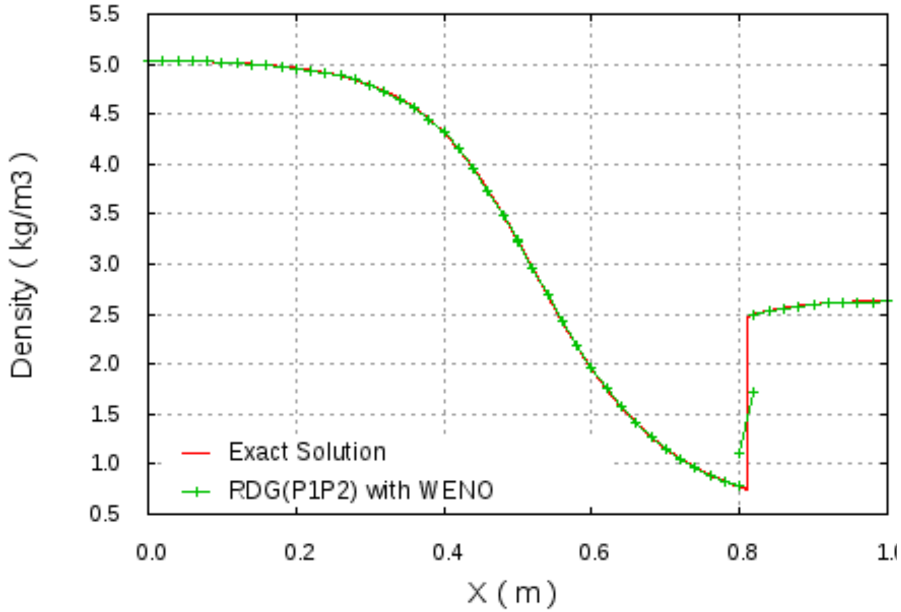

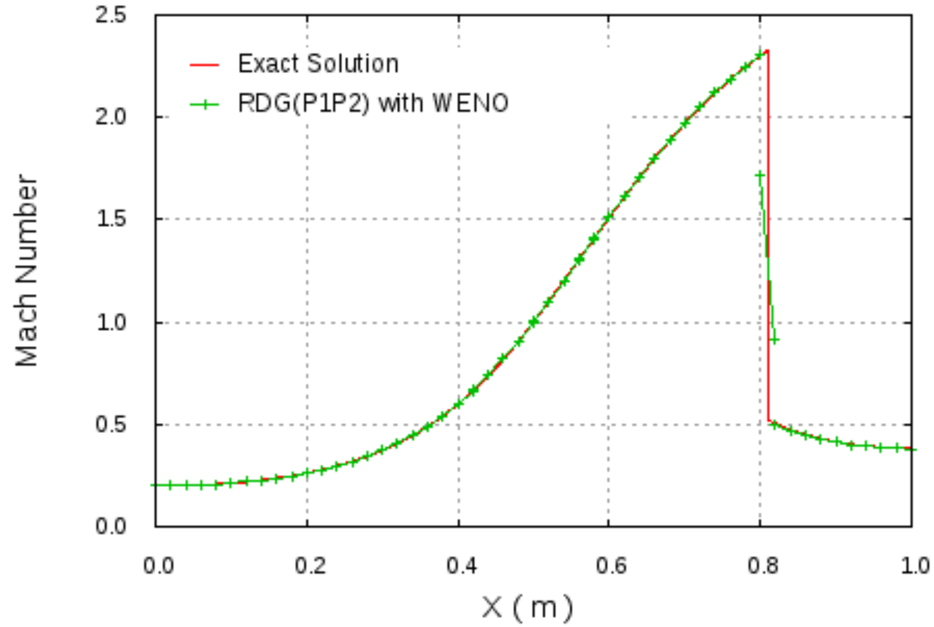

Stiffened EOS

No single parameter is changed !!!

No time-derivative preconditioner is required !!!

Example 2. Low Mach Number Flow past a Sphere

- Access the accuracy for solving low Mach number flow problems.

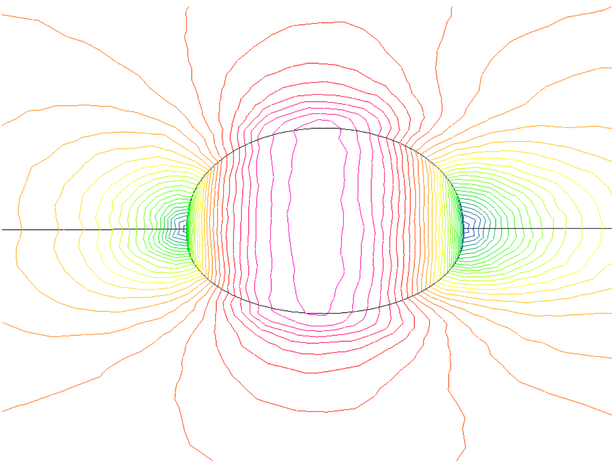

Obtained by the RDG(P_0P_1) on the finest grid

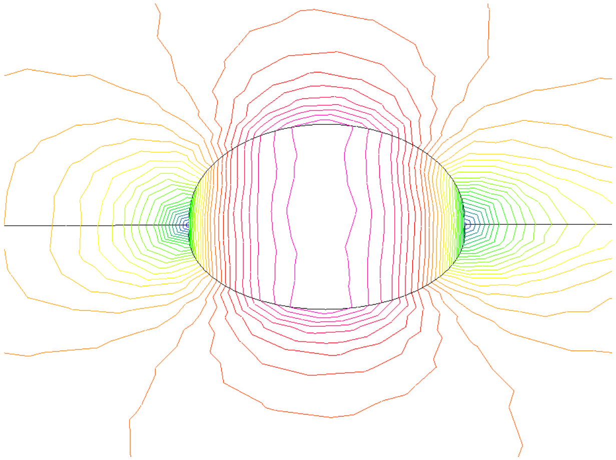

Obtained by the RDG(P_1P_1) on the fine grid

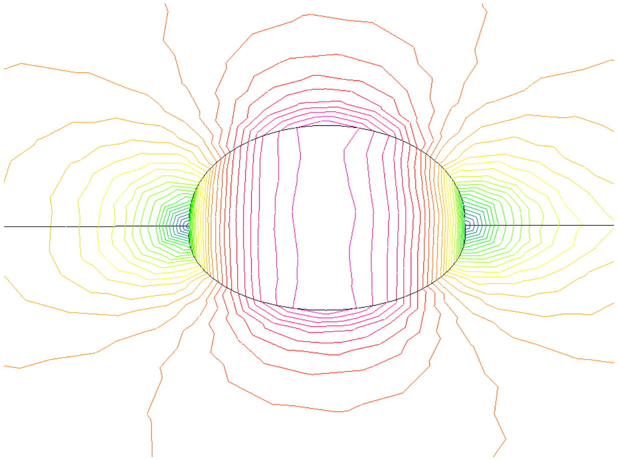

Obtained by the RDG(P_1P_2) on the fine grid

Comparison of the Computed Velocity Distributions on the Surface of the Sphere

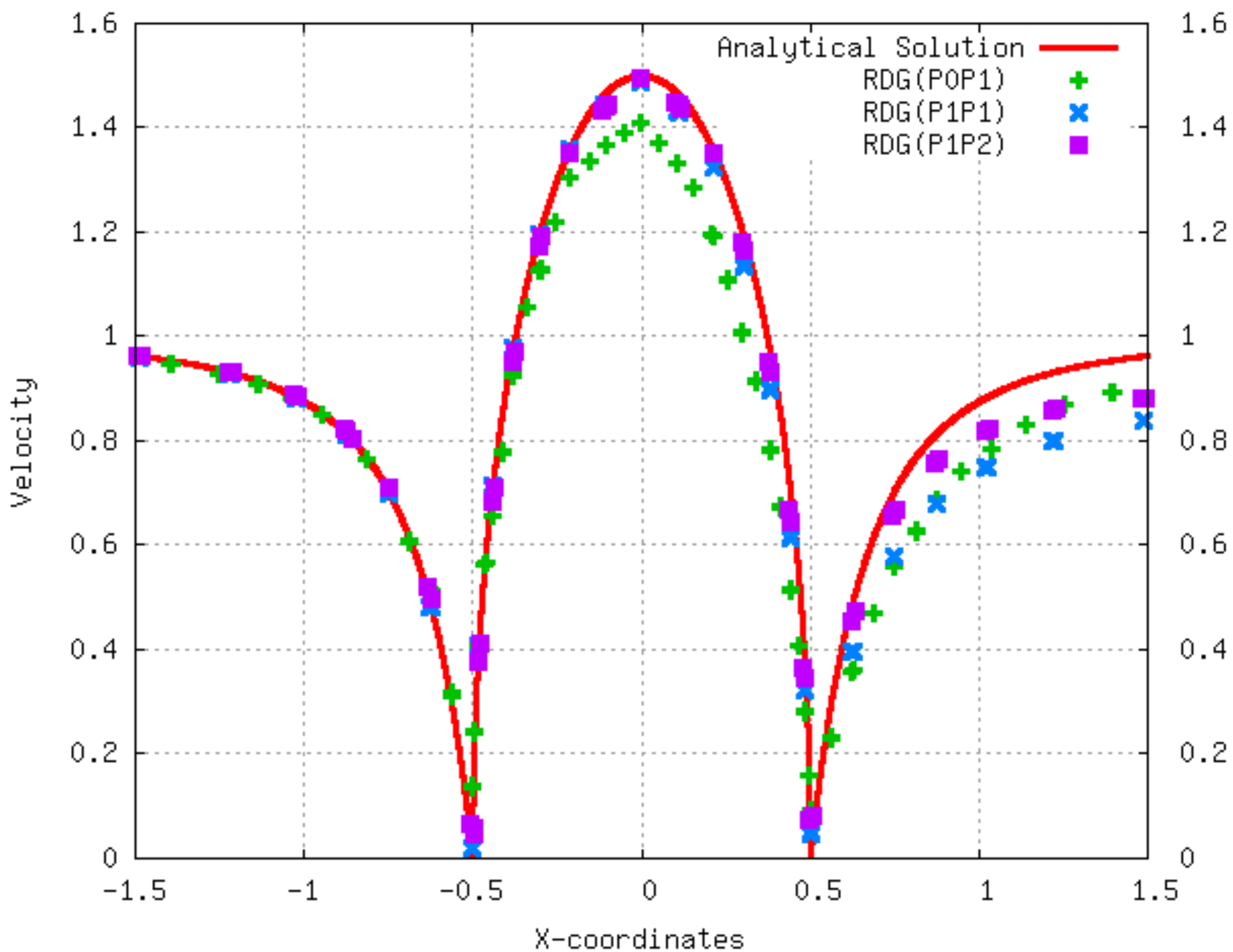

Strengths of the RDG method

Essentially oscillation-free property

Example 1. Transonic Flow past an ONERA M6 Wing (M_∞=0.84, α=3.06°)

- Access the accuracy and non-oscillatory property of the HWENO(P_1P_2) method for flows with discontinuities.

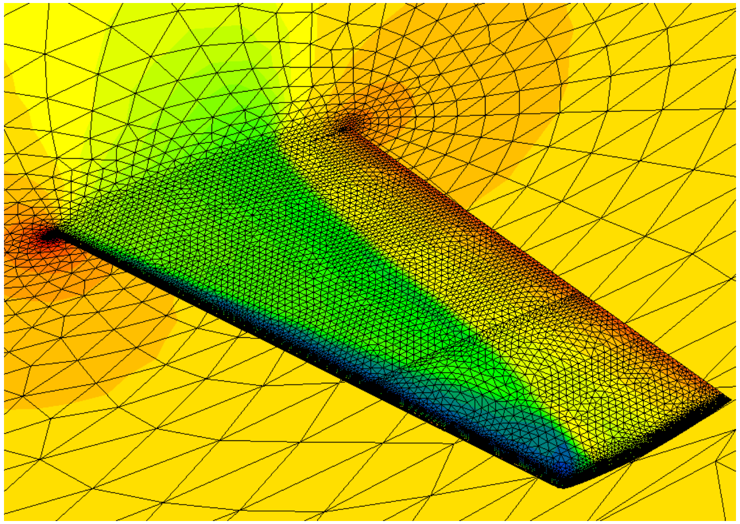

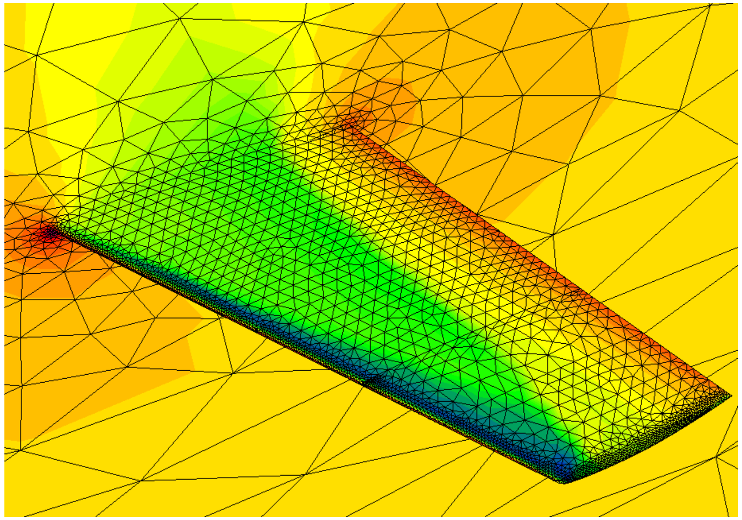

Computed Pressure Contours

WENO(P_0P_1)	HWENO(P_1P_2)
nelem = 593,169	nelem = 95,266
npoin = 110,282	npoin = 18,806
nboun = 19,887	nboun = 5,287

Example 1. Computed Pressure Coefficient and Entropy Production Distributions at different spanwise locations

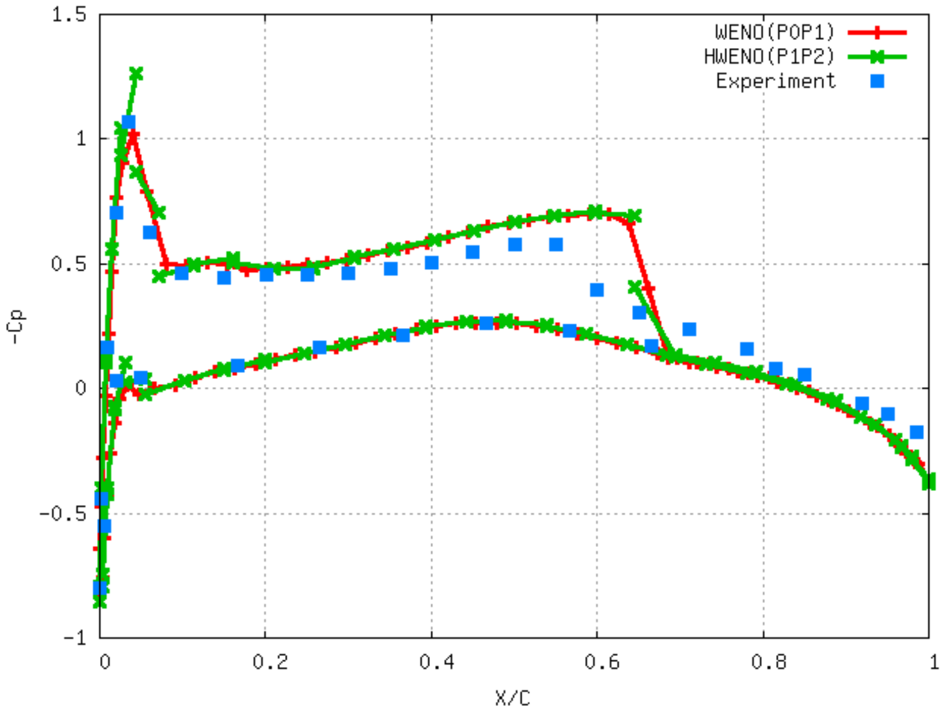

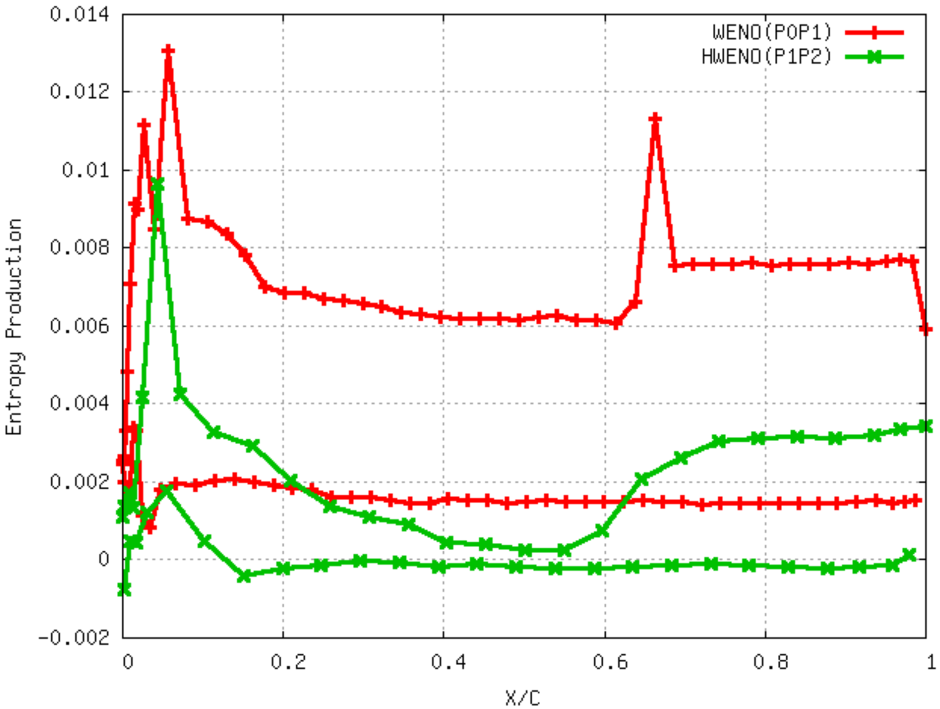

η=0.20

Computed Pressure Coefficient and Entropy Production Distributions at different spanwise locations

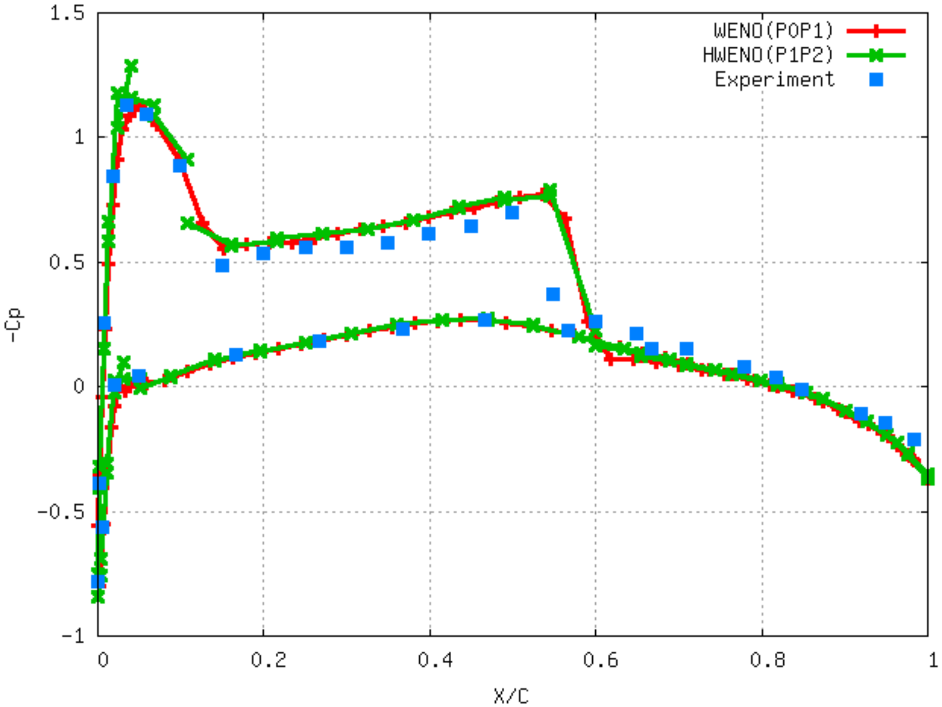

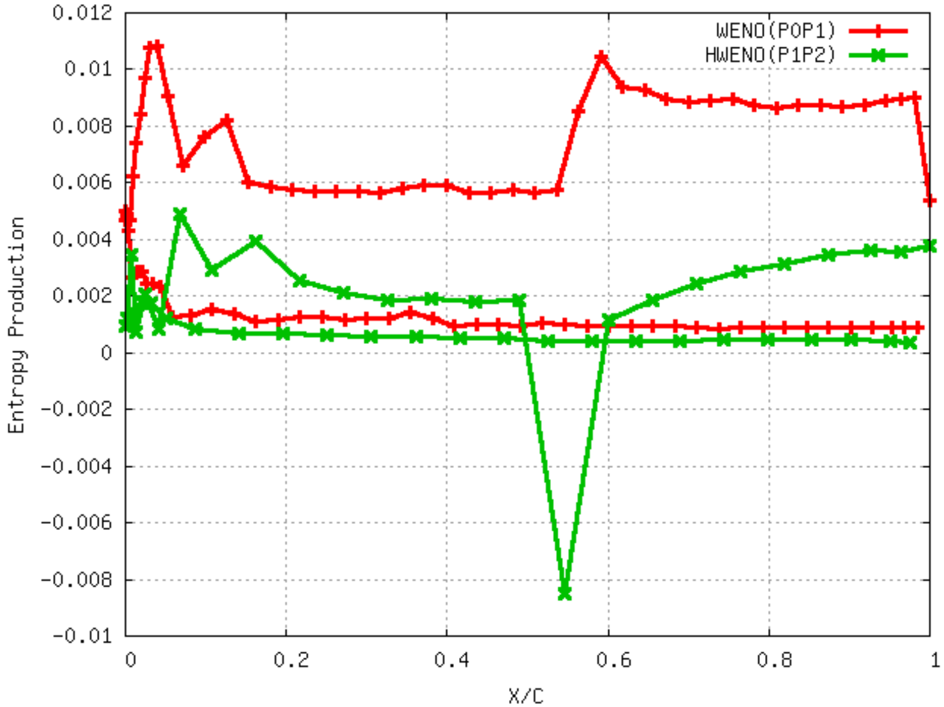

η=0.44

Computed Pressure Coefficient and Entropy Production Distributions at different spanwise locations

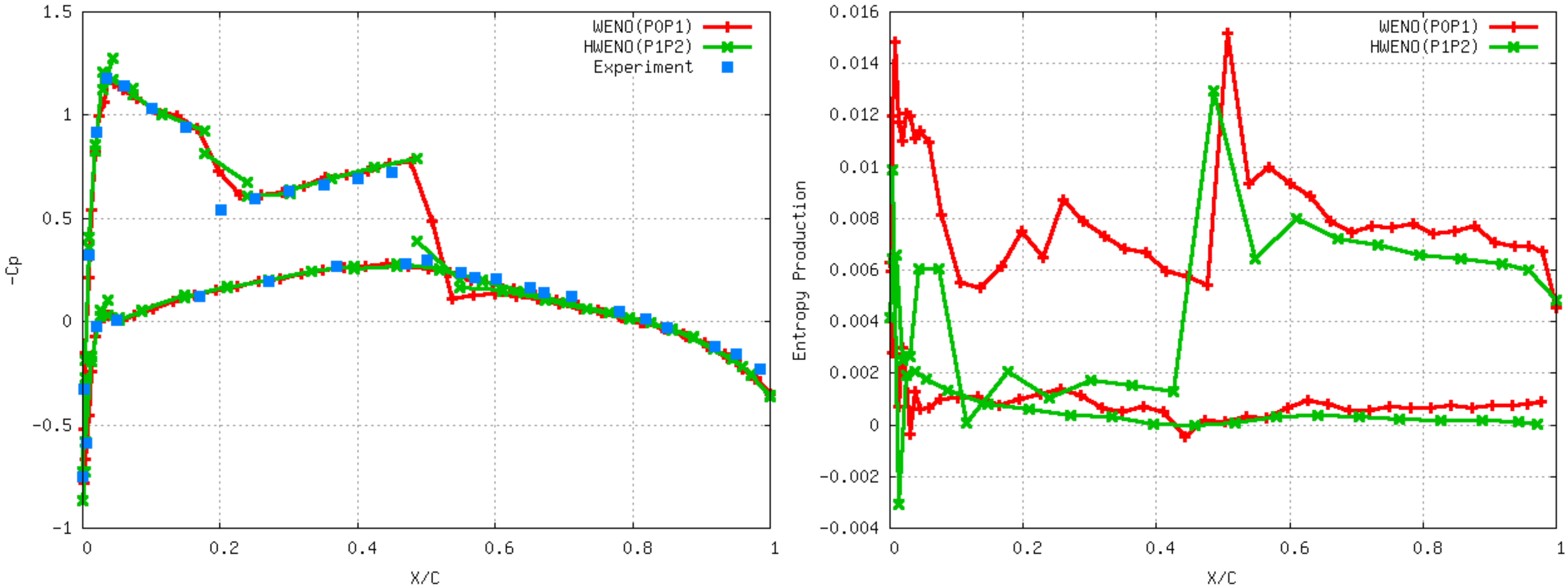

η=0.65

Computed Pressure Coefficient and Entropy Production Distributions at different spanwise locations

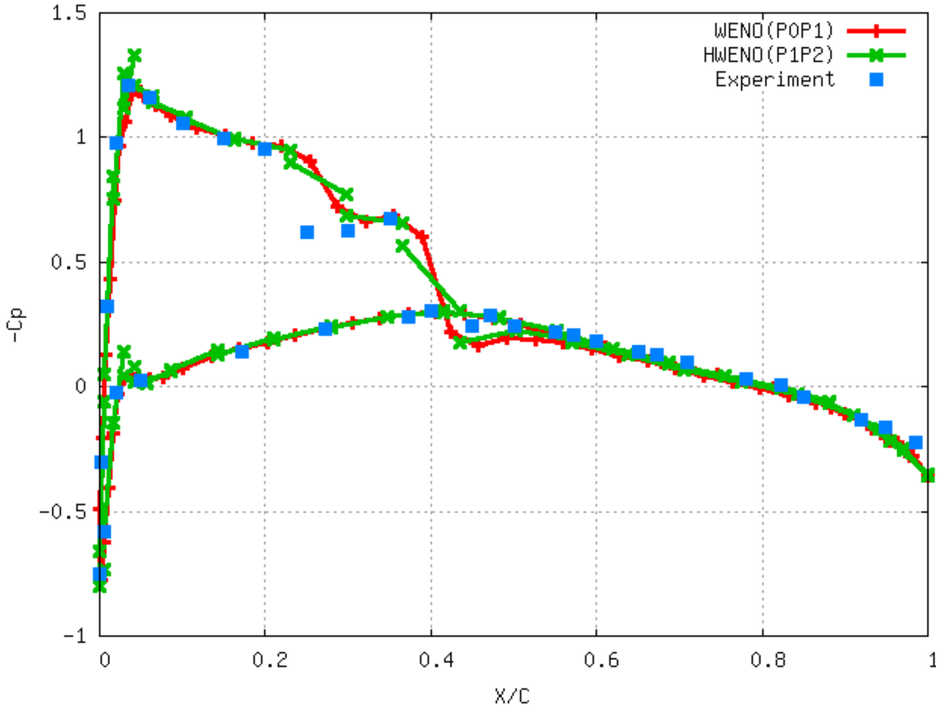

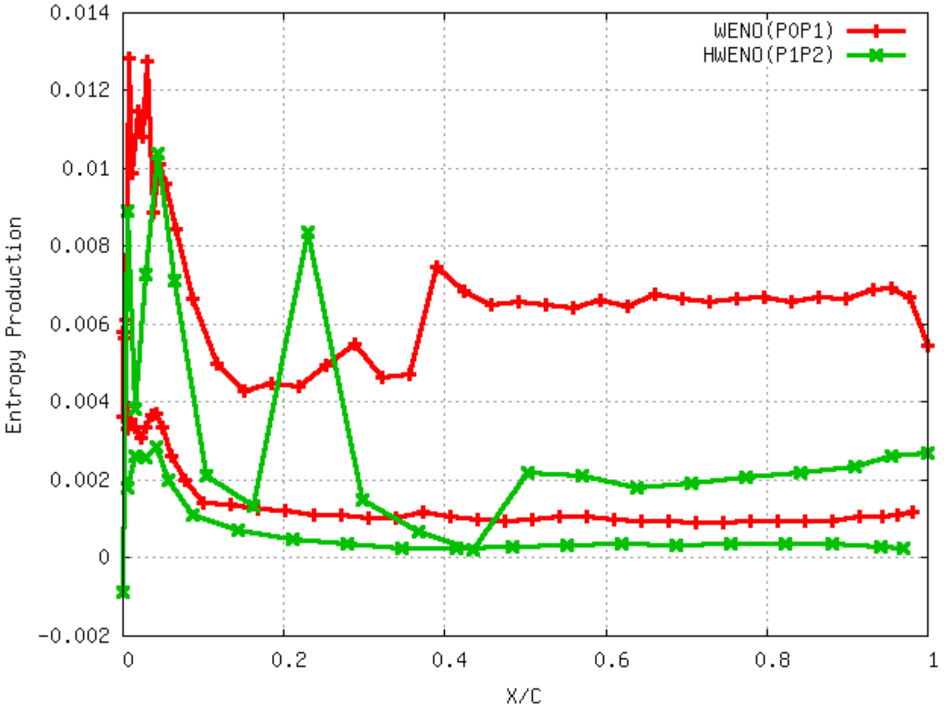

η=0.80

Computed Pressure Coefficient and Entropy Production Distributions at different spanwise locations

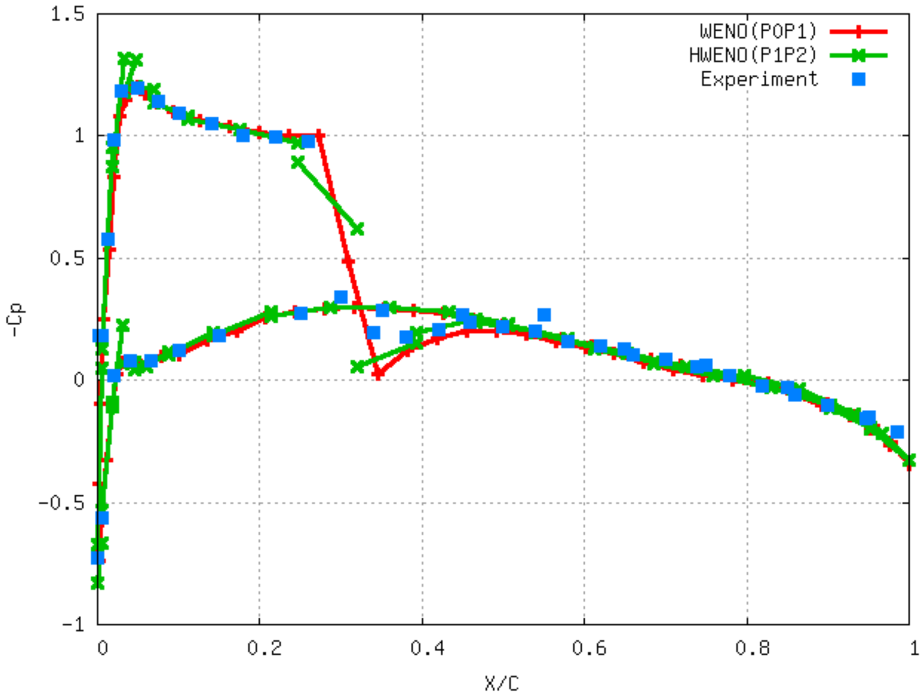

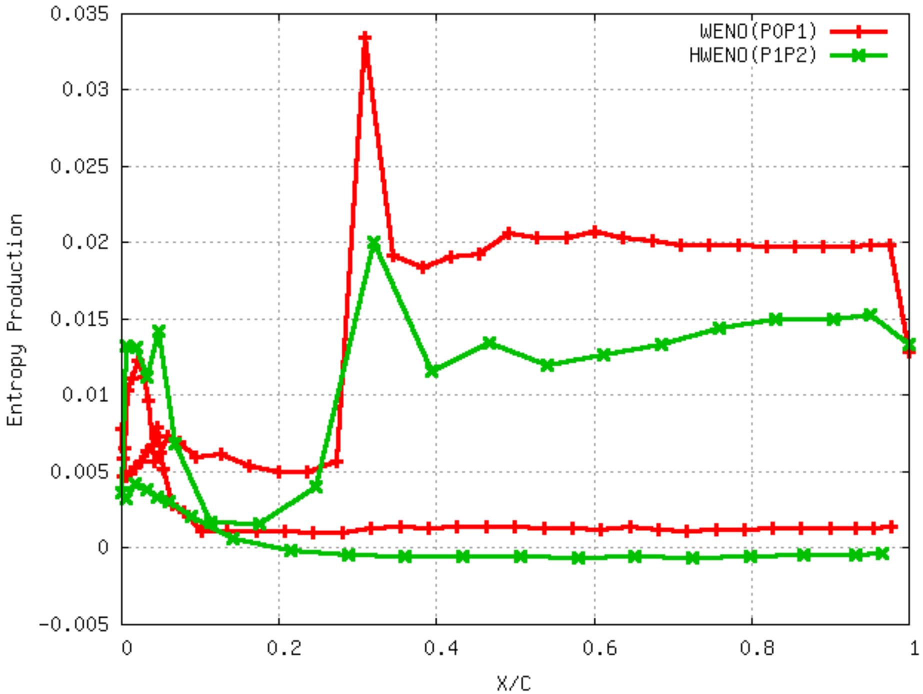

η=0.90

Computed Pressure Coefficient and Entropy Production Distributions at different spanwise locations

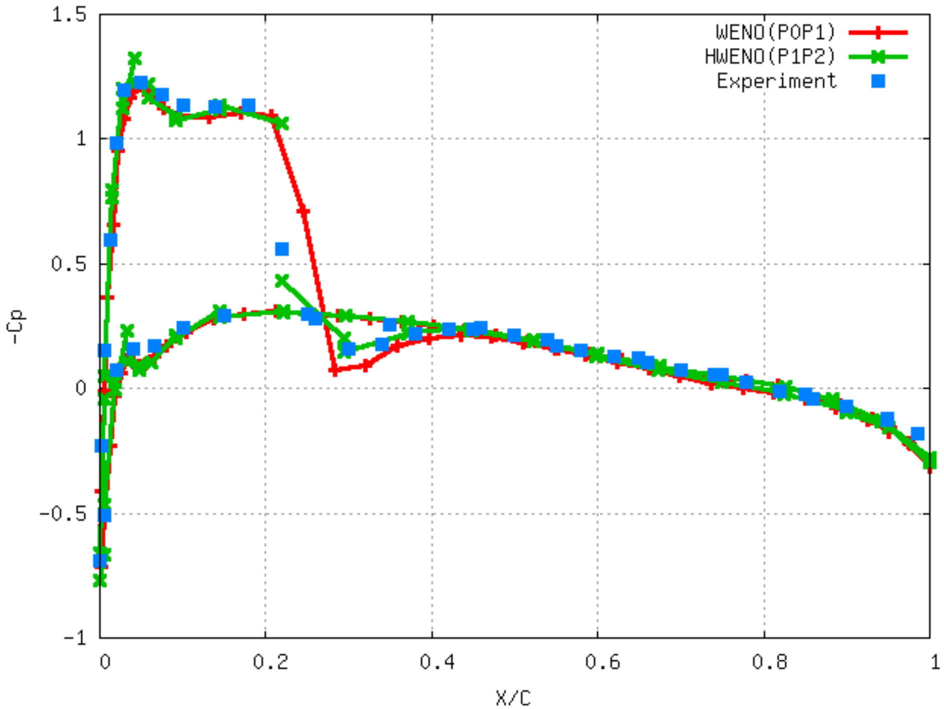

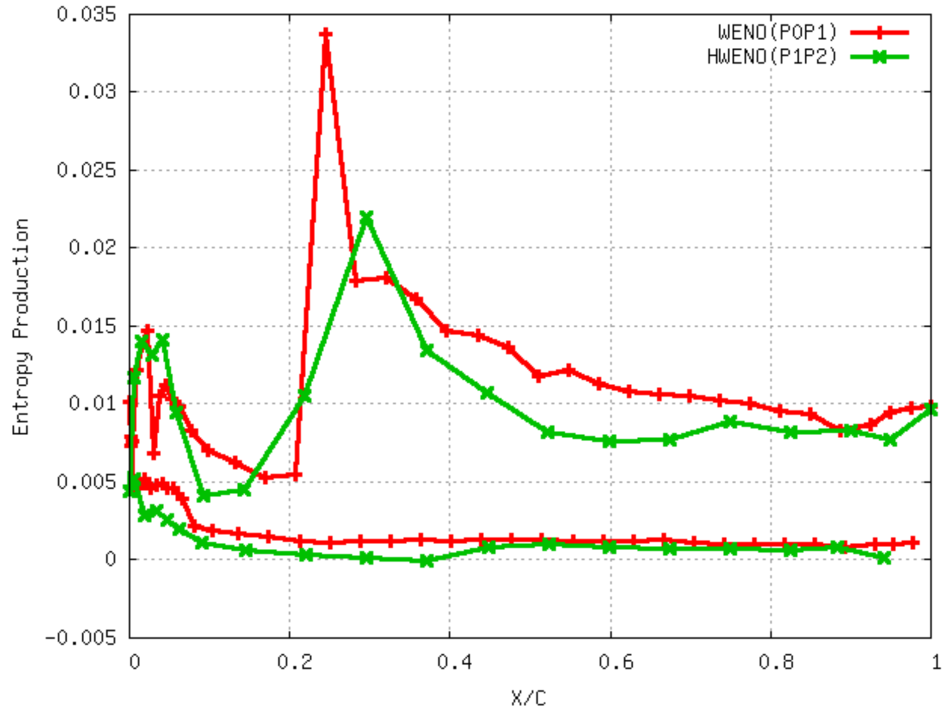

η=0.95

Example 2. Transonic Flow past past a Wing/Pylon/Finned-Store Configuration (M_∞=0.95, α=0°)

- Access the accuracy and non-oscillatory property of the HWENO(P_1P_2) method for flows with strong discontinuities.

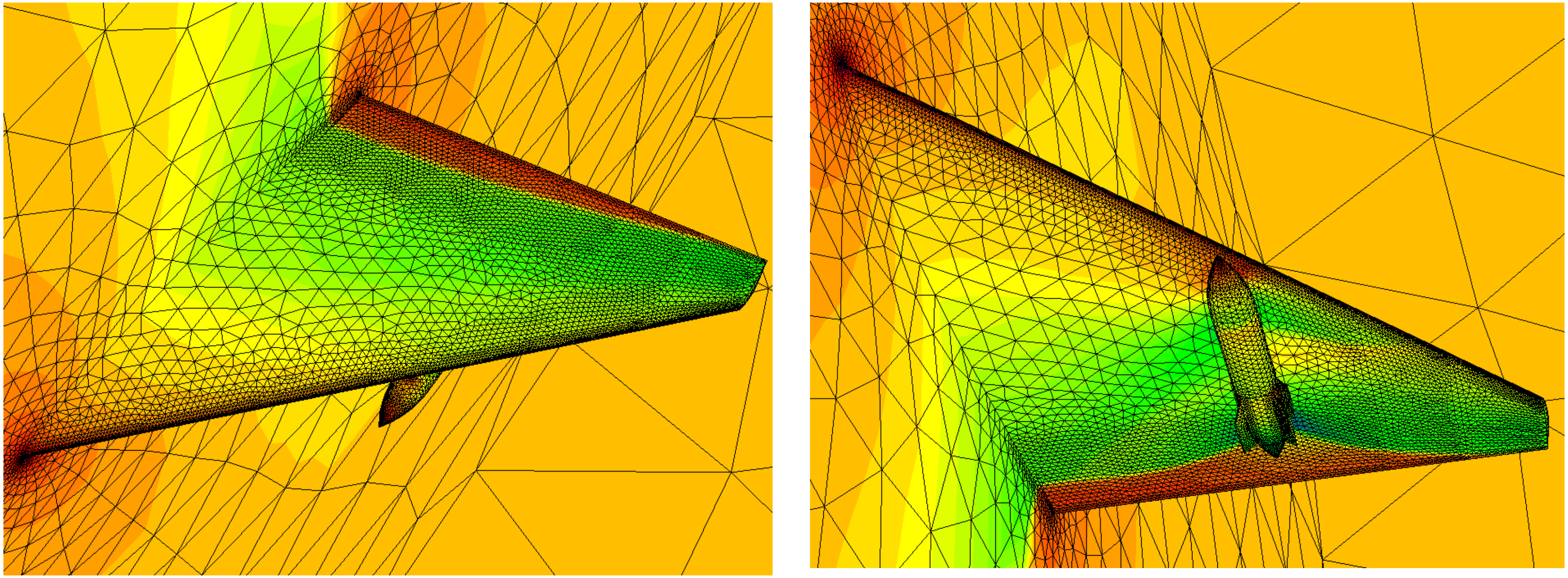

Computed Pressure Contours
(nelem=319,134, npoin=61,075, nboun=14,373)

Computed Pressure Coefficient Distributions at different spanwise locations

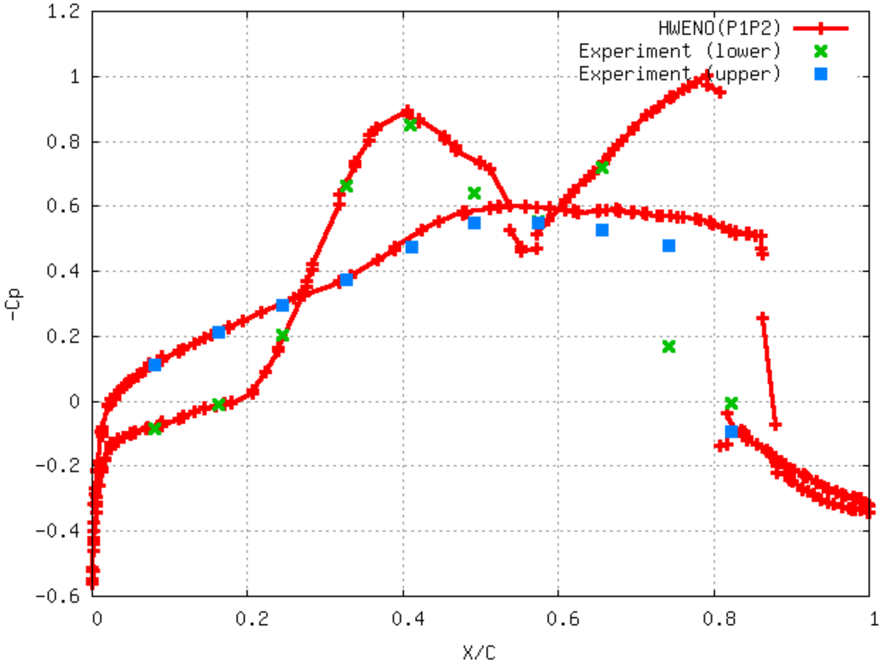

η=0.4077

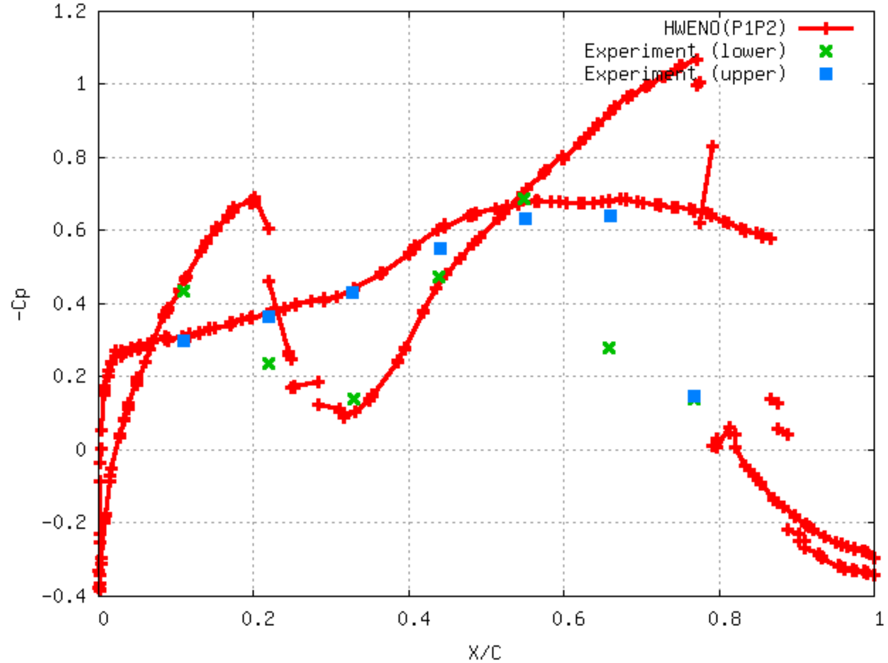

η=0.51

Parallel Performance

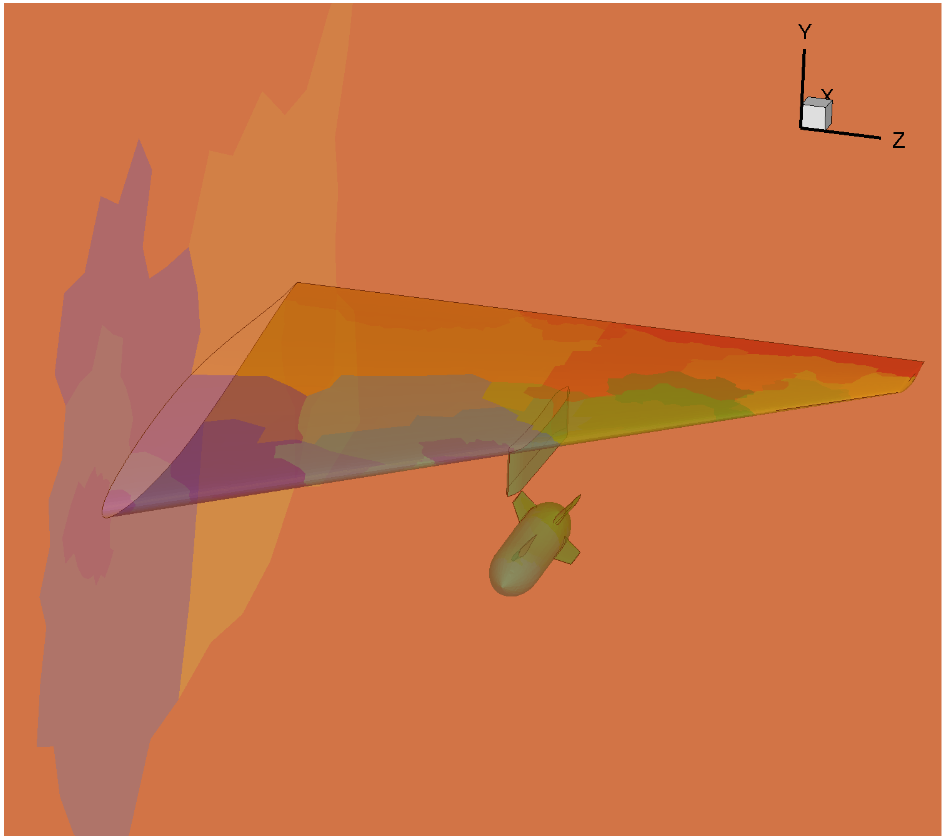

Graph of domain decomposition by METIS
128 partitions and 124,706 elements

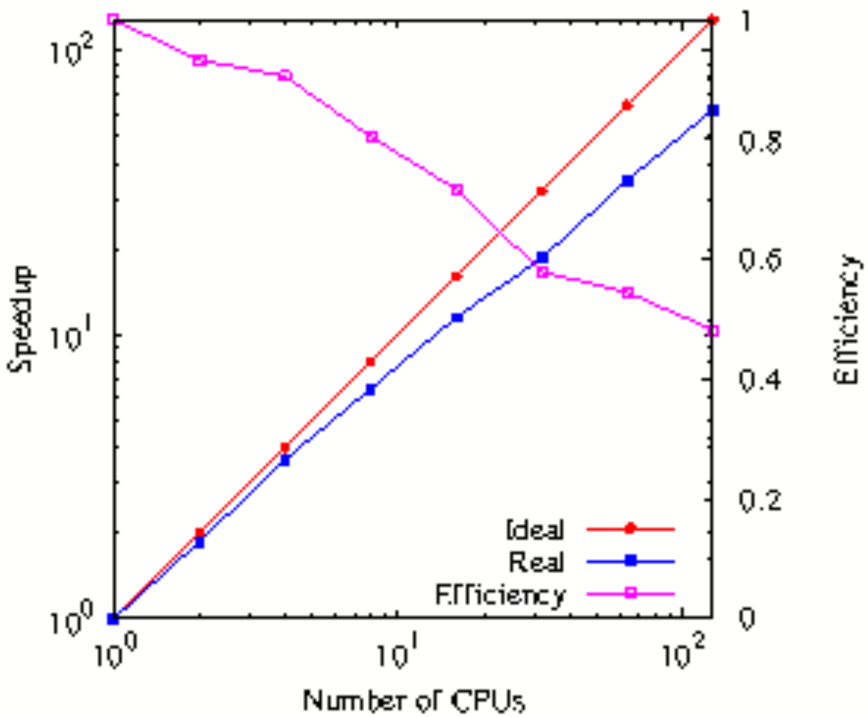

Explicit Method

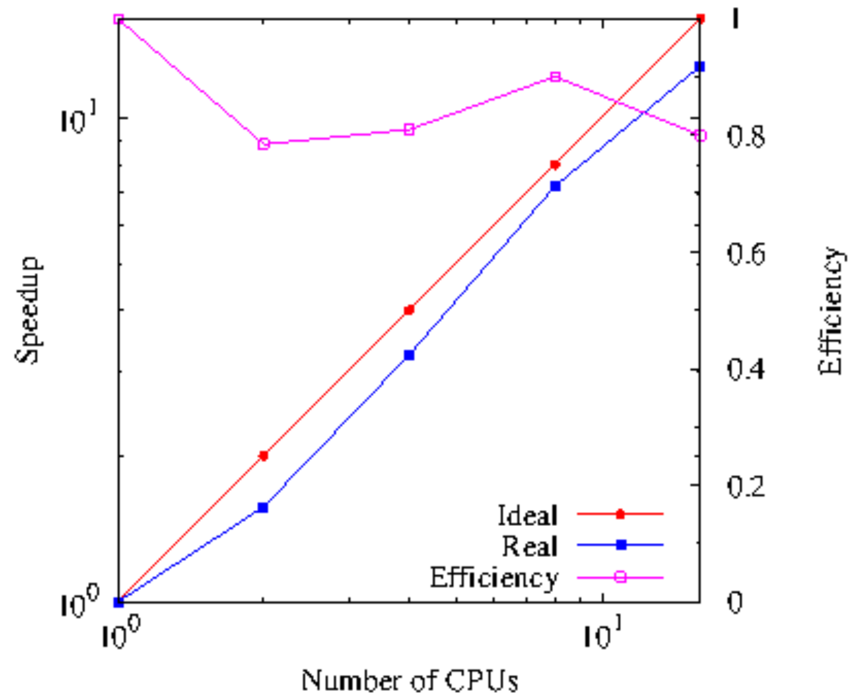

Implicit Method

Parallel speedup and efficiency on a single node (up to 16 CPUs)

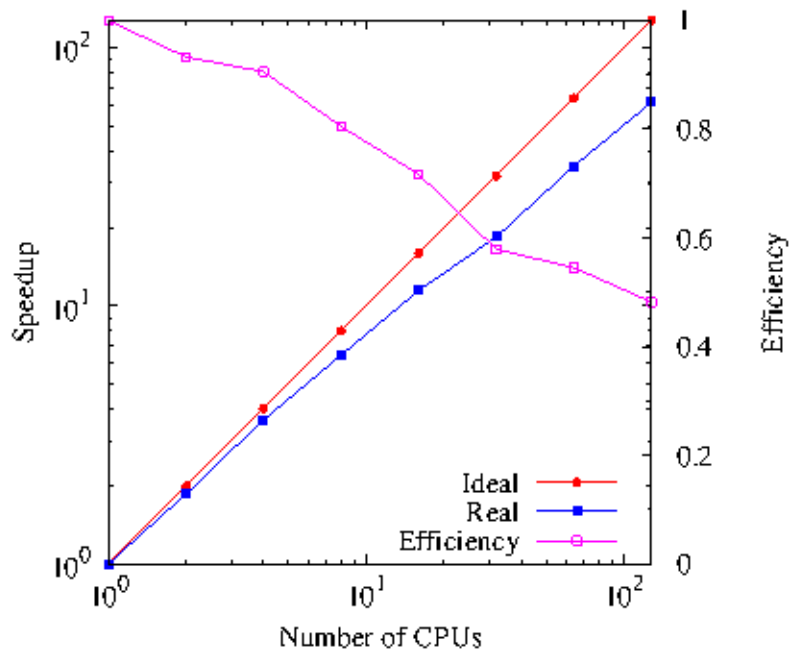

Explicit Method

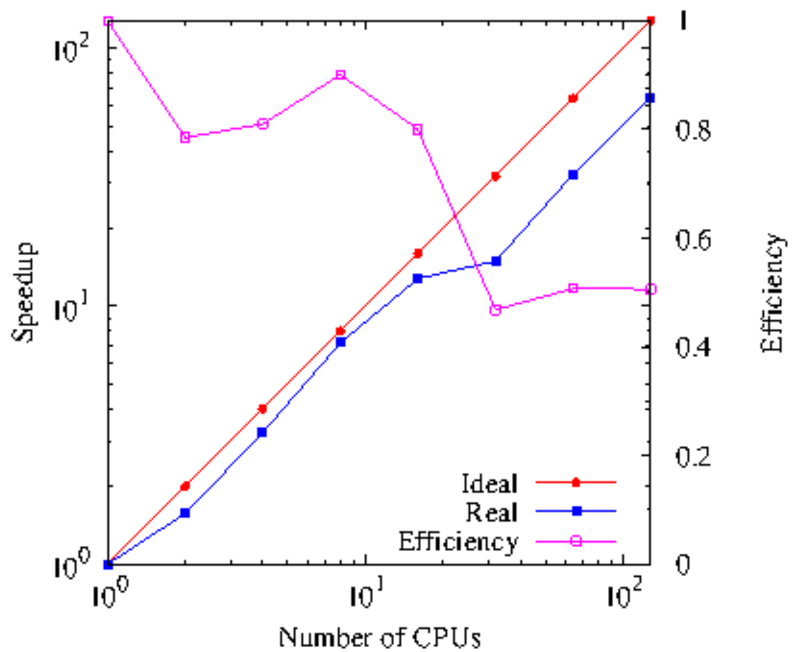

Implicit Method

Parallel speedup and efficiency on a multiple nodes (up to 8 nodes with16 CPUs per node)

Applications

Transonic flow past a B747 configuration

- Demonstrate that the HWENO(P_1P_2) method can be used for computing complicated flows of practical interest.
- Flow condition: M_∞=0.85, α=2°

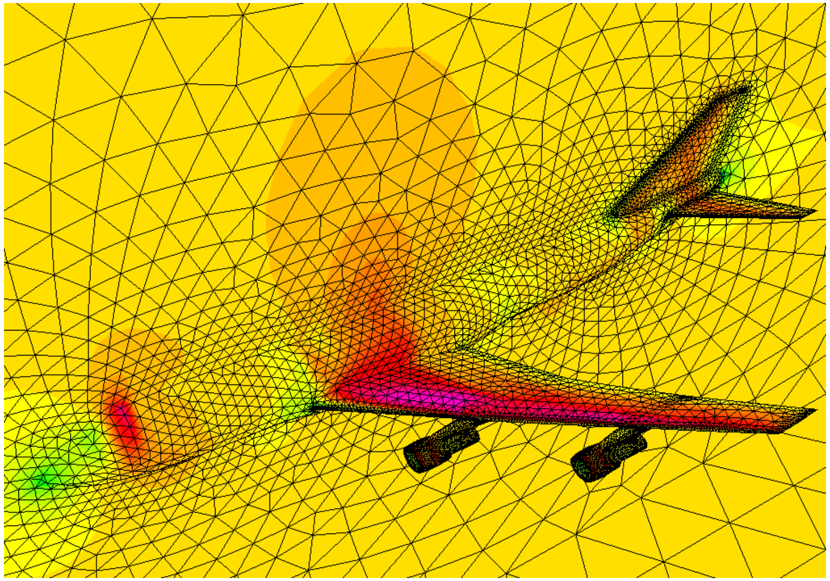

(nelem = 253,577, npoin = 48,851, nboun = 11,802)

Computed Mach Number Contours

Unsteady Viscous Flow over Tandem Airfoils
M=0.2, Re=10,000, α=0

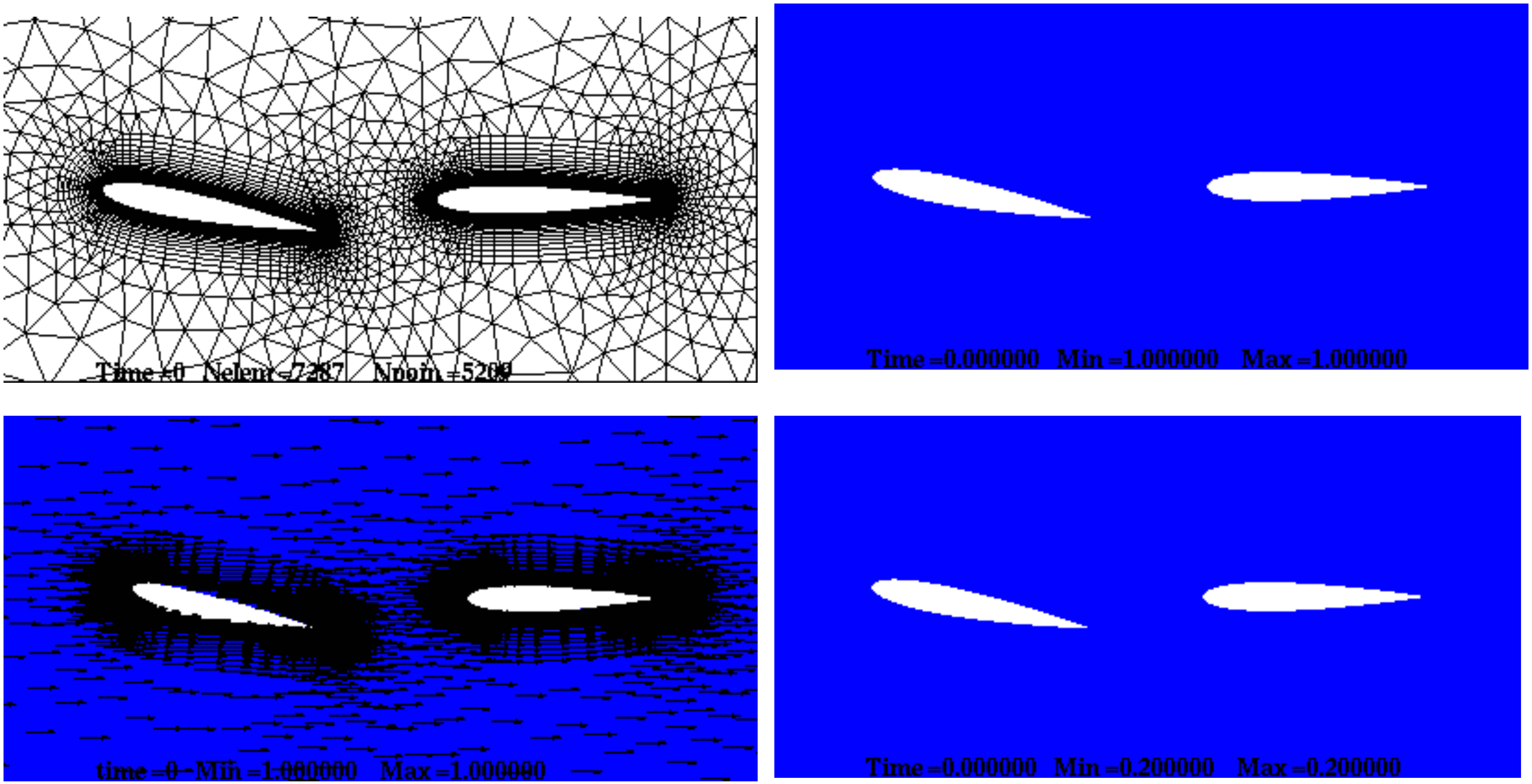

2,902 hexahedral elements, 4,385 prisms, 10,418 grid points,

Subsonic Flow past a Delta Wing

- Demonstrate that the WENO(P_1P_2) method can be used for computing vortex flows of practical interest.
- Flow condition: M_∞=0.3, Re=4,000

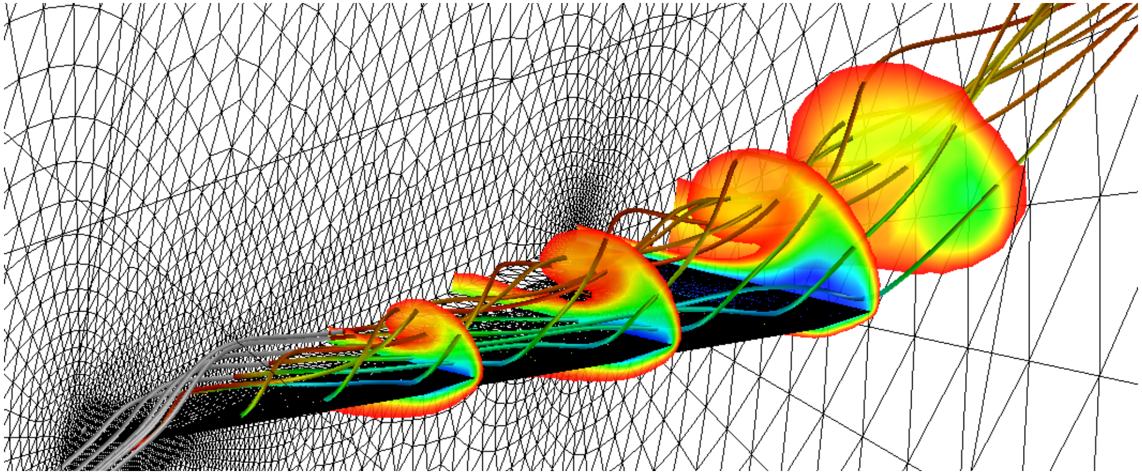

(Tetrahedral grid: Nelem = 674,260, Npoin = 120,531, Nboun = 12,991)

Computed Mach Number Contours and streamlines

Implicit Solutions

Computational Results

- **Numerical Examples**
  - 1. Inviscid shedding flow past a triangular wedge
  - 2. Kármán vortex street at Re = 200
  - 3. Viscous flow past an SD7003 airfoil
  - 4. Implicit large eddy simulation of a lid driven cavity
- **Default parameters for solving the pseudo-time system**
  - Linear solver: LU-SGS preconditioned GMRES algorithm
  - The pseudo time-step term is off, which is equivalent to solving a quasi-Newton system at each implicit Runge-Kutta stage
  - The relative residual tolerance is 1.0×10^{-4}.
  - The maximum iteration number is 5.
- **Compilation and runtime toolkit**
  - METIS for domain partitioning
  - PGI Fortran compiler + OpenMPI

Example 1. Inviscid shedding flow past a triangular wedge

- **Objective**: illustrate the importance of the temporal discretization schemes on the accuracy of the numerical solutions
- **Grid**: 13, 250 hexahedral elements, 27, 026 grid point, and 27, 026 quadrilateral faces
- **Initial condition**: we use intermediate solution ($M_\infty = 0.5$, $\alpha=0°$) obtained by DG(P0) as IC for the unsteady shedding flow

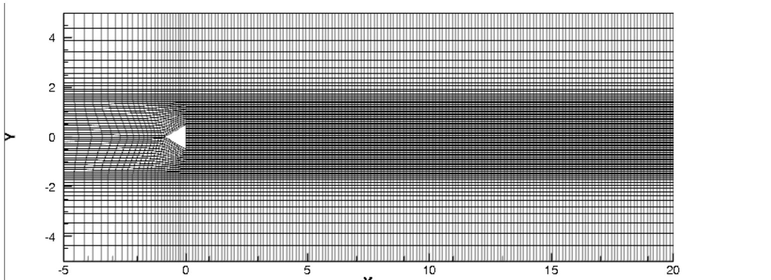

Global view of the grid

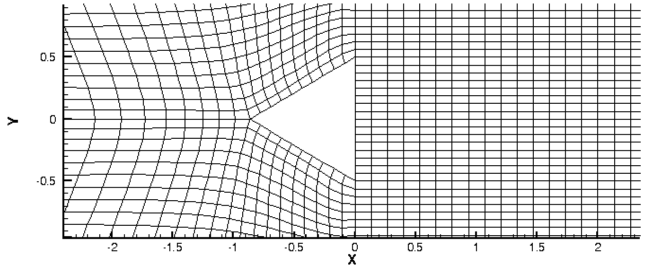

Local view of the grid

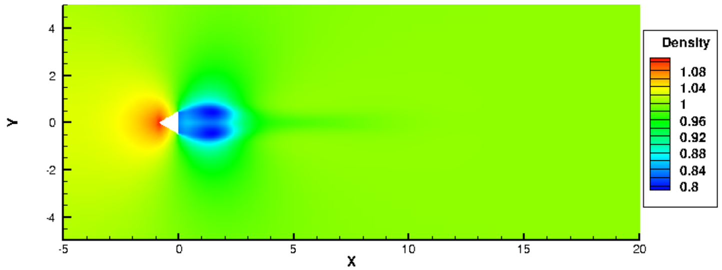

Density contour by P0 solution

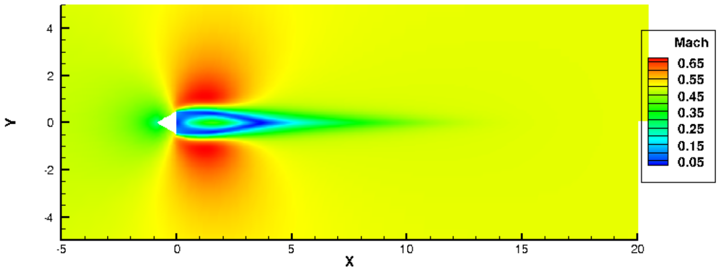

Mach number contour by P0 solution

Example 1. Inviscid shedding flow past a triangular wedge

- Comparison of computed density contours at t = 400 ($M_\infty = 0.5$, $\alpha = 0°$)
  - With a fixed time-step size of dt = 0.05

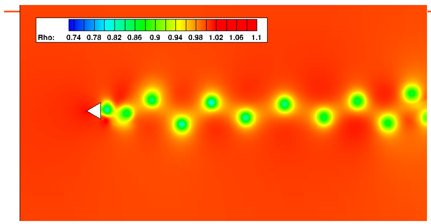

BDF1 + RDG(P1P2)

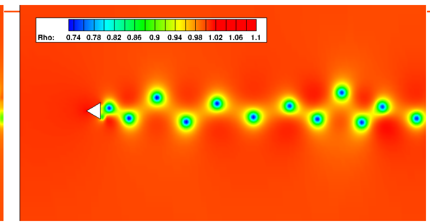

IRK2 +RDG(P1P2)

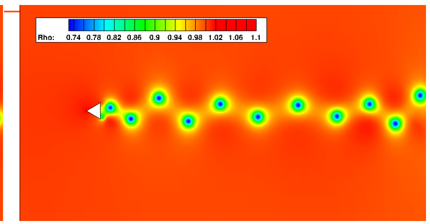

IRK3+RDG(P1P2)

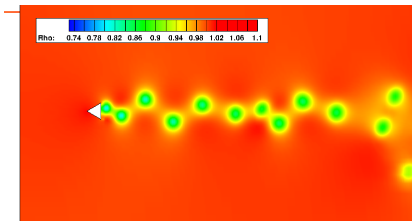

IRK3+DG(P1)

  - With a fixed time-step size of dt = 0.10

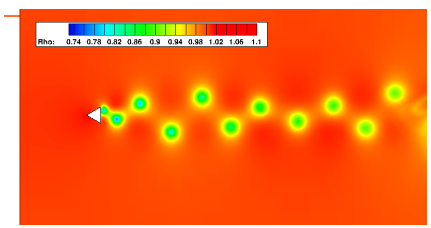

BDF1 + RDG(P1P2)

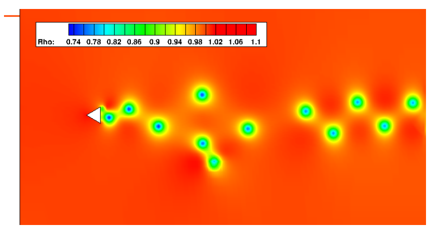

IRK2 + RDG(P1P2)

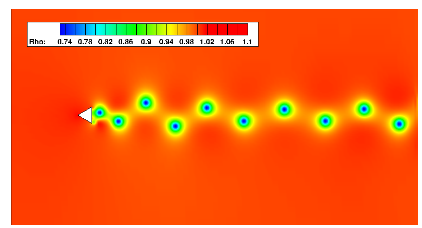

IRK3 + RDG(P1P2)

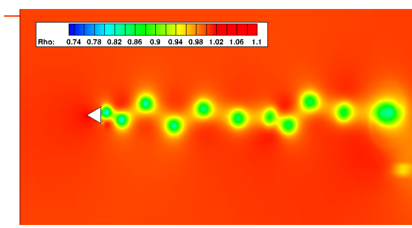

IRK3 + DG(P1)

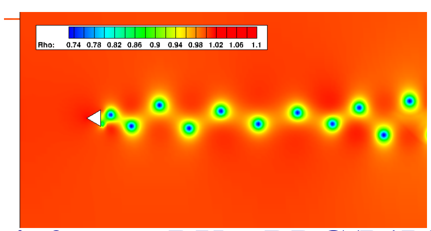

Reference solution: explicit 3-stage RK + RDG(P1P2) with a fixed dt = 0.0004

Example 1. Inviscid shedding flow past a triangular wedge

- Animations (up to solution time t = 400)
  - With a fixed time-step size of dt = 0.10

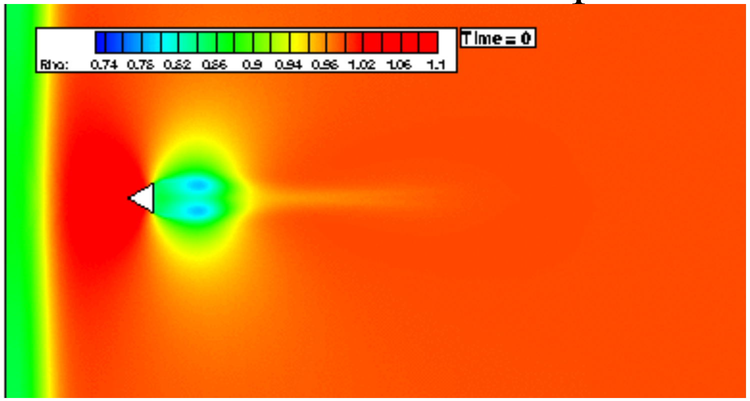

BDF1 + RDG(P1P2)

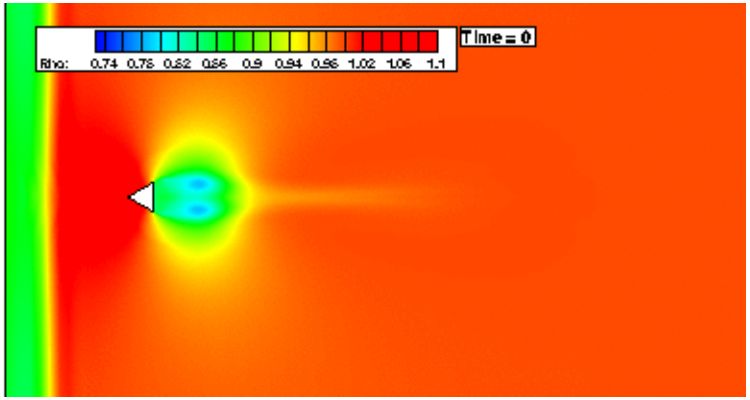

IRK3+DG(P1)

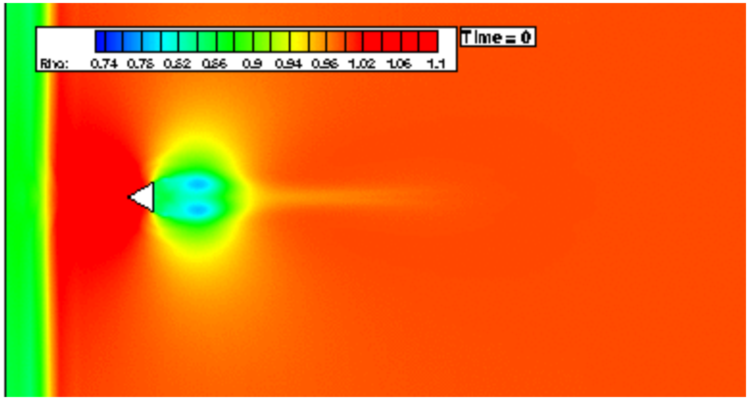

IRK2 + RDG(P1P2)

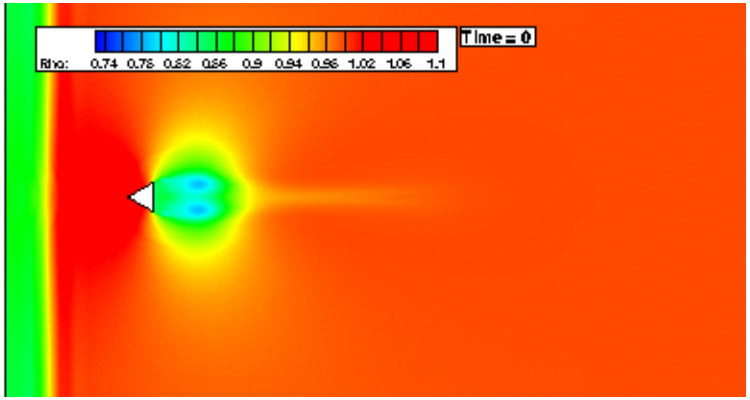

IRK3+RDG(P1P2)

Example 1. Inviscid shedding flow past a triangular wedge

- Comparison of the CPU time (evaluated by running on 64 cores) between the explicit and implicit methods.

For solution at t = 40	Time-step size	Time steps	CPU time (sec)
IRK2 + RDG(P1P2)	dt = 0.05	800	1,770
IRK3 + RDG(P1P2)	dt = 0.05	800	5,182
IRK2 + RDG(P1P2)	dt = 0.10	400	1,008
IRK3 + RDG(P1P2)	dt = 0.10	400	2,825
Explicit RK3 + RDG(P1P2)	dt = 0.0004	800,000	13,498

- Performance of the LU-SGS preconditioned GMRES solver
  - In average, a drop of **4** orders of magnitude for the unsteady residual can be achieved within **5** inner iterations at each implicit RK stage

The IRK3+RDG(P1P2) method provides accurate solutions in space and time and requires much less CPU time compared with its explicit counterpart!

Example 2. Kármán vortex street at Re = 200

- **Grid**: 10,204 hexahedral elements, 20,800 grid points, and 20,800 boundary faces. The normal grid spacing near the cylinder surface is 0.001 (normalized by the cylinder diameter)
- **Boundary condition**: no-slip, adiabatic condition on cylinder surface, symmetry condition on spanwise wall, characteristic condition at far-field.
- **Initial condition**: we use steady-state solution (M_∞ = 0.2, α=3°, Re = 50) obtained by DG(P0) as IC for the vortex shedding

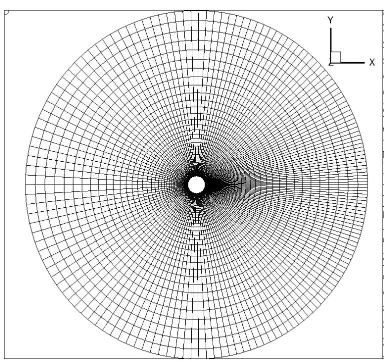

Grid: global view

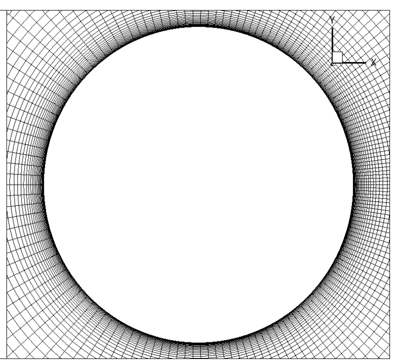

Grid: local View

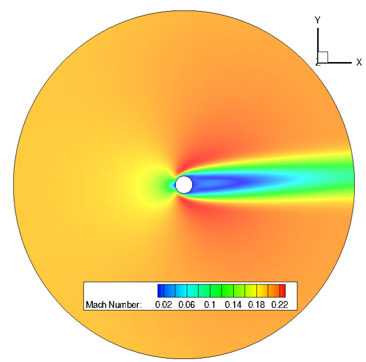

Mach Number

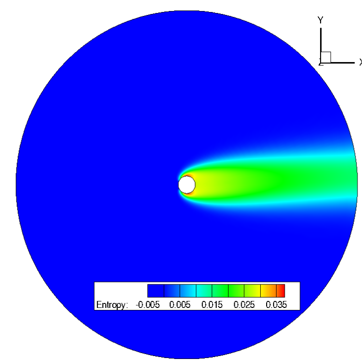

Entropy

You can find the grid and report at the NASA website
http://www.grc.nasa.gov/WWW/Acoustics/code/adpac/sample/CYLINDER_VORTEX_SHEDDING/

Example 2. Kármán vortex street at Re = 200

- Comparison of the computed instantaneous Mach number and entropy contours (M_∞ = 0.2, α = 0°, Re = 200)

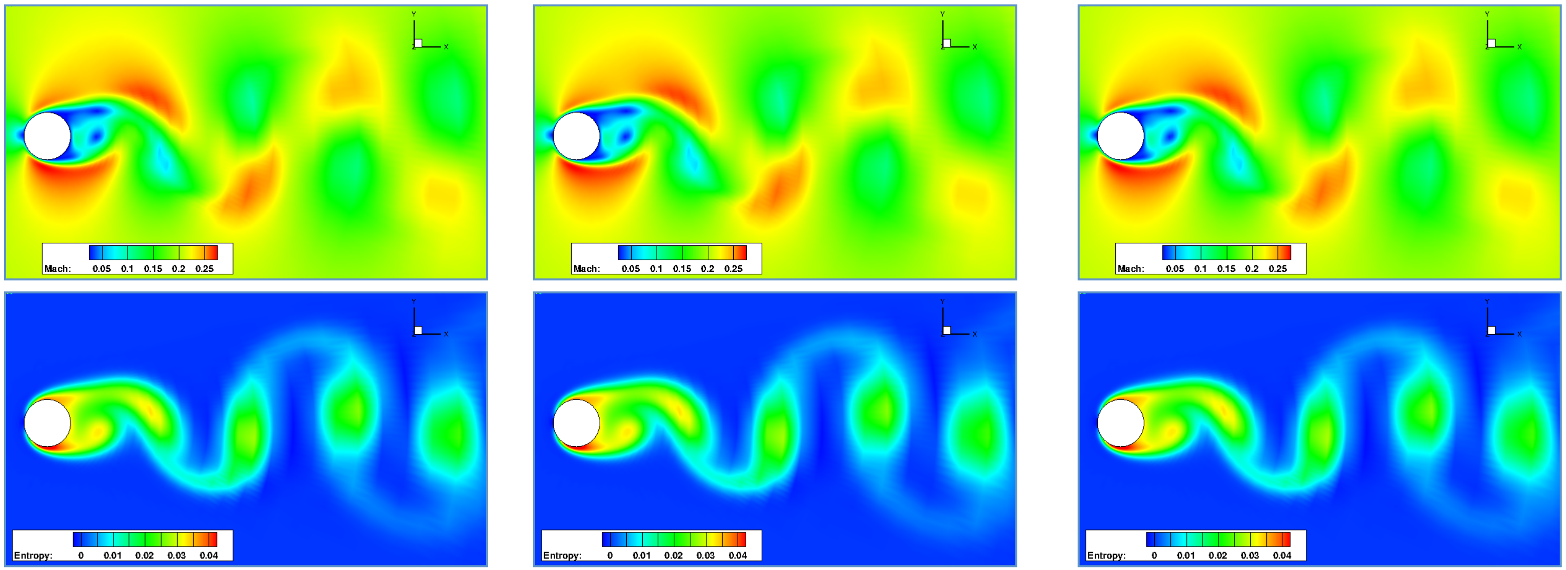

IRK2+RDG(P1P2), dt=0.05 **IRK3+RDG(P1P2), dt=0.05** **IRK3+RDG(P1P2), dt=0.5**

- Animations (up to solution time t = 40)

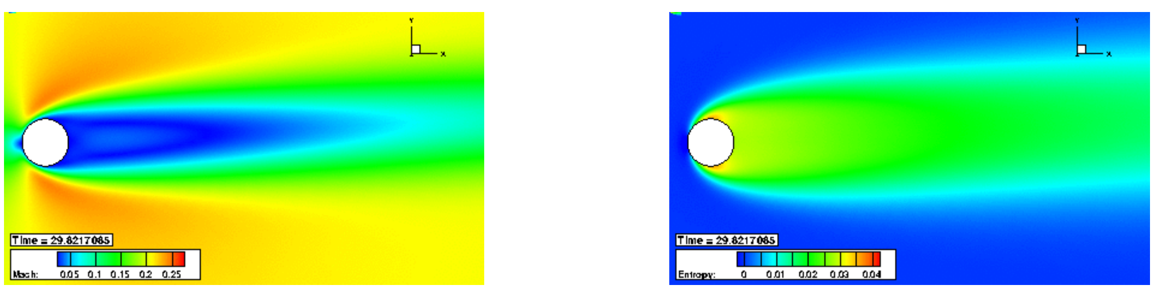

Example 2. Kármán vortex street at Re = 20

- Time histories of lift and drag coefficients (Strouhal number = 1.923)

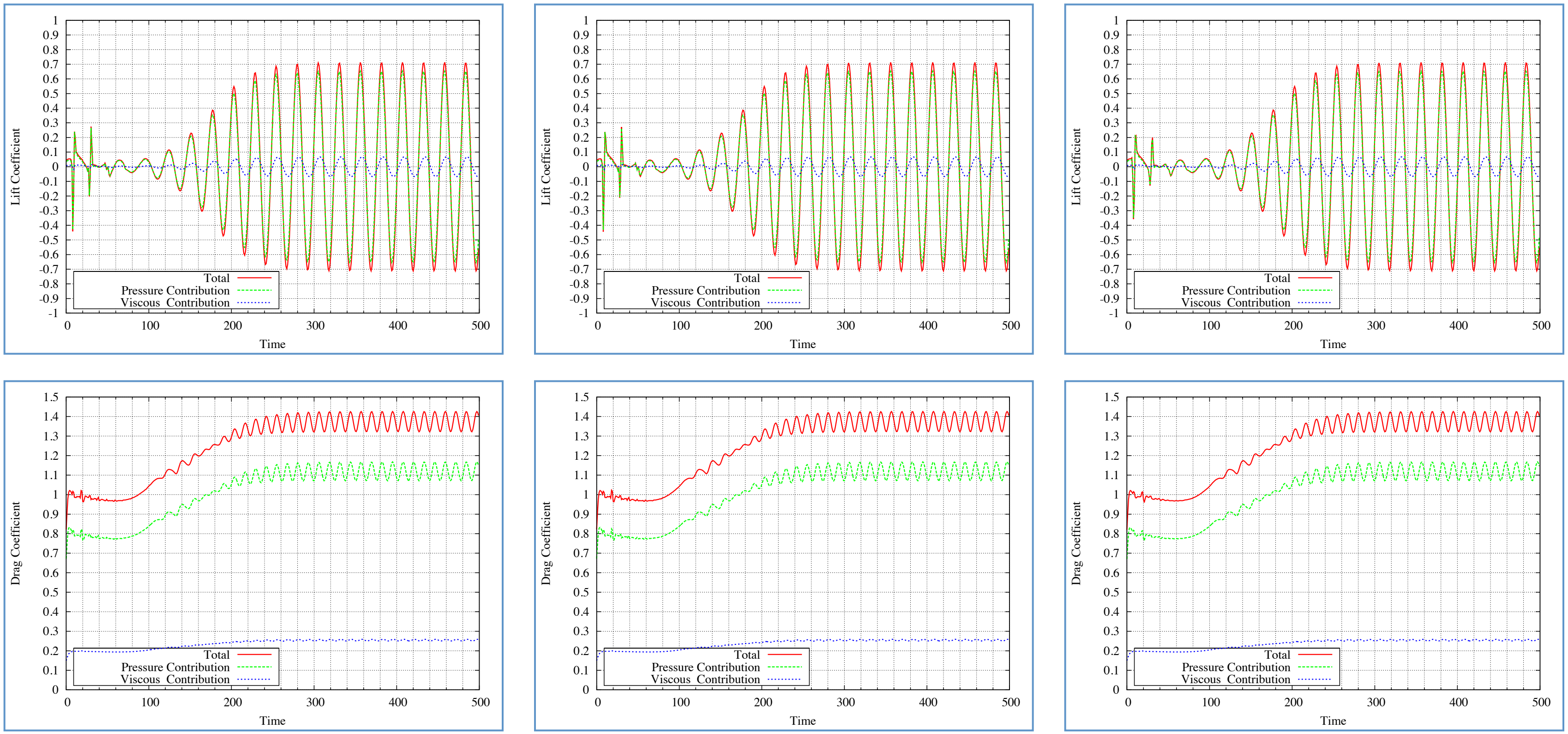

IRK2+RDG(P1P2), dt=0.05 **IRK3+RDG(P1P2), dt=0.05** **IRK3+RDG(P1P2), dt=0.5**

Agree well with the results in the referred literature!

Example 2. Kármán vortex street at Re = 200

- Comparison of the CPU time (evaluated by running on 128 cores) between the explicit and implicit methods.

For solution at t = 40	Time-step size	Time steps	CPU time (sec)
IRK2 + RDG(P1P2)	dt = 0.05	10,000	1,603
IRK3 + RDG(P1P2)	dt = 0.05	10,000	5,524
IRK3 + RDG(P1P2)	dt = 0.50	1,000	1,047
Explicit RK3 + RDG(P1P2)	dt = 0.00005	10,000,000	Estimated 77,960

- Performance of the LU-SGS preconditioned GMRES solver
  - In average, a drop of **4** orders of magnitude for the unsteady residual can be achieved within **5** inner iterations at each implicit RK stage

- The IRK's can greatly accelerate the solution over its explicit counterpart, while rendering accurate solution in time and space for viscous flows.
- The IRK3 enables the use of much larger time-step size and thus can improve the overall efficiency.

Example 3. Viscous flow past an SD7003 airfoil

- **Grid**: 50,781 prismatic elements, 52,176 grid points, 101,562 triangular boundary faces, and 279 quadrilateral boundary faces.
- **Boundary condition**: no-slip, adiabatic condition on the airfoil surface, symmetry condition on spanwise wall, characteristic condition on far-field.
- **Initial condition**: uniform flow ($M_\infty = 0.1$, $\alpha=4°$, $Re = 10{,}000$) in the field.

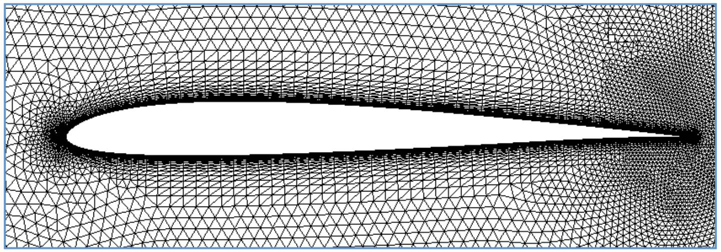

Airfoil: global view

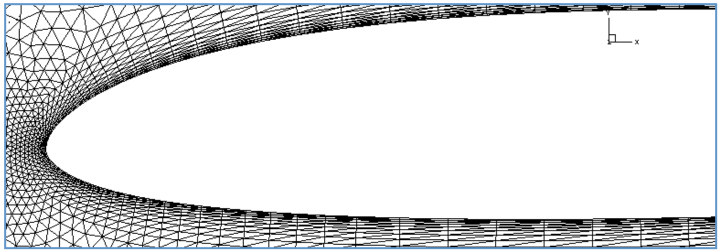

Airfoil: leading edge

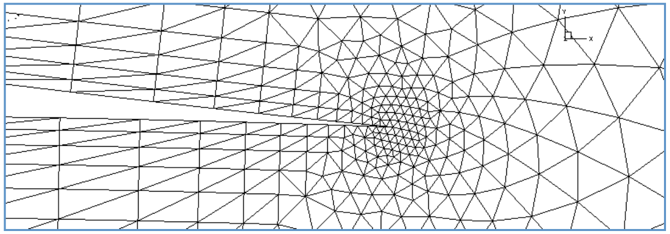

Airfoil: trailing edge

Example 3. Viscous flow past an SD7003 airfoil

- Comparison of the computed instantaneous pressure number contours

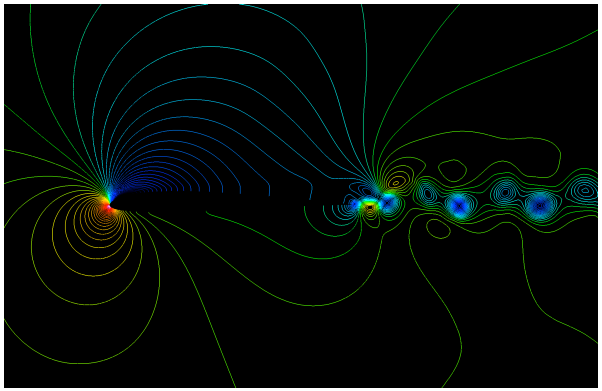

By the compact method*

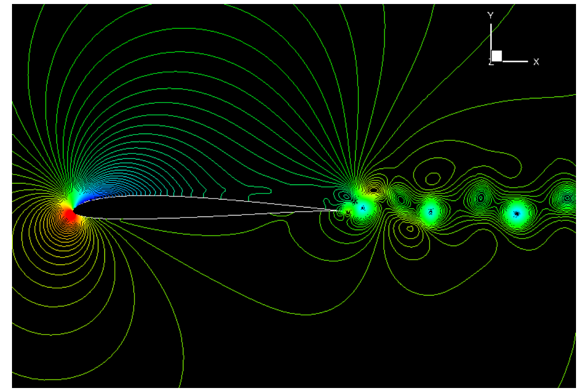

By IRK3+RDG(P1P2), dt = 0.01

- Comparison of the computed

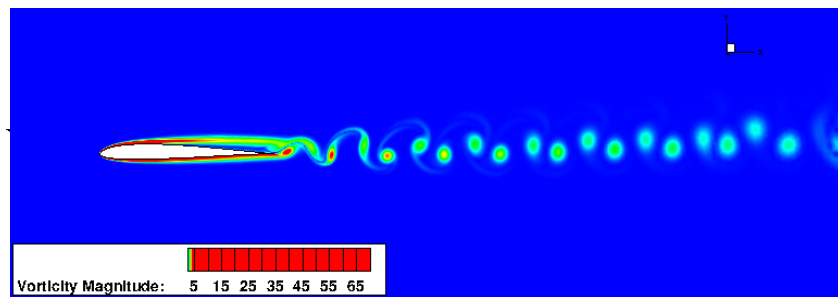

By the compact method*

By IRK3+RDG(P1P2), dt = 0.01

*** Raymond E Gordnier and Miguel R Visbal. Compact Difference Scheme Applied to Simulation of Low-Sweep Delta Wing Flow. AIAA journal, 43(8):1744–1752, 2005.**

Example 3. Viscous flow past an SD7003 airfoil

- Local details of the computed instantaneous solution by

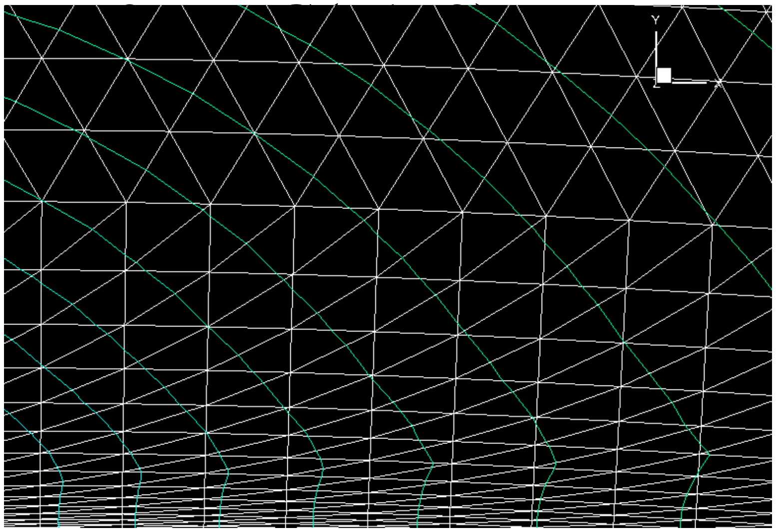

Pressure contours near the upper surface

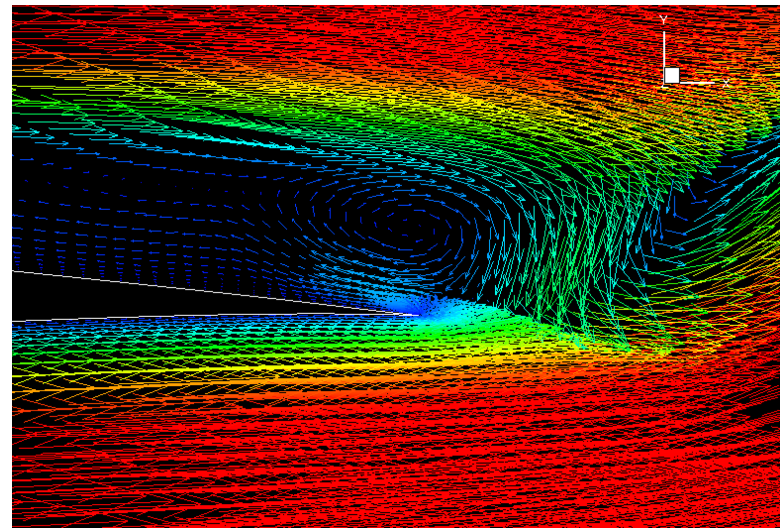

Velocity vectors near the trailing edge

- Animations (up to solution time t = 100 with dt = 0.01 and 1 sec / frame)

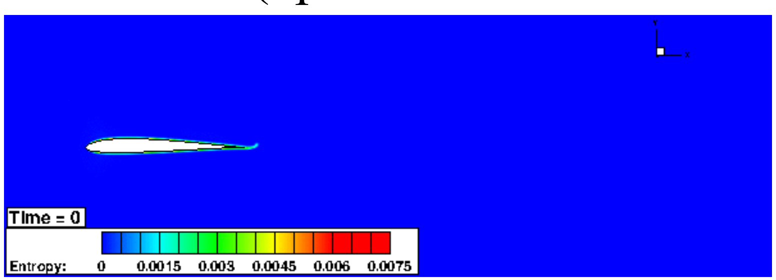

Entropy contours

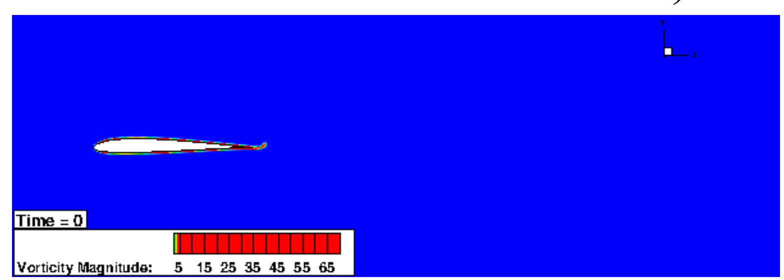

vorticity Magnitude contiurs

Example 3. Viscous flow past an SD7003 airfoil

- Comparison of the CPU time (evaluated by running on 256 cores) between the explicit and implicit methods.

For solution at t = 100	Time-step size	Time steps	CPU time (sec)
IRK3 + RDG(P1P2)	dt = 0.01	10,000	83,178
Explicit RK3 + RDG(P1P2)	dt = 0.00001	10,000,000	Estimated 1,669,400

A speedup factor of more than 200 by IRK3 over its explicit counterpart !

- Performance of the LU-SGS preconditioned GMRES solver
  - In average, a drop of **4** orders of magnitude for the unsteady residual can be achieved within **5** inner iterations at each implicit RK stage

Indeed, the relative tol. = 10^{-4} is a overkill in running these problems.
If we use relative tol. = 10^{-2}, even higher speedup may be achieved.

Example 4. Implicit LES of a lid driven cavit

- **Implicit LES**
  - Without the use of an explicit sub-grid scale model.
- **Why DG methods?**
  - The DG methods only dissipate the scales that the model is not able to capture correctly, thus acting like a sub-grid scale model.
- **Why RDG methods?**
  - DG methods like P2, P3, and P4 have shown the ability of helping improve the solution accuracy in a few benchmark DNS and LES problems. Yet they are expensive in terms of computing time and storage requirement.
  - Assess the RDG methods like P1P2 and even P2P3 for computing large-scale.
- **Why 3D lid driven cavity?**
  - The 3D lid driven cavity presents complex physical phenomena, though the geometry is simple. Therefore it is an adequate example to assess the performance of the implicit LES with the developed methods.

Example 4. Implicit LES of a lid driven cavit

- **Problem description**
  - Domain: x = [0, 1], y = [0, 1], and z = [-0.25, 0.25] (x: y: z = 1: 1: 0.5).
  - Top lid velocity $\mathbf{v}_b$ = (0.2, 0, 0), Re = 10,000.
  - No-slip, adiabatic conditions for the rest of boundary walls.
  - Grid: 64x64x32 grid points; h_{min} = 0.005 in x-y plane (y^+ = 3.535); uniform grid distribution in spanwise z-direction.

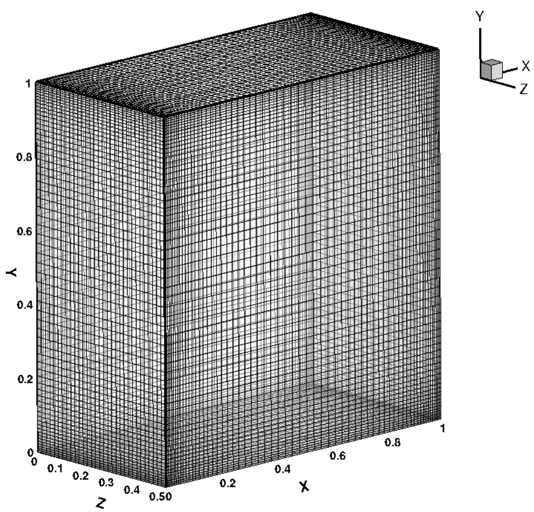

The 64x64x32 grid surface

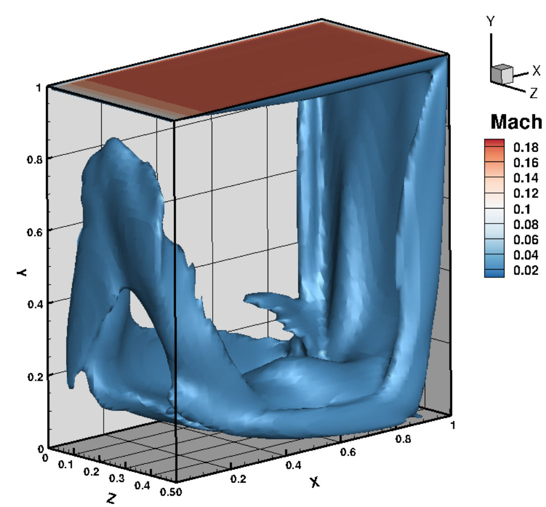

Instantaneous Mach No. iso-surface

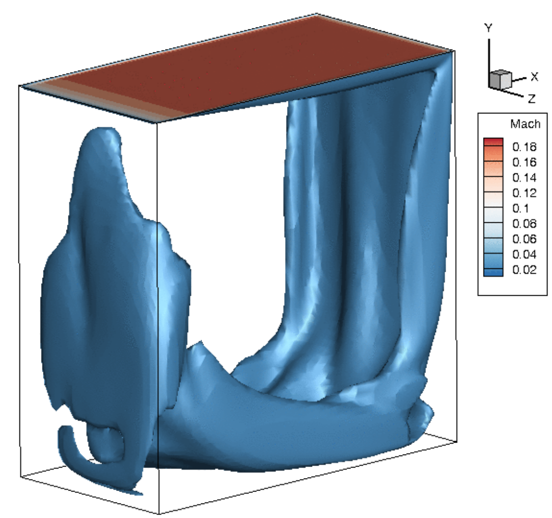

Animated Mach No. iso-

Example 4. Implicit LES of a lid driven cavity

- **Problem setup**
  - Step 1. Run 5000 time steps with BDF1+DG(P1) and CFL = 500 from zero-velocity field, so that the flow filed reaches a cyclically oscillating status.
  - Step 2. Restart the computation with a fixed time-step size of dt = 0.1, and use a desired method as shown below. The width of window for time averaging is 30 second per frame (every 300 steps).

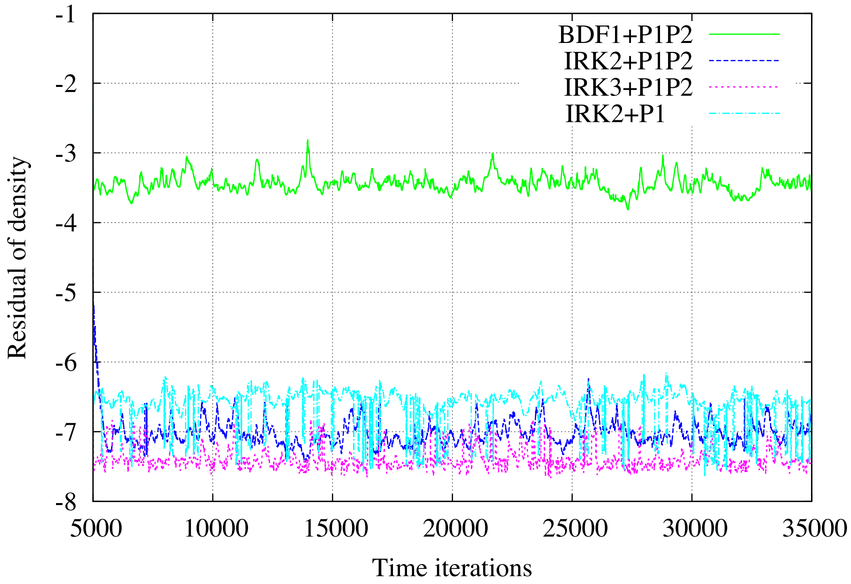

Density residual vs. time steps (fixed dt = 0.1)

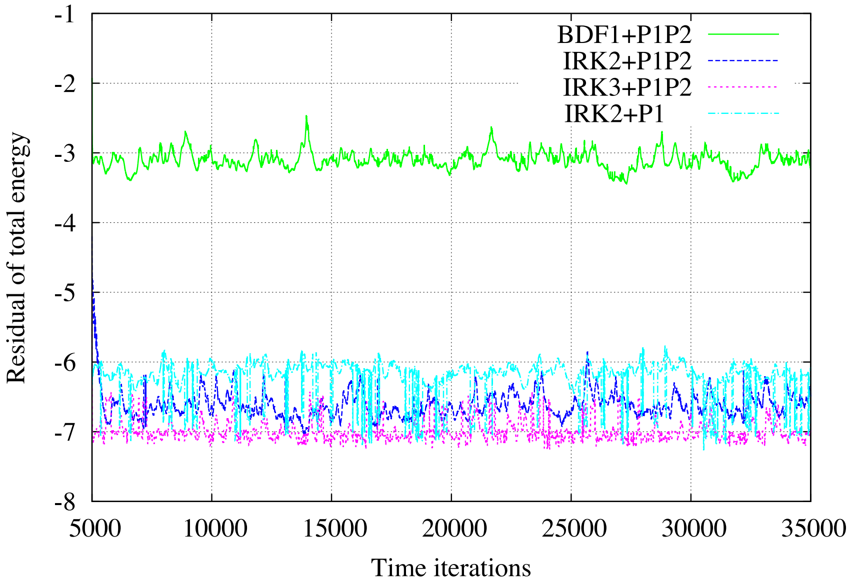

Total energy residual vs. time steps (fixed dt = 0.1)

Example 4. Implicit LES of a lid driven cavit

- **Mean velocities**
  - Exp. (Prasad&Koseff,1989)
  - LES (Zang et al., 1993)
  - BDF1+RDG(P1P2)
  - IRK2+RDG(P1P2)
  - IRK3+RDG(P1P2)
  - IRK2+DG(P1)

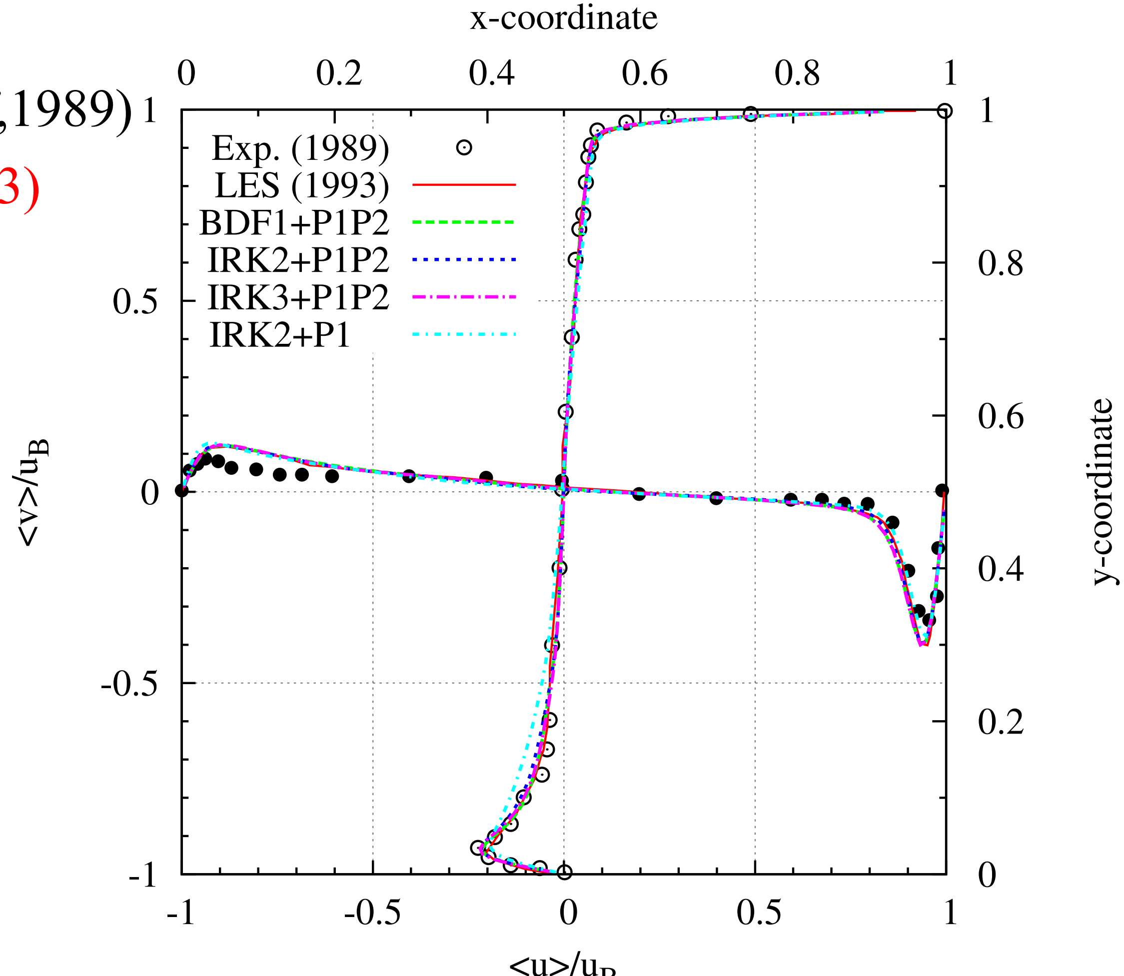

Profiles along the x and y centerlines on spanwise mid-plane (z = 0)

- RDG(P1P2) match all well.
- DG(P1) is a little off near bottom region.

Example 4. Implicit LES of a lid driven cavit

- **RMS velocities**
  - Exp. (Prasad&Koseff,1989)
  - LES (Zang et al., 1993)
  - BDF1+RDG(P1P2)
  - IRK2+RDG(P1P2)
  - IRK3+RDG(P1P2)
  - IRK2+DG(P1)

- DG(P1) is not accurate enough.
- RDG(P1P2) matches exp. data well!
- IRK's are slightly better than BDF1.
- IRK3 is close to IRK2.

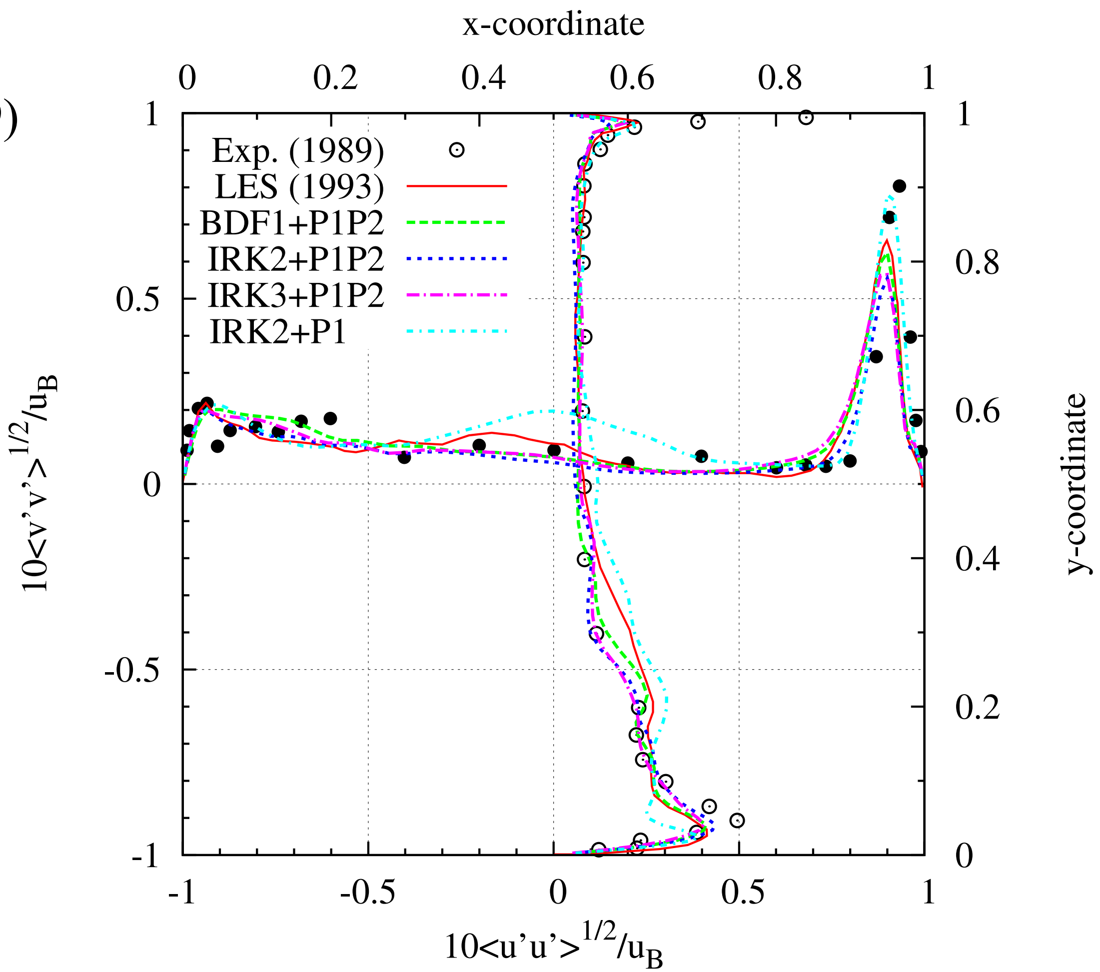

Profiles along the x and y centerlines on spanwise mid-plane (z = 0)

Example 4. Implicit LES of a lid driven cavit

- **Reynolds stress tensor component <u'v'>**
  - Exp. (Prasad&Koseff,1989)
  - LES (Zang et al., 1993)
  - BDF1+RDG(P1P2)
  - IRK2+RDG(P1P2)
  - IRK3+RDG(P1P2)
  - IRK2+DG(P1)

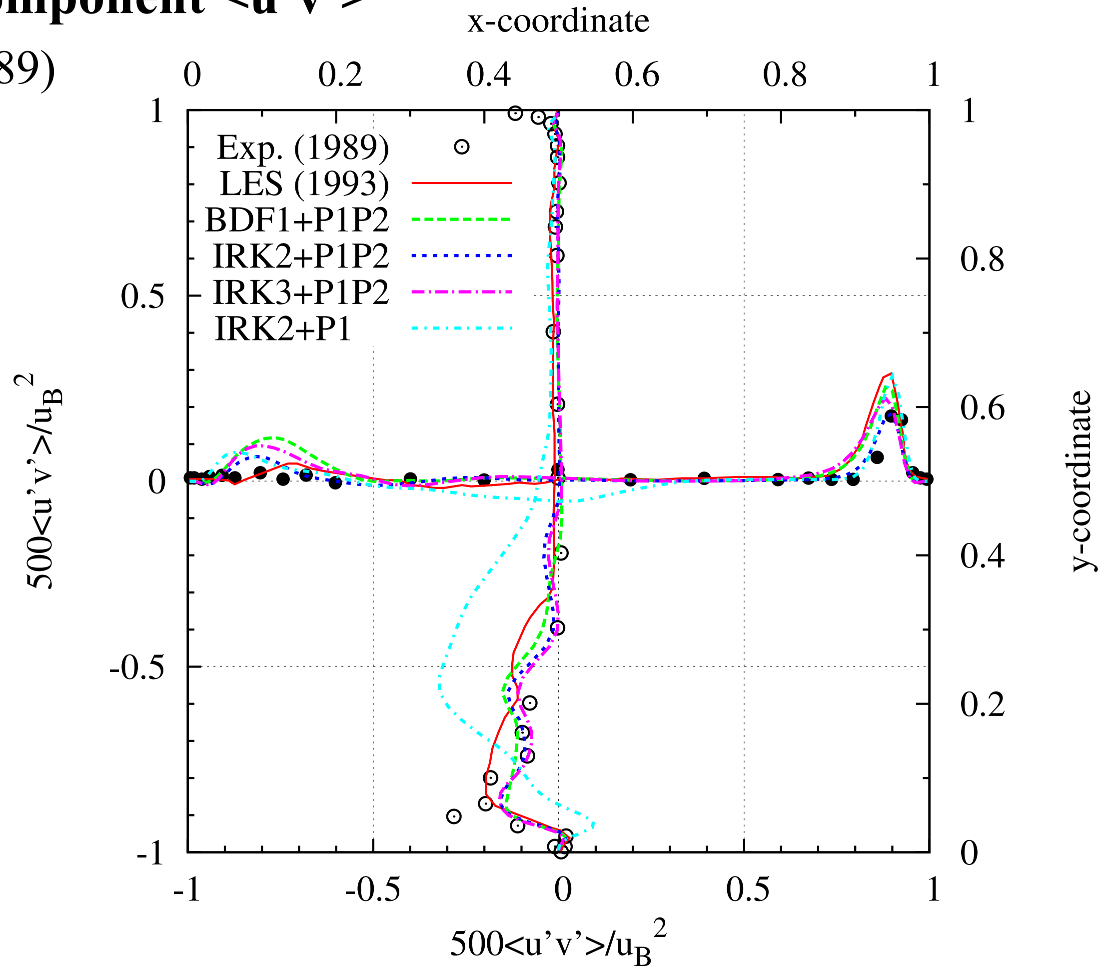

Profiles along the x and y centerlines on spanwise mid-plane (z = 0)

- DG(P1) is far from good in lower region.
- RDG(P1P2) matches exp. data well!
- IRK's are better than BDF1 in some regions.
- IRK3 is close to IRK2.

Example 4. Implicit LES of a lid driven cavity

- Comparison of the CPU time (evaluated by running on 256 cores) between the explicit and implicit methods.

For solution at t = 3000	Time-step size	Time steps	CPU time (sec)
BDF1 + RDG(P1P2)	dt = 0.1	30,000	52,542
IRK2 + RDG(P1P2)	dt = 0.1	30,000	86,066
IRK3 + RDG(P1P2)	dt = 0.1	30,000	263,010
IRK2 + DG(P1)	dt = 0.1	30,000	69,050
Explicit RK3 + RDG(P1P2)	dt = 0.0001	30,000,000	Estimated 7,347,942

- LU-SGS preconditioned GMRES solver
  - In average, a drop of **4** orders of magnitude for the unsteady residual can be achieved within **5** inner iterations at each implicit RK stage.

- A speedup factor of more than 85 by IRK over its explicit counterpart!
- IRK+RDG(P1P2) greatly improve solution accuracy for implicit LES without much extra cost than the underlying IRK+DG(P1)!

Concluding Remarks

- A reconstructed discontinuous Galerkin method based on a Hierarchical WENO reconstruction, HWENO(P_1P_2) has been developed for compressible flows at all speeds on hybrid grids.

- The HWENO(P_1P_2) method is able to provide sharp resolution of shock waves essentially without over- and under-shoots for discontinuities and achieve the designed third-order of accuracy for smooth flows.

- RDG methods have the potential to provide a superior alternative to the traditional FV methods, and to become a main choice for the next generation of CFD codes.

- A higher-order RDG-based CFD code will ultimately deliver a more accurate, efficient, robust, and reliable simulation tool with confidence that will enable us to solve flow problems at resolutions never before possible by the current state-of-the-art CFD technology.

Thank You !